Condensed phase and dark reactions of atmospheric nitrogen oxides

by

Hannah Schaefer Kenagy

A dissertation submitted in partial satisfaction of the

requirements for the degree of

Doctor of Philosophy

in

Chemistry

in the

Graduate Division

of the

University of California, Berkeley

Committee in charge:

Professor Ronald C. Cohen, Chair
Professor Kristie A. Boering
Professor Allen H. Goldstein

Summer 2021

Condensed phase and dark reactions of atmospheric nitrogen oxides

Abstract

Condensed phase and dark reactions of atmospheric nitrogen oxides

by

Hannah Schaefer Kenagy

Doctor of Philosophy in Chemistry

University of California, Berkeley

Professor Ronald C. Cohen, Chair

Nitrogen oxides ($NO_x \equiv NO + NO_2$) influence both the gas and aerosol phases of tropospheric chemistry, with impacts on air quality, climate, and nutrient cycling in ecosystems. The lifetime of NO_x in the atmosphere is controlled by conversion to its permanent oxidative sinks: organic nitrates ($RONO_2$) and nitric acid (HNO_3). Much of the previous observational work to understand the lifetime and fate of NO_x has focused on summer conditions when the daytime NO_x lifetime is relatively short (2-4 hr) and NO_x plays a key role in tropospheric O_3 production. Here I use observations from four aircraft experiments to provide new constraints on the lifetime and fate of NO_x and its oxidation products in urban areas by exploring the importance of condensed phase and dark reactions. First, I examine the lifetime and fate of NO_x during wintertime conditions in the Northeast US and show that NO_x loss is dominated by nocturnal, condensed phase reactions that produce HNO_3. Second, I examine the importance of nocturnal production of $RONO_2$ as a loss pathway for NO_x in three chemically distinct locations in the US and Korea. Finally, I examine the fate of $RONO_2$, an important oxidative sink of NO_x, by assessing its partitioning into the condensed phase and its role in secondary organic aerosol (SOA) formation using observations from Korea as an example of urban chemistry.

Although urban NO_x lifetimes have been examined extensively during summertime conditions, wintertime NO_x chemistry has been comparatively less studied. I use measurements of NO_x and its oxidation products from the aircraft-based WINTER (Wintertime INvestigation of Transport, Emissions, and Reactivity) experiment over the northeastern United States during February – March 2015 to describe the urban NO_x lifetime during conditions when days are shorter, actinic flux is reduced, and temperatures are colder. By analyzing regional outflow from the East Coast, I show that NO_x is long lived during the winter, with a longer daytime lifetime (29 hr) than nighttime lifetime (6.3 hr). Moreover, I demonstrate that wintertime urban NO_x emissions have an overall lifetime controlled by the nighttime conversion of NO_x to HNO_3 via heterogeneous chemistry.

In warm, rural environments dominated by biogenic emissions, nocturnal NO_3-initiated production of $RONO_2$ is known to be competitive with daytime OH-initiated $RONO_2$ production. However, in urban areas, OH-initiated production of $RONO_2$ has been assumed dominant and NO_3-initiated production considered negligible. I show evidence for nighttime $RONO_2$ production similar in magnitude to daytime production during the three aircraft campaigns in chemically distinct summertime environments: Studies of Emissions and Atmospheric Composition, Clouds, and Climate Coupling by Regional Surveys (SEAC[4]RS, 2013) in the rural Southeastern United States, Front Range Air Pollution and Photochemistry Experiment (FRAPPÉ, 2014) in the Colorado Front Range, and Korea-United States Air Quality Study (KORUS-AQ, 2016) around the megacity of Seoul, South Korea. During each campaign, morning observations show $RONO_2$ enhancements at constant, near-background O_x ($\equiv O_3 + NO_2$) concentrations, indicating that the $RONO_2$ are from a non-photochemical source, whereas afternoon observations show a strong correlation between $RONO_2$ and Ox resulting from photochemical production. Furthermore, I show that there are sufficient precursors for nocturnal $RONO_2$ formation during all three campaigns.

Finally, I examine the fate of $RONO_2$ using observations from KORUS-AQ during May – June 2016. I use measurements of particle-phase $RONO_2$ and total (gas + particle) $RONO_2$ to explore the phase partitioning of $RONO_2$ and the contribution of organic nitrates to SOA production. These measurements show that about 1/4 of $RONO_2$ is in the condensed phase, and from our observations, I estimate that $\approx 15\%$ of the organic aerosol (OA) mass can be attributed to $RONO_2$. I observe that the fraction of $RONO_2$ in the condensed phase increases with total OA concentration, evidence that equilibrium absorptive partitioning controls the phase distribution of $RONO_2$. I use our observations in conjunction with the Community Multiscale Air Quality (CMAQ) Modeling System to show that our current understanding of $RONO_2$ chemistry can only account for one third of the observed $RONO_2$; there is a large missing source of semi-volatile, anthropogenically-derived $RONO_2$ around Seoul.

Dedication

To all those who have been told they can't, they don't know enough, they're not good enough, or they don't belong;

To all those who have worked tirelessly with no credit, those who have been pushed out because of their 'otherness';

You are seen, you are heard, you are worthy, and you belong.

Contents

List of Figures

List of Tables

Acknowledgments

Thank you to my advisor Ron Cohen who has always had confidence in me, even when I didn't have any in myself. You have always treated me like a colleague, and I wouldn't be where I am today without your unwavering confidence, your encouragements to creatively focus on the bigger picture, all of the opportunities you've provided me, and the ways you've helped me improve my scientific communication skills. And many thanks for having a sense of humor and not firing me after I got the whole group to dress up as you for Halloween!

Thank you to all of my lab mates, who have been there through the tears, laughter, and the daily grind. I only wish the pandemic hadn't forced us to not share an office for the last year of my time at Berkeley!

Special shout-out to Tamara, Alexis, Josh, and Paul for showing me the ropes and welcoming me to the group. Many thanks to Helen for all of our cathartic walks and lunches, Qindan for always willing to help me de-bug and for taking classes with me, Jinsol for sitting next to me all those years, Bryan for all of your pranks and jokes, Erin for all of the laughs we shared, Alex for being the most appreciative of all of my ridiculous gifs, and to Garima and Amy for all of the distractions you provided me. And a big thank you to my undergrad mentees, Lindsey and Jennifer. You are both wonderful, smart, kind women, and I learned so much from both of you! Working with you both was a highlight of my time in graduate school, and I can't wait to see where life takes you.

Thank you to the whole group for the best grad school birthday celebrations. No one else has ever given me a minion piñata with my own face on it, nor has anyone ever given me a giant inflatable flamingo and accompanied me to various campus ponds to take it for a ride.

Thank you to Catherine and Trevor for all of the laughs and tears we shared in the 'chalkboard room' as we struggled through our first year of grad school and beyond. I couldn't have done it without you!

Thank you to the many other people who have provided mentorship to me during my time in graduate school. Many thanks to Jay Al-Saadi for teaching me everything I know about field campaign flight planning, Xuan Zhang for being such a great chamber experimentalist, and to my committee members (Kristie Boering and Allen Goldstein) for their encouragements and suggestions on this work.

Thank you to my entire family, which is filled with role models of empowered women, for all of your encouragement and support! Special thanks to my moms for always believing in me, always loving me, and always encouraging me to be the best Hannah I could be. And a big thank you to my sister, Anja, for being the best sister I could have ever asked for. Our laughs and giggles, phone calls, and mutual encouragement are one of the main reasons I made it through grad school!

Thank you to all of the mentors I have had along the way, from my elementary school teachers to my high school science teachers and my undergrad research mentors. You all helped me along this journey, encouraging me when I needed it and providing space for me to develop my scientific creativity.

Chapter 1

Introduction

1.1 Impacts of NO_x in the atmosphere

Though atmospheric trace gases make up less than 0.1% of the gases in the atmosphere, they drive chemistry in the atmosphere that affects human health, climate, and ecosystem health. Nitrogen oxides ($NO_x \equiv NO + NO_2$) are one class of such trace gases that affect both the gas and aerosol phases of tropospheric chemistry.

NO_x regulates the concentrations of atmospheric oxidants, including hydroxyl radicals (OH), nitrate radicals (NO_3), and ozone (O_3). O_3 production is a non-linear function of NO_x concentration, and NO_x also affects the formation of inorganic nitrate aerosol through production of nitric acid (HNO_3). Through its impact on tropospheric oxidation and through production of organic nitrates, NO_x plays a role in secondary organic aerosol (SOA) production.

NO_x, O_3, and aerosol particles are all detrimental to human health, and air pollution causes 3.3 million premature deaths every year worldwide (Lelieveld et al., 2015). Improvements in air quality in the United States have been made since the passage of the Clean Air Act in 1970, thereby increasing life expectancy (Pope, Ezzati, and Dockery, 2009). However, there are still areas in the United States with poor air quality, and poor air quality in the United States disproportionately affects the poor and people of color (e.g., Maantay, 2007; Miranda et al., 2011; Demetillo et al., 2020).

Trace gases, including NO_x, affect climate by influencing aerosol particle composition and concentration, which has both direct and indirect effects on radiative forcing. Moreover, the oxidative capacity of the atmosphere, which is influenced by NO_x concentrations, controls the lifetime of greenhouse gases such as methane.

Nitrogen oxides also affect the health of ecosystems and agricultural crops. O_3, produced via chemistry involving NO_x, is detrimental to crop health. Oxidation of NO_x generates nitric acid (HNO_3) which contributes to acid rain and nitrogen deposition.

1.2   Nitrogen oxides: sources and sinks

NO_x is emitted to the atmosphere as NO through a variety of combustion processes, including fossil fuel combustion and biomass burning. Such anthropogenic processes are the dominant NO_x sources in and around urban areas. Natural sources of NO_x to the atmosphere include soil bacteria and lightning.

In recent decades, the US has made large strides in decreasing NO_x emissions. Consistent NO_x reductions of 7% per year in US cities (Russell, Valin, and Cohen, 2012; Laughner and Cohen, 2019) have been achieved using catalytic converters on vehicles and through engineering emission controls on power plants (e.g., Frost et al., 2006; Kim et al., 2006; Ban-Weiss et al., 2008; Bishop and Stedman, 2008; Millstein and Harley, 2010; Dallmann and Harley, 2010; Parrish et al., 2011).

Photochemical NO_x loss

During the daytime when photochemistry is dominant, NO_x is lost through radical termination reactions with HO_x ($\equiv OH + HO_2 + RO_2$) radicals. Reaction of NO_2 with OH produces nitric acid (HNO_3, R1). The minor products of reaction of NO with RO_2 (branching ratio α) are alkyl and multifunctional organic nitrates ($RONO_2$, R2). Finally, reaction of NO_2 and RO_2 radicals generates peroxy nitrates (RO_2NO_2, R3).

$$NO_2 + OH \rightarrow HNO_3 \tag{R1}$$

$$NO + RO_2 \xrightarrow{\alpha} RONO_2 \tag{R2}$$

$$NO_2 + RO_2 \rightarrow RO_2NO_2 \tag{R3}$$

In the troposphere, HNO_3 and $RONO_2$ are both considered relatively permanent sinks of NO_x. HNO_3 typically undergoes wet and dry deposition, with a lifetime of a few days, or can be incorporated into aerosol particles as inorganic nitrate (NO_3^-). $RONO_2$ can also deposit, condense onto aerosol particles, or hydrolyze to produce HNO_3. Peroxy nitrates, however, are temporary sinks of NO_x, as they easily dissociate to regenerate NO_2. RO_2NO_2 are stabilized by lower temperatures like those of the upper troposphere. When lofted after production in an urban area, RO_2NO_2 can be transported downwind, resulting in the release of NO_2 away from the urban core.

Historically, HNO_3 production was considered the primary pathway for NO_x loss. However, production of $RONO_2$ competitive with HNO_3 production has been observed in urban areas, including Houston, TX (Rosen et al., 2004) and Mexico City (Farmer et al., 2011), as well as in rural regions, including over the boreal forest (Browne et al., 2013), in the southeast US (Romer et al., 2016), and in a forested region of southwest Germany (Sobanski et al., 2017).

Understanding the balance of NO_x sinks is important as it affects the overall lifetime of NO_x (Romer et al., 2016), including the dependence of NO_x loss on temperature (Romer

et al., 2018). Formation of low volatility $RONO_2$ can also contribute to secondary organic aerosol formation (e.g., Rollins et al., 2012; Pye et al., 2015; Zare et al., 2019). Moreover, the balance of radical termination reactions affects O_3 production rates (Perring et al., 2010; Farmer et al., 2011; Edwards et al., 2013; Lee et al., 2014b). As NO_x emissions in the US have decreased over the last two decades (Russell, Valin, and Cohen, 2012; Laughner and Cohen, 2019), many US cities have shifted from a regime in which HNO_3 is the dominant NO_x sink to one in which $RONO_2$ is the dominant sink of NO_x (Romer Present, Zare, and Cohen, 2020).

Nocturnal NO_x loss

At night, NO_x is also lost to HNO_3 and $RONO_2$ through dark reactions initiated by NO_3 oxidation. NO_3 is produced by reaction of NO_2 with O_3 (R4) and is lost via photolysis (R5, R6) and reaction with NO (R7). NO_3 concentrations can build up in the residual layer at night where there is neither sunlight nor fresh NO emissions.

$$NO_2 + O_3 \rightarrow NO_3 + O_2 \tag{R4}$$

$$NO_3 \xrightarrow{h\nu} NO + O_2 \tag{R5}$$

$$NO_3 \xrightarrow{h\nu} NO_2 + O(^3P) \tag{R6}$$

$$NO_3 + NO \rightarrow 2\,NO_2 \tag{R7}$$

Nocturnal NO_3-initiated production of HNO_3 involves multi-phase chemistry. First, NO_3 reacts with NO_2 to produce N_2O_5 in reversible thermal equilibrium (R8). N_2O_5 can undergo heterogeneous hydrolysis to produce 2 HNO_3 (R9). In the presence of aerosol containing chloride ions (e.g., sea salt aerosol), reaction of N_2O_5 with HCl will produce $ClNO_2$ and HNO_3 (R10). HNO_3 is also a product of NO_3 oxidation of aldehydes.

$$NO_3 + NO_2 \rightleftharpoons N_2O_5 + M \tag{R8}$$

$$N_2O_5 + H_2O \xrightarrow{het\cdot} 2\,HNO_3 \tag{R9}$$

$$N_2O_5 + HCl \xrightarrow{het\cdot} HNO_3 + ClNO_2 \tag{R10}$$
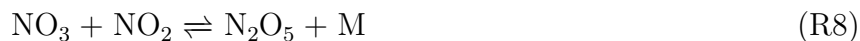
Nocturnal production of $RONO_2$ involves NO_3 oxidation of alkenes, via addition to the double bond (R11) with yield β.

$$NO_3 + alkene \xrightarrow{\beta} RONO_2 \tag{R11}$$

Significant production of $RONO_2$ from NO_3 oxidation has been observed previously in areas dominated by biogenic emissions, including forested regions of Colorado (Fry et al.,

2013), Finland (Sobanski et al., 2017), and Germany (Liebmann et al., 2019). Studies focused on $RONO_2$ derived from isoprene have found NO_3-initiated production to be competitive with OH-initiated production of isoprene nitrates using measurements from the Southeastern US (Starn et al., 1998; Xiong et al., 2015), using an observationally-constrained model of the eastern US (Horowitz et al., 2007), and using a global model (Kuhlmann et al., 2004).

1.3 Current understanding of organic nitrate chemistry

Our understanding of organic nitrates in the atmosphere has improved in recent years, due in large part to advances in measurement techniques for both total organic nitrates $tRONO_2$, speciated $RONO_2$, and particle phase organic nitrates $pRONO_2$.

Instruments combining thermal dissociation (TD) with a method of NO_2 detection can measure $tRONO_2$. In such a measurement scheme, $tRONO_2$ is thermally dissociated into RO and NO_2, NO_2 is detected, and the $tRONO_2$ concentration is determined by subtracting off the ambient NO_2 concentration. Such schemes were first developed with laser induced fluorescence (LIF) detection of NO_2 (Day et al., 2002) and have since also been used with cavity ring down spectroscopy (CRDS) (Thieser et al., 2016; Womack et al., 2017).

Recent advances in using chemical ionization mass spectrometry (CIMS) have allowed for detailed measurements of speciated nitrates, including many nitrates derived from isoprene (Crounse et al., 2013; Lee et al., 2016). Other mass spectrometry techniques (e.g., GC-MS, PTR-MS) have also been used to measure speciated organic nitrates (e.g., Schneider et al., 1998; deGouw et al., 2003).

Laboratory studies over recent years have also allowed for better constraints on α and β, the yields of $RONO_2$ production in the NO + RO_2 reaction (R2) and the NO_3 + alkene reaction (R11), respectively. Many of these advances have been made for isoprene, one of the most ubiquitous volatile organic compounds (VOCs) in the atmosphere. The yield of $RONO_2$ from reaction of isoprene-derived RO_2 radicals with NO is now understood to be 11-15%, higher than previously recognized (Teng, Crounse, and Wennberg, 2017; Wennberg et al., 2018). Yield of $RONO_2$ from NO_3 oxidation of isoprene is higher, varying in the range of 65-80% (Perring et al., 2009; Rollins et al., 2009; Kwan et al., 2012).

Depending on the properties of the backbone R group of $RONO_2$, $RONO_2$ lifetimes can vary from hours to days. Loss of $RONO_2$ can occur through photolysis, oxidation, deposition, partitioning into the aerosol phase, and/or hydrolysis to form HNO_3. Oxidation and photolysis may recycle NO_x to the atmosphere, whereas deposition and hydrolysis serve as permanent sinks of NO_x. Recent studies have shown that 45% of $RONO_2$ in the Southeast US undergo rapid hydrolysis to form HNO_3, which is quickly lost to deposition (Romer et al., 2016; Zare et al., 2019). $RONO_2$ that partition into the aerosol phase have recently emerged as an important constituent of organic aerosol (OA) (e.g., Rollins et al., 2012; Pye et al., 2015; Lee et al., 2016; Kiendler-Scharr et al., 2016; Zare et al., 2019).

1.4 Current understanding of the contribution of RONO$_2$ to organic aerosol

Organic aerosol constitutes a large, and often dominant, fraction of tropospheric aerosol mass (Heald et al., 2005; Murphy et al., 2006a; Zhang et al., 2007). Much of this organic aerosol is secondary, produced from the volatile organic compounds that are sufficiently oxidized in the atmosphere to be condensable and/or water soluble (Gouw et al., 2005; Goldstein and Galbally, 2007; Zhang et al., 2007; Gouw et al., 2008). The chemical and physical processes that control SOA production, however, are complex and currently highly uncertain (Heald et al., 2005; Volkamer et al., 2006; Hallquist et al., 2009; Heald et al., 2010; Hayes et al., 2015; Woody et al., 2016; Ma et al., 2017; Shrivastava et al., 2017; Tsimpidi et al., 2017; Nault et al., 2018).

The partitioning of semi-volatile organic compounds (SVOCs) and water-soluble organic compounds between the gas and condensed phases is an important source of SOA (Donahue et al., 2006; Ding et al., 2008; Wozniak, Bauer, and Dickhut, 2012). Typically, gas-particle partitioning of SVOCs is described by equilibrium absorptive partitioning theory, where the fraction of a given SVOC in the particle phase is controlled exclusively by its vapor pressure and the mass of the absorbing (in this case, organic) aerosol (Pankow, 1994; Donahue et al., 2006). If the VOC is water-soluble, then its gas-particle partitioning is generally described by Henry's Law, where the fraction in the aqueous aerosol phase is defined by its solubility in pure water (Kroll et al., 2005; Ervens, Turpin, and Weber, 2011).

Particle phase organic nitrates (pRONO$_2$) have recently emerged as a crucial but poorly understood component of SOA (e.g., Rollins et al., 2012; Fry et al., 2013; Ayres et al., 2015; Xu et al., 2015b; Pye et al., 2015; Fisher et al., 2016; Lee et al., 2016; Lee et al., 2019). The addition of a nitrate functional group reduces the saturation concentration of a given molecule by approximately 2.5 orders of magnitude (Pankow and Asher, 2008), thereby generating a lower volatility compound that may condense to form SOA. Moreover, ^{14}C measurements have indicated that the carbon in OA is largely biogenic in origin, but correlations between OA and anthropogenic trace gases (e.g., NO$_x$) indicate SOA has an anthropogenic origin (Weber et al., 2007). Because many of the lowest volatility organic nitrates are produced from the oxidation of monoterpenes in the presence of anthropogenically emitted NO$_x$, it is plausible to assume that a large fraction of organic nitrate aerosol will have a biogenically-derived carbon backbone despite being produced in a series of reactions involving anthropogenically-produced NO$_x$.

Recent lab studies have improved our understanding of the yield of pRONO$_2$ from VOC oxidation in the presence of NO$_x$ (Ng et al., 2008; Brown et al., 2009; Rollins et al., 2009; Fry et al., 2009; Fry et al., 2014). Field and modeling studies have shown that pRONO$_2$ are an important component of SOA in areas dominated by biogenic emissions, including the Southeast US (Ayres et al., 2015; Xu et al., 2015b; Pye et al., 2015; Fisher et al., 2016; Lee et al., 2016; Zare et al., 2019), in the Rocky Mountains (Fry et al., 2013), across Europe (Kiendler-Scharr et al., 2016), in the boreal forest (Hao et al., 2014), in the Central Valley

of California (Rollins et al., 2012; Rollins et al., 2013), and in rural areas of both northern and southern China (Zhu et al., 2016; Xu et al., 2020; Zhu et al., 2021). A number of field studies have also found significant contributions of pRONO$_2$ to SOA in regions of oil and gas production, including the Alberta Oil Sands (Lee et al., 2019) and in the Uintah Basin (Lee et al., 2015), and in Chinese cities (Zhang et al., 2016; Yu et al., 2019).

1.5   Dissertation aims

In this dissertation, I use observations from four aircraft experiments to provide new constraints on the lifetime and fate of NO$_x$ and its oxidation products in urban areas by exploring the importance of condensed phase and dark reactions. In each urban area, I show that condensed phase and dark reactions of NO$_x$ are significant sinks of tropospheric NO$_x$.

In Chapter 2, I examine wintertime conditions in the Northeastern United States using data from the WINTER (Wintertime INvestigation of Transport, Emissions, and Reactivity) campaign in 2015. I show that most NO$_x$ loss occurs from dark, condensed phase conversion of NO$_x$ to HNO$_3$ via heterogeneous hydrolysis of N$_2$O$_5$.

In Chapter 3, I examine data from three different summertime chemical environments: Studies of Emissions and Atmospheric Composition, Clouds, and Climate Coupling by Regional Surveys (SEAC^{4}RS, 2013) in the rural Southeastern United States, Front Range Air Pollution and Photochemistry Experiment (FRAPPÉ, 2014) in the Colorado Front Range, and Korea-United States Air Quality Study (KORUS-AQ, 2016) around the mega-city of Seoul, South Korea. In each distinct environment, I show that nocturnal NO$_3$-initiated production of RONO$_2$ is competitive with daytime OH-initiated production of RONO$_2$.

In Chapter 4, I examine the phase partitioning of RONO$_2$ and its role in SOA production in the mega-city of Seoul, South Korea using data from KORUS-AQ. I show that $\approx$ 15% of the organic aerosol mass can be attributed to RONO$_2$, but our current state-of-the-science understanding of RONO$_2$ chemistry can only account for one third of the observed RONO$_2$. I propose some possible mechanisms for this large missing source of semi-volatile, anthropogenically-derived RONO$_2$ around Seoul.

Lastly, I conclude by offering some predictions about the future role of RONO$_2$ in urban NO$_x$ and SOA chemistry, and I suggest questions to guide future research in this area.

Chapter 2

NO$_x$ lifetime and NO$_y$ partitioning during WINTER

2.1 Introduction

Nitrogen oxides (NO$_x$ $\equiv$ NO + NO$_2$) influence both the gas and aerosol phases of tropospheric chemistry, with impacts on air quality, climate, and nutrient cycling in ecosystems. In the atmosphere, NO$_x$ regulates oxidants, such as nitrate radicals (NO$_3$), hydroxyl radicals (OH), and ozone (O$_3$). Ozone is both a respiratory irritant and a greenhouse gas, and its production is a non-linear function of NO$_x$ concentration. Through its influence on the tropospheric oxidant budget, NO$_x$ also controls the lifetime of greenhouse gases such as methane. Moreover, NO$_x$ affects the formation of inorganic nitrate aerosol (e.g., Guo et al., 2016; Mezuman, Bauer, and Tsigaridis, 2016; Bian et al., 2017) and secondary organic aerosol (SOA) through its impacts on tropospheric oxidation and through the formation of organic nitrates (e.g., Rollins et al., 2012; Fry et al., 2014; Lee et al., 2014b; Ayres et al., 2015; Fisher et al., 2016; Kiendler-Scharr et al., 2016; Lee et al., 2016; Ng et al., 2017).

NO$_x$ is emitted to the atmosphere as NO both anthropogenically, through fossil fuel combustion, agriculture, and biomass burning, (e.g., Dallmann and Harley, 2010; Mebust and Cohen, 2014) as well as naturally, from soil bacteria and lightning (e.g., Schumann and Huntrieser, 2007; Hudman et al., 2012). Once emitted, NO$_x$ typically undergoes a series of oxidative transformations to higher oxides of nitrogen, some of which are then removed from the atmosphere via deposition.

In the presence of sunlight, NO$_x$ is oxidized by HO$_x$ radicals (HO$_x$ $\equiv$ HO$_2$ + RO$_2$ + OH), which are produced mainly through photolytic reactions. Oxidation reactions R12, R13, and R14, as shown in Fig. 2.1, are the primary daytime NO$_x$ sinks with the products: peroxy
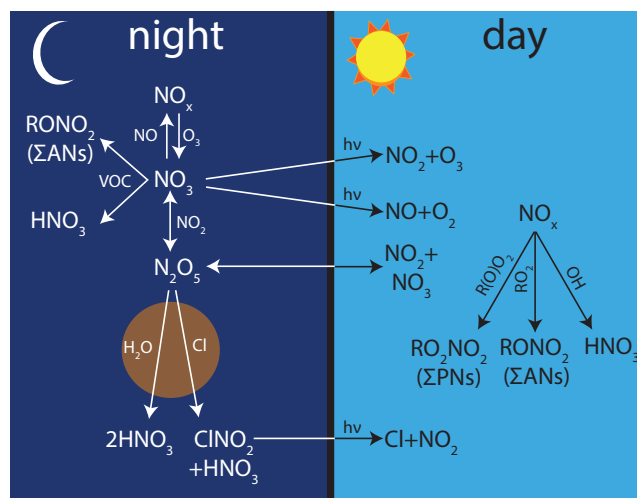
Figure 2.1: Schematic of NO_x oxidation reactions. The right panel contains daytime reactions, while the left panel contains nighttime reactions.

nitrates (RO_2NO_2, noted as a class as $\Sigma\,PNs$), alkyl nitrates ($RONO_2$, noted as a class as $\Sigma\,ANs$), and nitric acid (HNO_3), respectively. Depending on the conditions, these NO_x sinks may be temporary, allowing NO_x to be re-released back to the atmosphere, or they may be permanent, with sink species eventually being deposited out of the atmosphere.

$$NO_2 + RO_2 \xrightarrow{\text{M}} RO_2NO_2\ (\Sigma PNs) \tag{R12}$$

$$NO + RO_2 \xrightarrow{\text{M}} RONO_2\ (\Sigma ANs) \tag{R13}$$

$$NO_2 + OH \xrightarrow{\text{M}} HNO_3 \tag{R14}$$
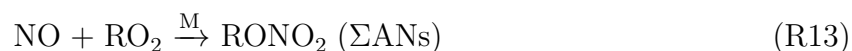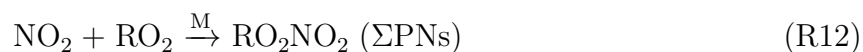
NO_3 is formed via reaction between NO_2 and O_3 (R15) and is lost via photolysis, reaction with NO, and reaction with VOCs (e.g., Aldener et al., 2006; Liebmann et al., 2018a; Liebmann et al., 2018b). NO_3 can be an important NO_x intermediate at night when there is neither sunlight nor high concentrations of NO present to remove it. At night, NO_3 can react with another NO_2 molecule to form N_2O_5 (R16), as shown in Fig. 2.1. Upon collision with aerosol, N_2O_5 can hydrolyze to form nitric acid (R17) or, in the presence of aerosol-phase chloride, will react to form nitryl chloride and nitric acid (R18). Alternatively, NO_3 reacts with alkenes at night (with branching ratio α) to generate alkyl nitrates (R19) and with volatile organic compounds (VOCs) to form nitric acid (R20). NO_3 also reacts with RO_2 and HO_2 radicals (R21, R22) to recycle NO_x (Stone et al., 2014).

$$NO_2 + O_3 \rightarrow NO_3 + O_2 \tag{R15}$$

$$NO_3 + NO_2 \overset{\text{M}}{\rightleftharpoons} N_2O_5 + M \tag{R16}$$

$$N_2O_5 + H_2O \xrightarrow{\text{het} \cdot} 2\,HNO_3 \tag{R17}$$

$$N_2O_5 + HCl \xrightarrow{\text{het} \cdot} HNO_3 + ClNO_2 \tag{R18}$$

$$NO_3 + \text{alkene} \xrightarrow{\text{M}} RONO_2 \,(\Sigma ANs) \tag{R19}$$

$$NO_3 + VOC \xrightarrow{\text{M}} HNO_3 + \text{products} \tag{R20}$$

$$NO_3 + RO_2 \rightarrow NO_2 + RO + O_2 \tag{R21}$$

$$NO_3 + HO_2 \rightarrow NO_2 + OH + O_2 \tag{R22}$$
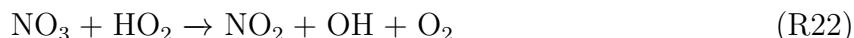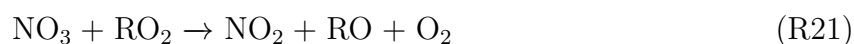
The rate of R17 depends on the heterogeneous uptake coefficient for N_2O_5 ($\gamma_{N_2O_5}$). $\gamma_{N_2O_5}$ represents the reaction probability of N_2O_5 on aerosol and depends on both aerosol composition and ambient conditions. The rate of R18 depends on the yield for $ClNO_2$ formation, which depends on aerosol liquid water content and particulate chloride concentrations (Bertram and Thornton, 2009). At sunrise, N_2O_5 will thermally dissociate and both NO_3 and $ClNO_2$ will photolyze, thereby re-releasing NO_x.

Urban NO_x chemistry and the reaction set above have been studied extensively during summertime conditions when typical daytime NO_x lifetimes are 2-11 h (e.g., Ryerson et al., 1998; Nunnermacker et al., 2000; Dillon et al., 2002; Ryerson, 2003; Alvarado et al., 2010; Valin, Russell, and Cohen, 2013; Romer et al., 2016). In contrast, wintertime NO_x chemistry, which we expect to differ from summertime chemistry, has been studied considerably less. Evaporative and biogenic VOC emissions are much less important in winter than in summer. The colder temperatures of wintertime slow reactions with activation barriers and accelerate 3-body reactions (e.g., Lee et al., 2014b). Moreover, winter is characterized by shorter days and reduced solar radiation, causing a decrease in the role of photolysis and shifting the balance of daytime oxidation and nighttime chemistry.

Previous model- and observation-based studies of wintertime chemistry have shown that a large fraction of NO_x loss occurs as a result of nighttime N_2O_5 chemistry (e.g., Dentener and Crutzen, 1993; Evans and Jacob, 2005; Davis, Bhave, and Foley, 2008; Alexander et al., 2009; Macintyre and Evans, 2010; Wagner et al., 2013; Wild et al., 2016) and that $ClNO_2$ can function as an important winter NO_x reservoir at night (Riedel et al., 2013). Crowley et al. (2011) showed that, during the late autumn in Southern Spain, nocturnal NO_x loss was dominated by the reaction of NO_3 with VOCs and that daytime and nighttime NO_x losses were comparable. During a wintertime field campaign in the Uintah Basin in Utah, USA (a rural region with intensive oil and gas operations), Lee et al. (2014b) observed that alkyl nitrate formation was accelerated at low temperatures and dominated chemical NO_x loss during the snow-free winter of 2012 when there was little NO_x oxidation. Wild et al. (2016) showed that HNO_3 production via heterogeneous chemistry of N_2O_5 dominated NO_x loss during 2013 and 2014 winters when there was more NO_x oxidation in the Uintah Basin.

These prior studies show that NO$_x$ lifetimes during winter vary and that key mechanisms depend on the interplay of emissions and meteorology. Here we explore that interplay in continental outflow to gain quantitative insights into processes and mechanisms. We use data from the 2015 aircraft-based WINTER (Wintertime INvestigation of Transport, Emissions, and Reactivity) campaign over the eastern United States to constrain the daytime and nighttime NO$_x$ lifetime under wintertime conditions in urban environments. We determine the most important wintertime sinks of NO$_x$ during both day and night, and we estimate wintertime rates of mixing between the boundary layer and the free troposphere and rates of HNO$_3$ deposition. Lastly, we investigate the impact of winter nighttime chemistry on the odd-oxygen budget.

2.2   Instrumentation/measurements

The WINTER campaign took place aboard the NSF/NCAR C-130 aircraft during February and March 2015. It consisted of 13 research flights out of Norfolk, VA which covered the eastern US as well as the Atlantic Ocean during both day and night.

The aircraft was outfitted with a suite of instruments measuring gas and aerosol composition. Those used in this analysis are detailed in Table 2.1. Additionally, the aircraft was outfitted with instrumentation measuring temperature, pressure, and wind speed. The GEOS-Chem chemical transport model (www.geos-chem.org) was run for each flight path. The WINTER campaign simulations used model version 10-01 driven by meteorological fields from NASA GMAO's GEOS-5 FP system. The model has been described in detail previously (Bey et al., 2001; Mao et al., 2010; Parrella et al., 2012; Travis et al., 2016).

2.3   Results and analysis

Imagery of NO$_2$ vertical column density from the OMI satellite during the period of the WINTER campaign in Fig. 2.2 shows that the corridor between Washington, D.C. and New York City (DC-NYC corridor) has high NO$_2$ concentrations relative to the surrounding regions. Here, we analyze the regional outflow that moves east from DC-NYC corridor over the Atlantic Ocean, since the average measured wind direction was 274° (i.e., from west to east), with a standard deviation of 33° (calculated using the Yamartino method (Yamartino, 1984)). We then analyze the isolated outflow since there are no important sources of NO$_x$ over the ocean aside from ship plumes, which were not sampled during the aircraft transects included in this analysis.

We parameterize the East Coast with a polynomial fit, as shown by the black line in Fig. 2.2. We then calculate the distance of each measurement from the East Coast and use the average wind speed measured on each flight during either day or night (shown in Table 2.2) to calculate the time each measured air parcel originated on the East Coast. We consider coastal measurements (time zero) to be those within 25 km of the black line in Fig. 2.2. We

Table 2.1: Summary of instrumentation from the WINTER campaign used in this analysis.

Instrument/Method	Species Measured	Reference
TD-LIF[a]	NO_2, ΣANs, ΣPNs	Day et al. (2002)
HRToF-CIMS[b]	HNO_3, N_2O_5, $ClNO_2$	Kercher, Riedel, and Thornton (2009) and Lee et al. (2014a)
CRDS[c]	NO, NO_2, O_3	Fuchs et al. (2009) and Wagner et al. (2011)
		Washenfelder et al. (2011) and Wild et al. (2014)
	N_2O_5	Dubé et al. (2006) and Fuchs et al. (2008)
		Wagner et al. (2011)
CRDS with thermal dissociation	total NO_y	Wild et al. (2014)
VUV resonance fluorescence	CO	Gerbig et al. (1999)
CL[d]	NO, O_3, total NO_y	Ridley et al. (1994)
TOGA[e]	suite of VOCs	Apel et al. (2015)
PCASP[f]	aerosol surface area	Strapp, Leaitch, and Liu (1992)
AMS[g]	aerosol nitrate (PM_1)	DeCarlo et al. (2006) and Canagaratna et al. (2007)
		Dunlea et al. (2009) and Schroder et al. (2018)
filter with IC	aerosol nitrate (PM_4)	Dibb et al. (1999) and Dibb, Talbot, and Scheuer (2000)

a Thermal Dissociation Laser Induced Fluorescence (University of California, Berkeley)
b Iodide-adduct High-Resolution Time-of-Flight Chemical Ionization Spectrometer (University of Washington)
c Cavity Ring Down Spectrometer (NOAA)
d Chemiluminescence detector (NCAR)
e Trace Organic Gas Analyzer (NCAR)
f Passive Cavity Aerosol Spectrometer Probe (NCAR)
g Aerosol Mass Spectrometer (University of Colorado, Boulder)
h filter-sampling system used to collect PM_4 with subsequent post-flight ion chromatography (University of New Hampshire)

categorize data into day (using flights 1, 3, and 4) and night (using flights 1, 3, 4, and 6) periods, considering only points whose entire trajectory from the East Coast to location of measurement took place during daylight or darkness, respectively. During WINTER, average sunrise occurred at 06:45 and sunset at 17:30. Although flights 5 and 8 measured nighttime outflow from the DC-NYC corridor, we omit these from our analysis due to anomalously high (flight 5, mean nighttime wind speed 16.1 m s^{-1}) and anomalously low (flight 8, mean nighttime wind speed 2.7 m s^{-1}) wind speeds, compared to the mean nighttime boundary layer wind speed over the ocean during the campaign of 8.1 m s^{-1}. Flight tracks used are shown in Fig. 2.3, and the average wind speed, temperature, and altitude sampled during each flight are shown in Table 2.2.
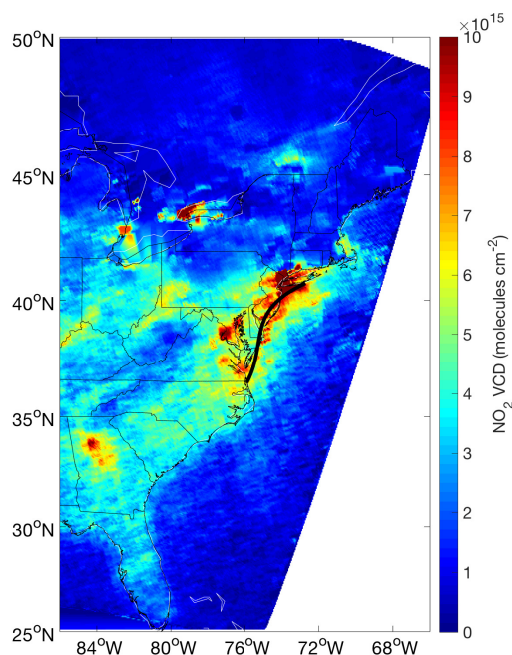
Figure 2.2: OMI NO_2 vertical column density (VCD) during the WINTER campaign. The DC-NYC corridor, represented by the black line, has high NO_2 concentrations. The outflow from this corridor moves out over the Atlantic Ocean since wind moves from west to east. For reference, 1° longitude corresponds to 85 km at 40° N.

We then analyze the average concentrations of components of NO_y (NO_x, $\Sigma\,PNs$, $\Sigma\,ANs$, HNO_3, N_2O_5, $ClNO_2$, and aerosol-phase NO_3^-) as a function of time elapsed since leaving the East Coast, as shown in Fig. 2.4. In this analysis, we use chemiluminescence measurements of NO and total NO_y; TD-LIF measurements of NO_2, $\Sigma\,ANs$, and $\Sigma\,PNs$; HRToF-CIMS measurements of HNO_3, N_2O_5, and $ClNO_2$; and CRDS measurements of O_3. For aerosol-

Table 2.2: Average ($\pm\ 1\sigma$) wind speeds, temperatures, and altitudes sampled below 1,000 m over the ocean during flights used in analysis.

	day			night		
Flight Num.	Wind Speed ($\mathrm{m\,s^{-1}}$)	Temperature (K)	Altitude (m)	Wind Speed ($\mathrm{m\,s^{-1}}$)	Temperature (K)	Altitude (m)
1	6.28 ± 1.81	267.7 ± 1.3	219 ± 142	7.79 ± 1.44	267.1 ± 2.4	303 ± 216
3	9.10 ± 1.64	272.5 ± 2.2	318 ± 117	9.79 ± 2.20	271.8 ± 2.4	386 ± 182
4	4.14 ± 3.31	270.7 ± 1.7	436 ± 199	3.75 ± 1.22	276.1 ± 2.3	416 ± 126
6	–	–	–	8.96 ± 1.32	277.1 ± 2.1	350 ± 192

phase NO_3^-, we use the maximum of the AMS measurements of aerosol-phase inorganic NO_3^- and the filter-collected IC-analyzed NO_3^-. We include in Fig. 2.4 only measurements taken in the boundary layer. We use GEOS-Chem estimates (Rienecker et al., 2008; Molod et al., 2012) of the boundary layer height (BLH) which agree with our aircraft observations of vertical profiles of relative humidity and ozone (not shown). Over the ocean during the day on flights 1, 3, and 4, the GEOS-Chem BLH was 780 m, and during the night on flights 1, 3, 4, and 6, the GEOS-Chem BLH was 610 m.
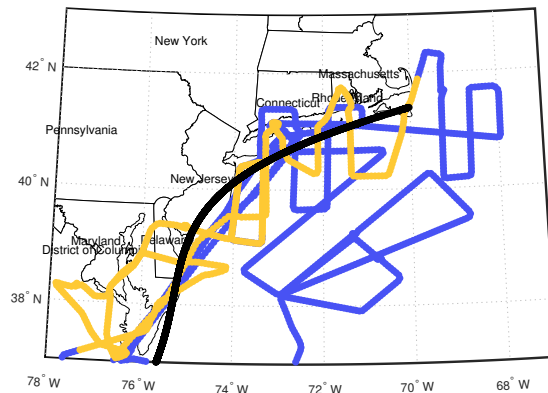
Figure 2.3: Map of flight tracks used in analysis of regional outflow. Blue tracks correspond to data taken at night (flights 1, 3, 4, and 6), whereas orange tracks correspond to data taken during the day (flights 1, 3, and 4). The parameterized coast line of the DC-NYC corridor is shown in black. We consider coastal measurements (time zero) to be those within 25 km of this line.

Our analysis assumes westerly winds that remain constant during a given flight, but yields a regional average of the observations of the East Coast outflow. Of course, there are local variations in all of the parameters assessed hereafter, but we present an average case

of the conditions during WINTER.

Daytime chemistry

The daytime evolution of the East Coast outflow shown in Fig. 2.4 suggests that NO$_x$ has an e-folding lifetime well in excess of 10 hours during winter daytime. Within the first 7 h of evolution, total NO$_y$ decreases by 16% which corresponds to a cumulative loss of 1 ppb of NO$_y$ to deposition and mixing with the free troposphere. After 7 h of evolution, NO$_x$ is still the dominant fraction of NO$_y$ (80%). Fitting the decay of NO$_x$ as a function of time elapsed since leaving the East Coast indicates the e-folding lifetime for NO$_x$ is 29 (-8, +16) h (range of lifetime estimates described in Appendix A.3). This lifetime estimate accounts for NO$_x$ loss due to chemistry, deposition, and mixing with the free troposphere. Of the NO$_x$ sinks present in the daytime in Fig. 2.4, HNO$_3$ is present in the highest concentration, which suggests it is the primary daytime chemical NO$_x$ sink.

We then calculate the production rates of each daytime NO$_x$ sink compound over the ocean, as described in Appendix A.1. We find the average ($\pm$ 95% confidence interval) $P(\Sigma \, \mathrm{ANs})$ is 0.39 ($\pm$ 0.07) ppt h^{-1}, the average $P(\Sigma \, \mathrm{PNs})$ is 5.1 ($\pm$ 0.4) ppt h^{-1}, and the average $P(\mathrm{HNO_3})$ is 50 ($\pm$ 4) ppt h^{-1}, using GEOS-Chem estimates of OH concentrations (average 0.01 ppt in boundary layer). These production rates confirm that $\Sigma \, \mathrm{ANs}$ and $\Sigma \, \mathrm{PNs}$ are relatively unimportant daytime NO$_x$ sinks whereas HNO$_3$ production is the dominant, albeit small, daytime NO$_x$ sink reaction pathway.

Nighttime chemistry

The nighttime outflow evolution shown in Fig. 2.4 demonstrates that NO$_x$ is shorter-lived at night than during the day. Fitting the decay of NO$_x$ as a function of time elapsed since leaving the East Coast yields an e-folding lifetime of 6.3 (-0.5, +0.6) h, which takes into account both chemical and physical loss processes. Initially, NO$_x$ is the dominant component (75%) of NO$_y$. 50% (4.5 ppb) of NO$_y$ is lost to deposition and mixing with the free troposphere during the first 9 h of evolution, and after 9 h of evolution, HNO$_3$ is the dominant fraction (55%) of NO$_y$.

At night, there is evidence of NO$_x$ conversion to NO$_3$, N$_2$O$_5$, $\Sigma \, \mathrm{ANs}$, HNO$_3$, and ClNO$_2$. Of these nighttime NO$_x$ sinks, on average HNO$_3$ is present in the highest concentration. There was significant variation observed during different flights in the ratio of ClNO$_2$ to HNO$_3$ (nighttime boundary layer outflow average = 0.26, standard deviation = 0.44), which is not captured in the averages shown in Fig. 2.4. We calculate the average production rate of HNO$_3$ (Eq. A.8) from N$_2$O$_5$ reactions on aerosol surfaces over the ocean at night, as described in Appendix A.2, assuming a constant ClNO$_2$ yield. We find the average $P(\mathrm{HNO_3})$ at night to be 350 ($\pm$ 30) ppt h^{-1}, seven times the daytime $P(\mathrm{HNO_3})$ of 50 ppt h^{-1}.

Table 2.3: Summary of calculated parameters related to NO$_x$ lifetime during the daytime and nighttime. Production rates of sinks with only minor contributions to the NO$_x$ lifetime are not shown.

	day	night
NO$_x$ lifetime (h)	29	6.3
P(HNO$_3$) (ppt h^{-1})	50	350

2.4   2-Box model to constrain mixing and deposition rates

To understand if the chemistry described above is sufficient to describe the observations, we construct a two-box model with detailed chemistry and observationally-constrained initial conditions, and solve iteratively to estimate mixing rates between the boundary layer and the free troposphere (k_{mix}), the heterogeneous uptake coefficient for N$_2$O$_5$ ($\gamma_{N_2O_5}$), and the rate of HNO$_3$ deposition (k_{dep}(HNO$_3$)). The bottom of the two boxes represents the boundary layer, with chemistry occurring at 273 K and 1000 hPa, and the top box represents the free troposphere, with chemistry occurring at 253 K and 600 hPa. These temperatures and pressures are representative of average conditions during WINTER and are shown schematically in Fig. 2.5. During WINTER, the continental air advecting over the ocean is colder than the water at the ocean's surface. This generates a convective mixing process that leads to a relatively deep marine boundary layer, making a two-box model appropriate for this analysis.

Reaction rates used in the model are detailed in Supplemental Information and were obtained from Burkholder et al. (2015), Master Chemical Mechanism v. 3.3.1 (Jenkin, Saunders, and Pilling, 1997; Saunders et al., 2003; Jenkin et al., 2003; Bloss et al., 2005; Jenkin, Young, and Rickard, 2015), Wilson et al. (2006), Tyndall et al. (2001), and Atkinson et al. (2006). For model runs representing daytime conditions, the reaction of NO$_2$ with OH (R14) is included and the model is run for 11 hours (average length of day during WINTER). HNO$_3$ photolysis is neglected since the average HNO$_3$ photolysis frequency measured during WINTER flights 1, 3, and 4 corresponds to a photolysis lifetime exceeding 10^3 h. For model runs representing nighttime conditions, reactions R15, R16, R17, R18, R19 (with included alkenes: butene, isoprene, α-pinene, and β-pinene), and R20 (with included VOCs: methane, ethane, propane, formaldehyde, acetaldehyde, propanal, butanal, MACR, ethyl benzene, o-xylene, m-xylene, p-xylene, 1,2,4-trimethyl benzene, 1,2,3-trimethyl benzene, dimethyl sulfide) and are included and the model is run for 13 hours (average length of night during WINTER).

Aerosol nitrate is not included in the box model analysis because there is no net partitioning of gas-phase nitric acid into aerosol nitrate observed during the evolution of the average outflow. Aerosol nitrate remains as 10% of total NO$_y$ throughout the outflow, as seen in Fig. 2.4. Because aerosol deposition is slow ($\sim$ 1 week) on the timescales of our model ($\sim$

hours), the constant proportion of NO$_y$ as aerosol nitrate indicates that any change in aerosol nitrate concentration is purely a product of dilution/mixing (i.e., not from net movement of gas-phase nitric acid into aerosol). Nitric acid remains in the gas phase because of low aerosol pH (Guo et al., 2016). Consequently, aerosol nitrate does not affect the net NO$_x$ loss on the timescales of our model.

Nighttime heterogeneous hydrolysis of N$_2$O$_5$ (R17) is included with rate $\frac{1}{4} \times \bar{c}_{\text{N}_2\text{O}_5} \times \text{SA} \times \gamma_{\text{N}_2\text{O}_5} \times [\text{N}_2\text{O}_5]$ (see Appendix A.2). Aerosol surface area (SA) was held constant at the median wet aerosol surface area measured over the ocean during WINTER (200 μm^{2}cm^{-3} in boundary layer, 27 μm^{2}cm^{-3} in free troposphere), though there was significant variation in the observed aerosol surface area. Surface area of sea salt aerosol (approximated as surface area of super-micron aerosols) were estimated to be 3% of total aerosol surface area in the DC-NYC outflow, so the heterogeneous reaction of N$_2$O$_5$ with chloride-containing aerosol is represented by $0.03 \times \frac{1}{4} \times \bar{c}_{\text{N}_2\text{O}_5} \times \text{SA} \times \gamma_{\text{N}_2\text{O}_5} \times [\text{N}_2\text{O}_5]$, ignoring chlorine displacement from sea spray and assuming $\gamma_{\text{N}_2\text{O}_5}$ does not vary significantly with sea salt content.

Initial conditions for all species in the model are set using the average measurements at the East Coast between Washington, D.C. and New York City. OH concentrations during the day are fixed to the average OH concentration estimated by GEOS-Chem (0.01 ppt in the boundary layer; 0.04 ppt in the free troposphere). Schroder et al. (2018) determined the GEOS-Chem estimates of OH to be reasonable in the NYC plume. Exchange of all species between boxes is allowed to represent mixing between the boundary layer and the free troposphere, and HNO$_3$ is removed from the bottom box via deposition.

We estimate the mixing rate (k_{mix}) by iteratively adjusting k_{mix} and solving the model until the model-to-observation percent root mean square deviation (RMSD) is minimized for CO. CO chemistry is negligible on the time scales included in our model, so it is only affected by mixing between the boundary layer and the free troposphere and by horizontal dispersion. Setting initial CO concentrations to the average measurements at the East Coast (161 ppb in the boundary layer, 98 ppb in the free troposphere) and solving iteratively yields a daytime estimate of the mixing lifetime of 24 h and a nighttime estimate of the mixing lifetime of 15 h. We attribute the difference in mixing lifetimes between night and day to a difference in observed wind speed. The median horizontal wind speed in the DC-NYC outflow during the day was 6.5 m s^{-1} whereas the median horizontal wind speed at night was 8.3 m s^{-1}. The average vertical gust component of the wind vector in the regional outflow was also larger at night (-0.14 m s^{-1}) than during the day (-0.082 m s^{-1}). A larger wind speed at night, which has been observed previously off the coast of the northeast US (Archer et al., 2016), would generate more turbulence and decrease the mixing lifetime. Additionally, during winter, the ocean surface temperature is typically warmer than the cold air outflow. At night this temperature gradient is larger, generating vertical instability and convective mixing (Archer et al., 2016).

During nighttime model runs, the heterogeneous uptake coefficient of N$_2$O$_5$ ($\gamma_{\text{N}_2\text{O}_5}$) was then estimated by iteratively adjusting $\gamma_{\text{N}_2\text{O}_5}$ while holding k_{mix} constant and solving the model until model-to-observation percent RMSD is minimized for N$_2$O$_5$. This step was not done for the daytime version of the model since N$_2$O$_5$ chemistry is not relevant during

the day. We estimate $\gamma_{N_2O_5} = 0.013$. This compares reasonably with the wintertime N$_2$O$_5$ uptake coefficients derived by McDuffie et al. (2018) for the entire WINTER campaign which ranged over four orders of magnitude with a median of 0.0143 and a most frequent value of 0.018. Over the ocean, McDuffie et al. (2018) derived a median N$_2$O$_5$ uptake coefficient of 0.017. McDuffie et al. (2018) also explore correlations between $\gamma_{N_2O_5}$ and both aerosol composition and meteorological conditions and compare observed values of $\gamma_{N_2O_5}$ during WINTER to available literature parameterizations. Fibiger et al. (2018) derived a very low uptake coefficient of 7×10^{-4} in a coal-fired power plant plume in Georgia during WINTER, but the low values observed in Georgia were not representative of the average values derived for flights over the ocean.

Finally, we estimate the deposition rate of HNO$_3$ (k_{dep}(HNO$_3$)) by varying k_{dep}(HNO$_3$) iteratively while holding k_{mix} and (at night) $\gamma_{N_2O_5}$ constant until the maximum HNO$_3$ in the model matches the maximum observed HNO$_3$. Our model analysis constrains the deposition lifetime of HNO$_3$ to 29 h during the day and 20 h at night. Like for the trend in k_{mix}, a larger wind speed at night generates more turbulence and increases the nighttime deposition rate of HNO$_3$.

Our estimation of the daytime deposition rate of HNO$_3$ is sensitive to model uncertainty in OH concentrations. Our estimation of the nighttime deposition rate of HNO$_3$ is linked to the yield of ClNO$_2$ from N$_2$O$_5$ heterogeneous reactions. In our model, we use a constant sea salt aerosol fraction as an estimate of ClNO$_2$ yield and assume a constant $\gamma_{N_2O_5}$ that does not vary with sea salt content. These constant parameters do not account for the observed variability in the ClNO$_2$/HNO$_3$ ratio. Additionally, if the sea salt aerosol fraction underestimates (overestimates) the ClNO$_2$ yield or if a single $\gamma_{N_2O_5}$ value underestimates (overestimates) $\gamma_{N_2O_5}$ on chloride-containing aerosols, k_{dep}(HNO$_3$) will be overestimated (underestimated). Moreover, we do not include deposition of N$_2$O$_5$ nor ClNO$_2$ to the ocean in our model, which could lead to an overestimation of $\gamma_{N_2O_5}$ and a slight overestimation of HNO$_3$ production, resulting in an overestimation of k_{dep}(HNO$_3$).

We estimate the deposition velocity (v_{dep}) of HNO$_3$ as

$$v_{dep} = \text{BLH} \times k_{dep}(\text{HNO}_3) \tag{2.1}$$

using GEOS-Chem estimates of the BLH. Over the ocean during the day on flights 1, 3, and 4, the GEOS-Chem BLH was 780 m, yielding a deposition velocity of 0.75 cm s^{-1}. Over the ocean during the night on flights 1, 3, 4, and 6, the GEOS-Chem BLH was 610 m, yielding a deposition velocity of 0.85 cm s^{-1}. Similarly, Brown et al. (2004) calculated a nitric acid deposition velocity of 1.2 cm s^{-1} off the East Coast of the US during summer. However, despite similar deposition velocities during both seasons, more nitric acid is deposited in coastal marine environments during winter than during summer. In summer, warm continental air advects over cold water, which isolates the shallow marine boundary layer and allows for long distance transport above the boundary layer where it is not subject to deposition near the coast (Neuman et al., 2006). In contrast, during winter, cold air advects over warmer water which generates mixing and leads to a deeper marine boundary layer (Seidel et al.,

Table 2.4: Table of parameters included in box model.

	day		night	
	boundary layer	free troposphere	boundary layer	free troposphere
[OH] (ppt)	0.01	0.04	–	–
SA ($\mu m^2 cm^{-3}$)	–	–	200	27
T (K)	273	253	273	253
P (hPa)	1000	600	1000	600
$k_{dep}(HNO_3)$ (h^{-1})	1/29	–	1/20	–
k_{mix} (h^{-1})	1/24	1/24	1/15	1/15
$\gamma(N_2O_5)$	–	–	0.013	0.013

2012) that allows for significant coastal nitric acid deposition.

A summary of the parameters included in the final two-box model is shown in Table 2.4 and the outputs of the two-box model with these parameters along with average observations are shown in Fig. 2.6. The output indicates that daytime chemistry can be described with reasonable accuracy by considering HNO_3 as the only chemical sink of NO_x. The nighttime model captures the conversion of NO_x to NO_3, N_2O_5, Σ ANs, HNO_3, and $ClNO_2$, with HNO_3 as the major NO_x sink. During both day and night, NO_y loss in the boundary layer is dominated by mixing into the free troposphere rather than by deposition.

2.5   Integrated NO_x loss and impacts on odd-oxygen budget

We integrate the production rates of each NO_x sink in our two-box model over the course of 24 h, with 11 h of day and 13 h of night, to calculate the integrated NO_x loss via each reaction. HNO_3 has the largest integrated production, and is thus the largest sink of NO_x. However, the nighttime multi-phase N_2O_5 chemistry that converts NO_x to HNO_3 has a more significant impact than the photochemical daytime reaction of NO_2 with OH that leads to HNO_3 production. During the day, 10% of initial NO_x (500 ppt) is lost to HNO_3, whereas 64% (4500 ppt) of initial nighttime NO_x is converted to HNO_3 overnight via N_2O_5 chemistry. At night, an additional 0.7% of initial NO_x (50 ppt) is lost to HNO_3 from reaction of NO_3 with VOCs and DMS, 0.9% of initial NO_x (60 ppt) is lost to alkyl nitrates produced via NO_3 reaction with alkenes, and 1.2% of initial NO_x (90 ppt) is converted to $ClNO_2$ via heterogeneous chemistry of N_2O_5 on sea salt aerosol (though $ClNO_2$ concentrations did vary significantly between flights, indicating variation in $ClNO_2$ yield not accounted for in our analysis). In the summer marine boundary layer off the East Coast of the US, only 1/3 of HNO_3 production occurs during the night (Brown et al., 2004), whereas during the East Coast outflow measured during WINTER, 90% of HNO_3 production occurs at night. The boundary layer is $\sim$ 25% shallower at night than during the day (610 m at night vs. 780

m during the day). This is not enough of a difference to perturb the balance of nighttime chemistry dominating NO$_x$ loss even after accounting for the volume over which the processes occur. Thus, in contrast to summertime when NO$_x$ chemistry is controlled by daytime photochemistry with OH serving as the primary oxidant, wintertime NO$_x$ loss is dominated by nighttime multi-phase oxidation with O$_3$ as the primary oxidant.

Most wintertime oxidation of NO$_x$ leads to the formation of HNO$_3$, which is then eventually deposited. Formation of peroxy nitrates is found to be negligible and have little effect in the near coastal region. However, some of the nighttime NO$_x$ sinks are temporary and re-release NO$_x$ when they are photolyzed or thermally dissociated at sunrise. The amount of NO$_x$ re-released in the morning corresponds to the amount of NO$_x$ stored in NO$_3$, N$_2$O$_5$, and ClNO$_2$ reservoirs. In our model, after one night of chemical evolution following emission, these NO$_x$ reservoirs contain 400 ppt of NO$_x$ (6% of NO$_x$ concentration at East Coast), which is re-released in the morning.

O$_3$ is lost overnight through conversion of NO$_x$ to HNO$_3$ via N$_2$O$_5$ dark reactions (R15, R16, R17). When HNO$_3$ is produced via heterogeneous hydrolysis of N$_2$O$_5$ (R17), the dominant NO$_x$ loss mechanism at night, each molecule of HNO$_3$ generated corresponds to a loss of 1.5 molecules of O$_3$ (Brown et al., 2006). In our two-box model, 4400 ppt of HNO$_3$ is produced overnight through N$_2$O$_5$ hydrolysis, implying a loss of 6600 ppt of O$_3$ overnight. The average nighttime O$_3$ concentration in the DC-NYC outflow is 38 ppb, so approximately 15% of O$_3$ is lost overnight through N$_2$O$_5$ dark reactions. O$_3$ concentrations in the boundary layer remain relatively constant throughout the region at night. This is because chemical loss of O$_3$ is roughly balanced by mixing down of higher O$_3$ concentrations from the free troposphere (49 ppb at the East Coast). This balance was confirmed by our model runs.

Photochemical O$_3$ production is reduced in the winter when compared to summer because of low sun angles and reduced daylight hours with precursor concentrations that are only slightly elevated. In addition to reduced O$_3$ production, we infer significant boundary layer loss of O$_3$ in the east coast outflow resulting from nighttime NO$_x$ chemistry during winter. The presence of VOCs influences the balance between daytime O$_3$ production and nighttime O$_3$ loss, as VOCs are required for photochemical O$_3$ production and can also react with NO$_3$ to destroy O$_3$ at night. The extent of nocturnal O$_3$ destruction is also dependent on the concentrations and composition of aerosol particles, since these affect the rate of heterogeneous reactions of N$_2$O$_5$.

2.6   Conclusions

Analysis of the DC-NYC marine outflow indicates that NO$_x$ has a longer daytime lifetime (29 h) than nighttime lifetime (6.3 h) during winter. We constrain the rates of the chemical and physical loss processes that contribute to the overall NO$_x$ lifetime during winter in urban areas. Chemically, we conclude that HNO$_3$ is the primary NO$_x$ sink during both day and night, whereas peroxy nitrates and alkyl nitrates are relatively small NO$_x$ sinks since VOC reactivity is so low. Thus, the wintertime NO$_x$ lifetime is controlled primarily by HNO$_3$

production, and nighttime chemistry removes more NO$_x$ than does daytime chemistry. The shorter days and reduced sunlight characteristic of winter slow daytime chemistry by reducing OH concentrations and, consequently, VOC reactivity. At night, a shallower planetary boundary layer increases NO$_x$ concentrations, thereby increasing the importance of N$_2$O$_5$ chemistry which scales with the square of NO$_x$ concentration (R15, R16). Additionally, colder temperatures shift N$_2$O$_5$ equilibrium to the right, further increasing the importance of nighttime chemistry. Physically, we estimate a winter daytime mixing rate of 24 h, a nighttime mixing rate of 15 h, a daytime HNO$_3$ deposition lifetime of 29 h, and a nighttime HNO$_3$ deposition lifetime of 20 h. Lastly, we observe that approximately 15% of O$_3$ is removed at night via the dark reactions of N$_2$O$_5$, demonstrating that urban NO$_x$ emissions impact O$_3$ concentrations differently in summer versus in winter.
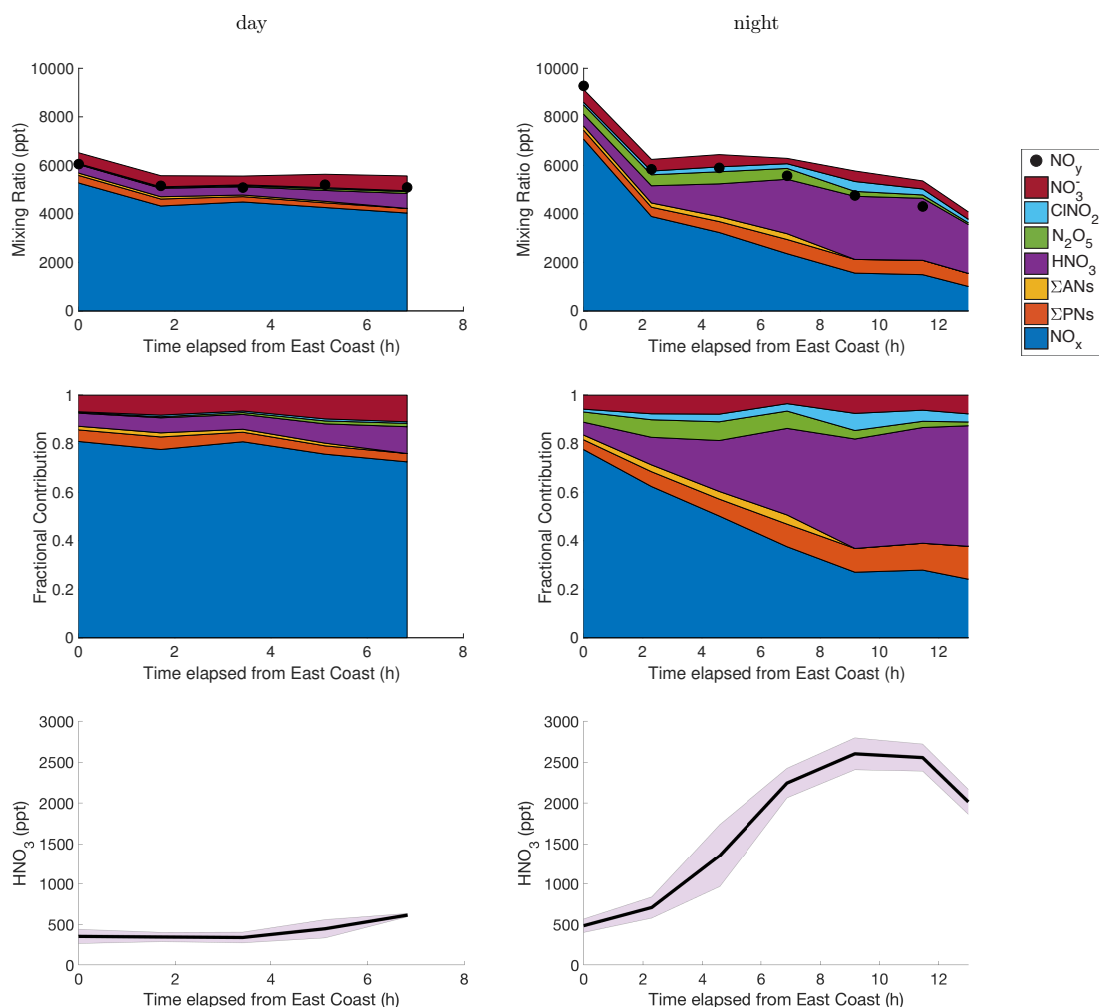
Figure 2.4: Mixing ratios (top) of species contributing to NO_y, fractional contribution (middle) of species contributing to NO_y, and growth of HNO_3 (bottom) during daytime hours (left) and nighttime hours (right) shown as a function time elapsed from the East Coast. Time elapsed from the East Coast is calculated by dividing the distance of each measurement from the East Coast by the average wind speed measured on each flight. Data are then binned and averaged as a function of time elapsed (day bins = 1.7 h; night bins = 2.3 h). In the bottom panel, shading represents a 95% confidence interval. Flights 1, 3, and 4 are used in daytime calculations and flights 1, 3, 4, and 6 are used in nighttime calculations. Only boundary layer data is included (below 780 m during the day, below 610 m at night).
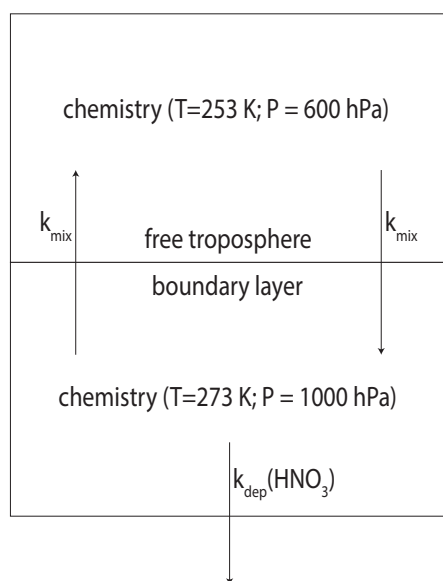
Figure 2.5: Schematic of the overall processes represented in the two-box model. k_{mix} represents the mixing rate of air between the boundary layer and the free troposphere. Chemistry occurs in both the boundary layer and the free troposphere, at temperatures and pressures representative of average conditions. HNO_3 has a deposition rate $k_{dep}(HNO_3)$.
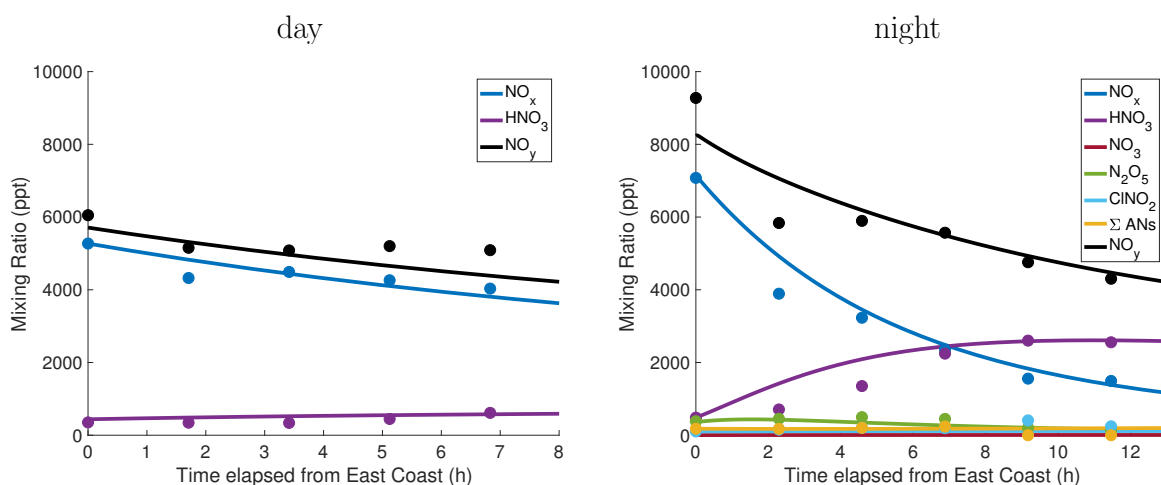
Figure 2.6: Concentrations in the boundary layer calculated in the 2-box model (lines) and average concentrations measured in the DC-NYC outflow (points) during the day (left) and at night (right).

Chapter 3

Evidence of nighttime production of organic nitrates during SEAC^{4}RS, FRAPPÉ, and KORUS-AQ

3.1   Introduction

Nitrogen oxides (NO$_x$≡NO + NO$_2$) are important tropospheric oxidants that contribute to ozone (O$_3$) formation, secondary aerosol production, and nitrogen deposition to ecosystems. Alkyl and multifunctional organic nitrates (RONO$_2$) are an oxidative sink of NO$_x$. Previous studies have shown that RONO$_2$ production is a significant NO$_x$ loss pathway (Day et al., 2003), especially as urban NO$_x$ concentrations decrease (Perring, Pusede, and Cohen, 2013; Romer Present, Zare, and Cohen, 2020). Organic nitrates can be generated through both daytime photochemical oxidation pathways initiated by OH and nighttime oxidation pathways initiated by NO$_3$.

During the day, RONO$_2$ is produced photochemically as a radical termination step in a series of reactions between oxidized VOCs (volatile organic compounds) and NO$_x$ (shown in Figure 3.1). VOCs are oxidized by OH to form organic peroxy radicals, RO$_2$ (R23). Reaction between NO and organic peroxy radicals can result in formation of an organic nitrate (R24, minor pathway, branching ratio α). The major pathway for the reaction between RO$_2$ and NO (R25), however, continues radical propagation to form two ozone molecules (R26, R27, R28). Consequently, this daytime chemistry produces both O$_x$ ($\equiv$ O$_3$ + NO$_2$) and RONO$_2$ so, if photochemistry is dominant, we expect a correlation between O$_x$ and RONO$_2$. Typically, chain lengths are such that we expect 6-20 O$_x$ for each RONO$_2$ (Perring, Pusede, and Cohen, 2013).

$$RH + OH \longrightarrow RO_2 + H_2O \tag{R23}$$
$$RO_2 + NO \longrightarrow RONO_2 \tag{R24}$$
$$RO_2 + NO \longrightarrow RO + NO_2 \tag{R25}$$
$$RO + O_2 \longrightarrow R'(O) + HO_2 \tag{R26}$$
$$HO_2 + NO \longrightarrow OH + NO_2 \tag{R27}$$
$$2\,NO_2 + h\nu \longrightarrow 2\,O(^3P) \longrightarrow 2\,O_3 \tag{R28}$$
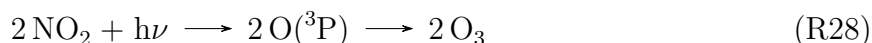
At night, $RONO_2$ is produced from alkenes via addition of NO_3 to a double bond (R31), as shown in Figure 3.1. NO_3 is formed from reaction between NO_2 and O_3 (R30). During the day, NO_3 is lost quickly via reaction with NO or via photolysis. In the nocturnal residual layer removed from fresh NO emissions, NO_3 concentrations can build up and react with alkenes. Two O_3 molecules are consumed in the production of NO_3 (R29 followed by R30), meaning that nighttime $RONO_2$ formation is a net sink of O_x. Consequently, we do not expect a positive correlation between $RONO_2$ and O_x if NO_3 is the dominant oxidant, and we might even expect a weak negative correlation.

$$NO + O_3 \longrightarrow NO_2 \tag{R29}$$
$$NO_2 + O_3 \longrightarrow NO_3 + O_2 \tag{R30}$$
$$NO_3 + R_1{=}R_2 \longrightarrow R_1(ONO_2){-}R_2 \tag{R31}$$
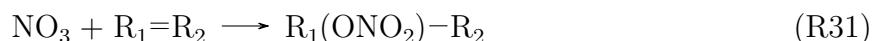
The fate of NO_x at night is controlled by the balance of two NO_3 reaction pathways. First, NO_x can be lost via NO_3 reaction with alkenes, as described above. Second, NO_3 can be lost at night via reaction with NO_2 to form N_2O_5 in thermal equilibrium, followed by aerosol uptake and heterogeneous hydrolysis to produce HNO_3 and $ClNO_2$. In certain environments, NO_3 may also react with species such as dimethyl sulfide, aldehydes, and peroxy radicals. The competition between these reaction pathways is controlled by both the relative availability of alkenes and by the fate of N_2O_5. Nighttime $RONO_2$ production increases in environments with high biogenic alkene emissions (isoprene, monoterpenes) and in environments with high anthropogenic alkene emissions, particularly where either of these two emission sources is sustained overnight. The N_2O_5 loss pathway becomes less competitive with $RONO_2$ formation in environments with low aerosol surface area and small heterogeneous uptake coefficients for N_2O_5 ($\gamma(N_2O_5)$), as these decrease the rate of heterogeneous hydrolysis of N_2O_5. Additionally, higher temperatures shift the N_2O_5 equilibrium towards dissociation, making N_2O_5 formation less favorable, while also increasing the rate of bimolecular NO_3 reactions with alkenes. Thus, nighttime $RONO_2$ formation is most favorable in environments with high alkene emissions, low aerosol surface area, small $\gamma(N_2O_5)$, and high temperatures.

There is reason to suspect that $RONO_2$ production from nighttime NO_3 oxidation of VOCs could be competitive with $RONO_2$ production from photochemical OH oxidation.

Because it is removed from fresh overnight NO emissions, a chemically active residual layer characteristic of many nighttime environments can contain elevated NO_3 concentrations as well as VOC emissions from late in the day. Moreover, $RONO_2$ yields from NO_3-initiated oxidation (20-80%) are far larger than $RONO_2$ yields from OH-initiated oxidation of VOCs (0.1-35%) (Perring, Pusede, and Cohen, 2013 and references within). Even if NO_3 oxidation represents a smaller fraction of total VOC oxidation than OH oxidation, the larger $RONO_2$ yields could make $RONO_2$ production from NO_3 oxidation competitive with $RONO_2$ production from OH oxidation.

A number of recent studies have shown that NO_3 oxidation can be a significant source of $RONO_2$ in regions dominated by biogenic VOC emissions. In forested regions of Colorado, Finland, and Germany, nighttime concentrations of $RONO_2$ were found to be comparable to daytime $RONO_2$ concentrations (Fry et al., 2013; Sobanski et al., 2017; Liebmann et al., 2019). Other studies have found NO_3-initiated formation of isoprene nitrates to be competitive with OH-initiated formation of isoprene nitrates in the Southeastern United States (Starn et al., 1998; Xiong et al., 2015), in an observationally-constrained model of the the eastern United States (Horowitz et al., 2007), and in a global model (Kuhlmann et al., 2004).

Moreover, NO_3 oxidation has been shown to be a significant source of organic aerosol in the Central Valley of California (Rollins et al., 2012), the Southeastern United States (Ayres et al., 2015; Lee et al., 2016; Xu et al., 2015b; Xu et al., 2015a; Pye et al., 2015; Fisher et al., 2016), in a forested region of Colorado (Fry et al., 2013), in rural Southwestern Germany (Huang et al., 2019), throughout Europe (Kiendler-Scharr et al., 2016), and in the Alberta oil sands (Lee et al., 2019).

Though NO_3 chemistry has been shown to be an important source of $RONO_2$ and secondary organic aerosol in rural regions dominated by biogenic emissions, nocturnal NO_3-initiated $RONO_2$ formation has often been considered negligible in comparison to daytime OH-initiated production of $RONO_2$ in urban environments. In this study, we present evidence for significant nighttime $RONO_2$ production using measurements of O_x and $RONO_2$ from three aircraft-based field campaigns in distinct summertime environments. First, we show evidence for significant nighttime $RONO_2$ production in the rural southeastern United States during SEAC[4]RS, an area with high biogenic emissions. Second, we show similarly high nighttime $RONO_2$ production in two urban areas: in the Colorado Front Range during FRAPPÉ, which is affected by both high urban and oil/gas emissions, as well as in and around the megacity of Seoul during KORUS-AQ. In each location, we show that the expected linear relationship between O_x and $RONO_2$ is observed during the afternoon. However, during the morning hours, the relationship between O_x and $RONO_2$ shows evidence of nighttime $RONO_2$ production. We support this conclusion further by assessing precursor availability for nighttime $RONO_2$ production.
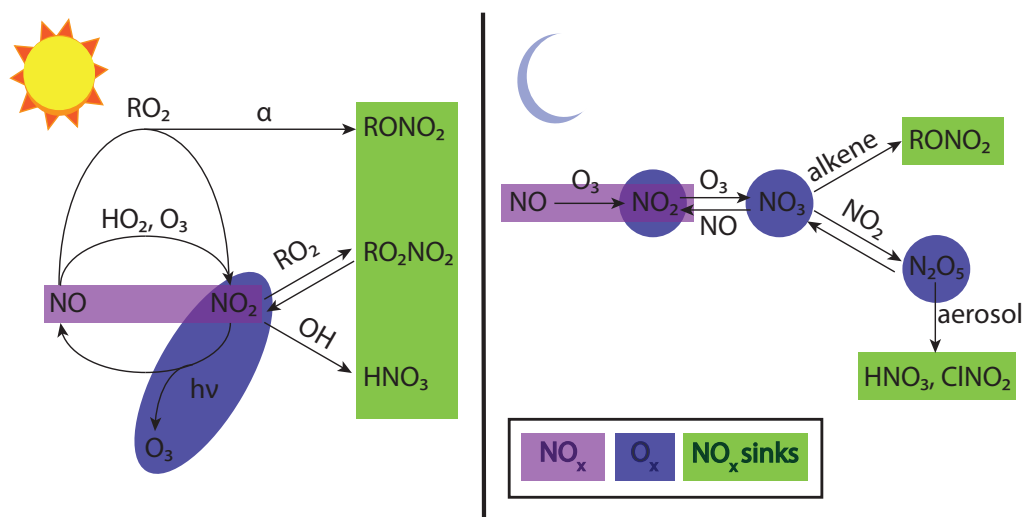
Figure 3.1: Schematic of daytime (left) and nighttime (right) NO_x chemistry.

3.2   Measurements

SEAC[4]RS, FRAPPÉ, and KORUS-AQ aircraft campaigns

The Studies of Emissions and Atmospheric Composition, Clouds, and Climate Coupling by
Regional Surveys (SEAC[4]RS) campaign took place during August-September 2013 in the
Southeastern and Western US (Toon et al., 2016). This analysis uses observations from the
NASA DC-8 aircraft which flew 19 primarily daytime research flights out of Ellington Field,
near Houston, TX.

The Front Range Air Pollution and Photochemistry Éxperiment (FRAPPÉ) took place
during July - August 2014 in the Northern Front Range Metropolitan Area (NFRMA) of
Colorado (Flocke et al., 2020). This analysis uses observations from the NSF/NCAR C-130
aircraft which flew fifteen daytime research flights out of the Rocky Mountain Metropolitan
Airport in Jefferson County, CO.

The Korea-United States Air Quality Study (KORUS-AQ) campaign took place during
May and June 2016 over South Korea and the Yellow Sea (Nault et al., 2018). This analysis
uses observations from the NASA DC-8 aircraft which flew 20 daytime research flights out
of Pyeongtaek, South Korea ($\approx$ 60 km south of Seoul).

Instrumentation

During all three campaigns, measurements of NO_2 and total $RONO_2$ (including both gas-phase and particle-phase $RONO_2$) were made by the UC Berkeley thermal dissociation laser induced fluorescence (TD-LIF) instrument (Day et al., 2002; Wooldridge et al., 2010). Briefly, one channel of the instrument measures NO_2 by laser induced fluorescence. Two other channels first flow air through a heated quartz oven. One channel is set at 180°C, the temperature at which peroxy nitrates (RO_2NO_2) dissociate into RO_2 and NO_2. The second is set at 360°C, the temperature at which $RONO_2$ dissociate into $RO + NO_2$. The difference in NO_2 detected in adjacent channels gives the mixing ratio for each class of compounds: the RO_2NO_2 mixing ratio is the difference between the 180°C channel and the unheated channel, and the $RONO_2$ mixing ratio is the difference between the 360°C channel and the 180°C channel.

O_3 and NO were measured by chemiluminescence. During SEAC^{4}RS, O_3 and NO were measured by the NOAA NO_yO_3 instrument (Ryerson et al., 1999; Ryerson, Williams, and Fehsenfeld, 2000). During FRAPPÉ and KORUS-AQ, O_3 and NO were measured by the NCAR chemiluminescence instrument (Ridley et al., 1994; Weinheimer et al., 1994).

Alkenes were measured by whole air sampling (WAS) (Colman et al., 2001; Simpson et al., 2011) and trace organic gas analyzer (TOGA) (Apel et al., 2015). For SEAC^{4}RS and KORUS-AQ, we use WAS measurements of propene, butenes, isoprene, α-pinene, and β-pinene. During FRAPPÉ, we use WAS measurements of propene, isoprene, α-pinene, and β-pinene and TOGA measurements of butenes and limonene.

Instrument details, including accuracy and sampling interval, can be found in Table S1 of the Supporting Information. We use 1-minute averaged data, and we consider only boundary layer data (below 1 km) during SEAC^{4}RS and KORUS-AQ and data below 2 km during FRAPPÉ.

3.3 Observations and results

O_x versus $RONO_2$

The relationship between O_x and $RONO_2$ during each campaign is shown in Figure 3.2 (plots of the relationship betwen O_x and $RONO_2$ during each flight within each each campaign are shown in Figures S1-S6). During all three campaigns, during the afternoon hours (13:00 - 19:00 local time) when photochemistry is most active, there is a positive, linear relationship between O_x and $RONO_2$, indicating that photochemical production of both O_x and $RONO_2$ is occurring. The slope of the relationship between O_x and $RONO_2$ mixing ratios is indicative of the branching ratio between O_x and $RONO_2$ production. From Figure 3.2, during SEAC^{4}RS, 29 O_x are produced for each $RONO_2$. Chain lengths are shorter during FRAPPÉ, where 13 O_x are produced for each $RONO_2$, and longer during KORUS-AQ, where 43 O_x are produced for each $RONO_2$.

During the morning hours (before 11:00 local time) before peak photochemistry occurs, however, the relationship between O_x mixing ratios and $RONO_2$ mixing ratios has a flat (zero) slope. At a relatively constant observed O_x mixing ratio, a wide range of $RONO_2$ mixing ratios were observed. This indicates that O_x and $RONO_2$ are not produced from the same pathway. Instead, the high levels of $RONO_2$ at relatively low levels of O_x suggest that many of the observed $RONO_2$ were produced via a non-photochemical pathway that produces $RONO_2$ without generating O_x. Since this trend is only observed in the morning, and not in the afternoon, it is indicative of a large source of $RONO_2$ produced from NO_3 oxidation overnight.

We also explored the effects of O_3 deposition and nighttime dynamics, but neither could sufficiently explain the observed trend. Estimating an approximate O_3 deposition velocity of $0.5\ \mathrm{cm\,s^{-1}}$ (e.g., Lenschow, Pearson, and Stankov, 1981; Colbeck and Harrison, 1985) and boundary layer height of 1 km, the lifetime of O_3 to deposition is 56 hours, far longer than the chemical timescales relevant to this analysis. Entrainment of air from aloft could also affect observed morning mixing ratios, but would have the same relative effect on both O_3 and $RONO_2$. Consequently, neither O_3 deposition nor entrainment can explain the lack of correlation between O_x and $RONO_2$ in the morning; the observed effect can only be explained by significant nocturnal production of $RONO_2$.

Precursors for nighttime $RONO_2$ production

As additional evidence for nighttime $RONO_2$ production, we assess the availability of precursors to $RONO_2$ production, namely NO_3 and alkenes. We report average morning (before 11:00 local time) mixing ratios of $RONO_2$, alkenes, and NO_x in Table 3.1. The abundance of NO_x and alkenes observed in the morning indicates that these precursors are not depleted by overnight chemistry; rather, the non-zero concentrations of precursors in the morning suggests that NO_3-initiated $RONO_2$ production chemistry is sustained overnight and occurs until daybreak.

During SEAC⁴RS, there were insufficient morning alkene measurements to report meaningful averages. However, Edwards et al. (2017) report airborne measurements which show that the nocturnal residual layer in the Southeastern US is rich in isoprene, evidence that there is an abundance of alkenes available overnight to form alkyl nitrates.

Moreover, we use the observed morning mixing ratios of NO_x, O_3, and alkenes to calculate lower bounds on the integrated overnight production of NO_3 (Eqn. 3.1), the instantaneous production rate of $RONO_2$ (Eqn. 3.2), and the instantaneous production rate of alkenes + O_3 (Eqn. 3.3).

$$\int P(\mathrm{NO_3}) = \mathrm{NO}_{\mathrm{x},initial}(1 - \exp(-t \times k_{\mathrm{NO_2+O_3}} \times \mathrm{O_3})) \tag{3.1}$$

$$P(\mathrm{RONO_2}) = \Sigma_i \alpha_i \times k_{\mathrm{NO_3\ +\ alkene_i}} \times [\mathrm{alkene}_i] \times [\mathrm{NO_3}] \tag{3.2}$$

$$Rate(\mathrm{O_3 + alkene}) = \Sigma_i k_{\mathrm{O_3\ +\ alkene_i}} \times [\mathrm{alkene}_i] \times [\mathrm{O_3}] \tag{3.3}$$

Table 3.1: Table of the average $RONO_2$, alkene, and NO_x concentrations in morning (before 11:00 local time), integrated overnight production of NO_3, instantaneous production rate of $RONO_2$, and instantaneous reaction rate of alkenes with O_3. All calculations were performed with morning precursor observations and can therefore be considered a lower bound. There are insufficient morning SEAC⁴RS measurements due to data sparsity to report meaningful morning average alkene mixing ratios.

	SEAC⁴RS	FRAPPÉ	KORUS-AQ
$RONO_2$ (ppb)	0.12	0.98	0.56
propene (ppt)	N/A	98	129
butene (ppt)	N/A	39	60
isoprene (ppt)	N/A	109	54
α-pinene (ppt)	N/A	11	15
β-pinene (ppt)	N/A	9.0	11
limonene (ppt)	N/A	4.8	N/A
NO_x (ppb)	0.43	8.1	4.4
$\int P(NO_3)$ (ppb)[a]	0.23	5.2	2.9
$P(RONO_2)$ (ppb/hour)[a,b,c]	N/A	2.3	1.3
alkene + O_3 rate (ppb/hour)[a,b]	N/A	0.021	0.108

[a]Calculated from morning (before 11:00 local time) precursor observations.
[b]Rate constants from MCM v3.3.1 are used.
[c]Nitrate yields used are from Perring, Pusede, and Cohen (2013) and references therein.

As shown in Table 3.1, the integrated production of NO_3 exceeds the observed morning mixing ratios of $RONO_2$, and the production rates of $RONO_2$ calculated from morning observations are more than sufficiently fast to account for the morning observations of $RONO_2$. Lastly, the rate of VOC (ethyne, ethene, propene, MACR, MVK, isoprene, butene, α-pinene, β-pinene, and limonene) oxidation by O_3 is at least an order of magnitude smaller than the production rate of $RONO_2$, indicating that NO_3 is the dominant nocturnal alkene oxidant in these environments.

3.4 Discussion and conclusion

We show evidence of significant nighttime $RONO_2$ production during three aircraft campaigns in three distinct locations: the rural southeastern United States dominated by biogenic emissions (SEAC⁴RS), the Colorado Front Range dominated by a combination of urban and oil/gas emissions (FRAPPÉ), and the megacity of Seoul dominated by urban emissions (KORUS-AQ). Though, in urban areas, nighttime production of $RONO_2$ has often been considered negligible in comparison to daytime production, we show evidence for nighttime $RONO_2$ production that results in morning $RONO_2$ mixing ratios of similar magnitude to afternoon observations of $RONO_2$ in all three of these distinct environments.
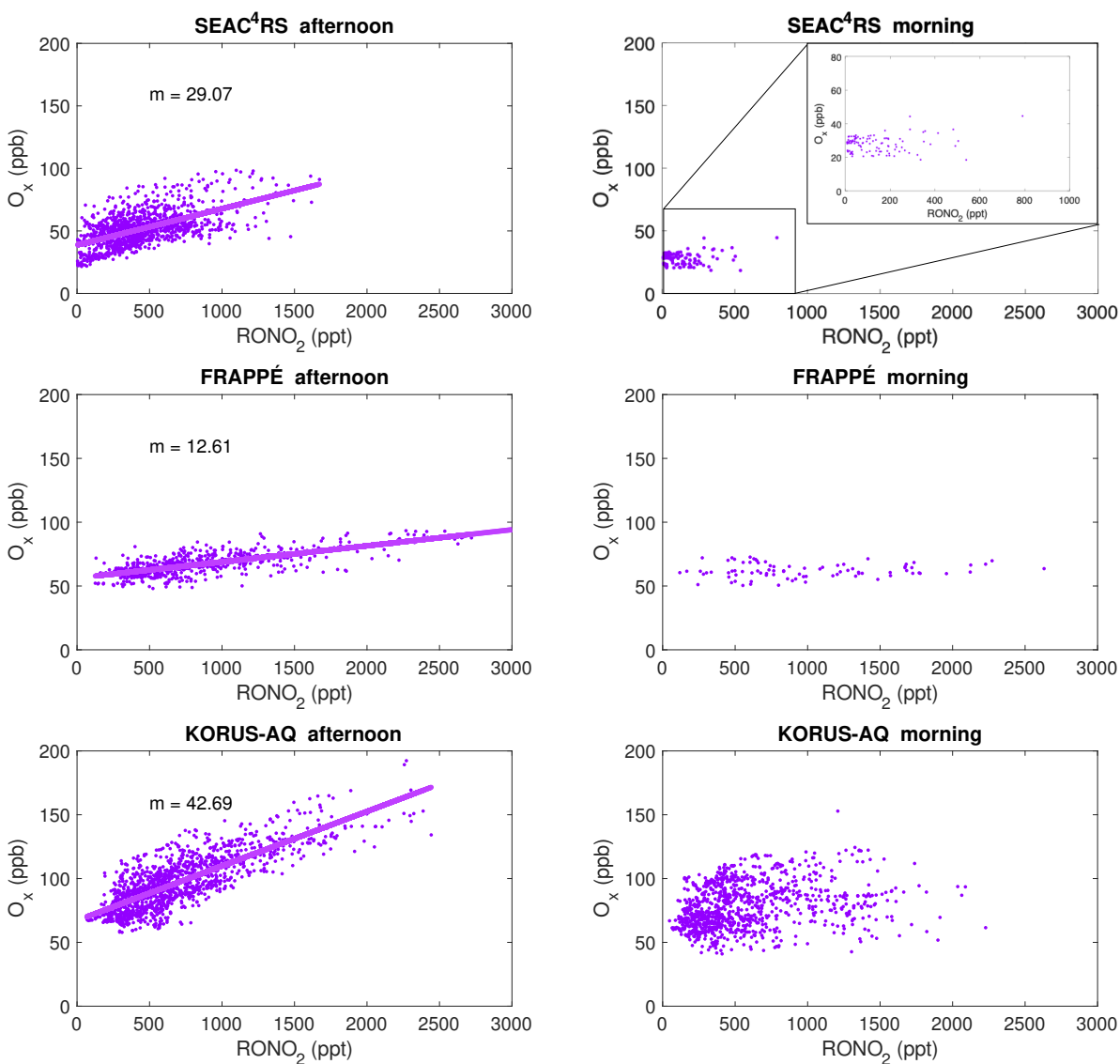
Figure 3.2: Plots of O_x vs. $RONO_2$ during SEAC[4]RS, FRAPPÉ, and KORUS-AQ during afternoon (left, 13:00 - 19:00 local time) and morning (right, before 11:00 local time). Only data in the boundary layer (< 1 km for SEAC[4]RS and KORUS-AQ, < 2 km for FRAPPÉ) are included. York linear fits (with slopes labeled as m) to the afternoon data are shown.

Rapid nighttime $RONO_2$ production impacts our understanding of the lifetime and fate of NO_x at night. Evidence for nighttime $RONO_2$ production indicates that HNO_3 and $ClNO_2$ produced via heterogeneous hydrolysis of N_2O_5 are not necessarily the dominant nighttime sinks of NO_x, consistent with other aircraft-based nighttime urban NO_3 budgets (Brown et al., 2011). In environments with low aerosol loading, high temperatures, and an abundance of alkenes, $RONO_2$ production can be the dominant nighttime NO_x sink. Significant nocturnal NO_3-initiated $RONO_2$ production in urban areas also has implications for substantial overnight secondary organic aerosol production in and around cities.

We explore the effects of temperature, alkenes, and aerosol surface area on the fraction of NO_x lost as $RONO_2$ (defined as $\frac{P(RONO_2)}{P(RONO_2)+P(HNO_3)}$) at night in Figure 3.3, assuming an initial NO_2 concentration, constant O_3, pressure, and $\gamma(N_2O_5)$, and NO_3 and N_2O_5 in steady-state (see Appendix A). Under these model conditions, the temperature, pressure, alkenes, NO_2, O_3 and aerosol surface area measured in the evening (after 16:30 local time) during FRAPPÉ and SEAC[4]RS indicate that $RONO_2$ is the dominant sink of NO_x at night, and during KORUS-AQ indicate that overnight NO_x loss is evenly split between N_2O_5 loss and $RONO_2$ production. This is consistent with a tower-based measurement in Seoul in 2015 which showed rapid NO_3-BVOC chemistry (Brown et al., 2017). For contrast, during the WINTER campaign (aircraft campaign over NE US, Feb-Mar 2015), low temperatures and low alkene concentrations lead to NO_x loss at night dominated by N_2O_5 hydrolysis (Kenagy et al., 2018). Histograms of the distribution of the fraction of NO_x lost as $RONO_2$ calculated from evening observations of NO_2, O_3, alkenes, temperature, and pressure during each campaign can be found in Figures S7-S9.

Here we have presented evidence for a significant, and sometimes dominant, nighttime source of $RONO_2$ using airborne, daytime measurements. Further measurements of the diel cycles of $RONO_2$ and its precursors would be of use to further elucidate the relative importance of the different mechanisms for $RONO_2$ formation. Additionally, measurements of the diel cycle of $RONO_2$ could provide insights into the fate of daytime- and nighttime-produced $RONO_2$ by showing whether they remain in the gas phase or partition into particles and whether hydrolysis, oxidation, or deposition dominates loss of $RONO_2$.
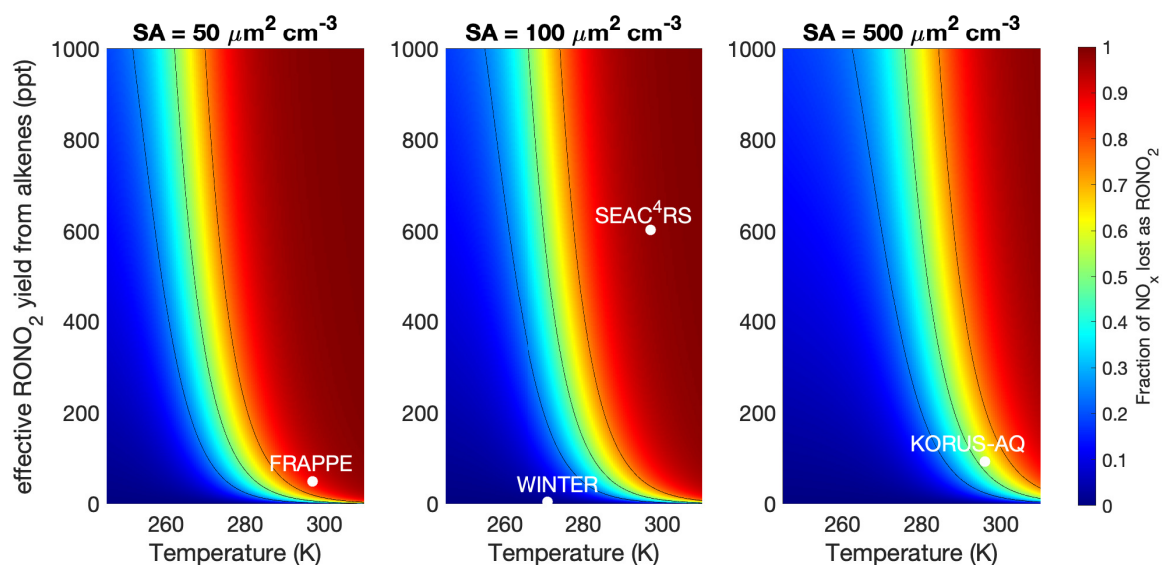
Figure 3.3: Fraction of NO_x lost as $RONO_2$ (defined as $\frac{P(RONO_2)}{P(RONO_2)+P(HNO_3)}$ overnight), shown as a function of temperature and effective $RONO_2$ yield from alkenes ($\Sigma_i\alpha_i[alkene]_i$) for three different aerosol surface areas (SA = 50, 100, and 500 $\mu m^2\,cm^{-3}$). We assume an initial NO_2 concentration (1 ppb), constant O_3 (40 ppb), constant pressure (1013 hPa), constant $\gamma(N_2O_5)$ (0.04), and NO_3 and N_2O_5 in steady-state. Black contour lines correspond to 25%, 50% and 75% of NO_x lost as $RONO_2$. Average evening (after 16:30 local time) conditions during SEAC[4]RS, FRAPPÉ, and KORUS-AQ are shown. Average conditions during WINTER (NSF aircraft campaign over Northeastern US during Feb-Mar 2015) are also shown as an example of conditions during which N_2O_5 loss is the dominant nighttime sink of NO_x (Kenagy et al., 2018).

Chapter 4

Contribution of organic nitrates to organic aerosol over South Korea during KORUS-AQ

4.1 Introduction

Organic aerosol (OA) constitutes a large, and often dominant, fraction of tropospheric aerosol mass (Heald et al., 2005; Murphy et al., 2006a; Zhang et al., 2007). Much of this organic aerosol is secondary (secondary organic aerosol, SOA), produced from volatile organic compounds (VOCs) that are sufficiently oxidized in the atmosphere to be condensable and/or water-soluble (Gouw et al., 2005; Gouw et al., 2008; Goldstein and Galbally, 2007; Jimenez et al., 2009; Hodzic et al., 2020). The chemical and physical processes that control SOA production, however, are complex and currently highly uncertain (Heald et al., 2005; Volkamer et al., 2006; Hallquist et al., 2009; Heald et al., 2010; Hayes et al., 2015; Woody et al., 2016; Ma et al., 2017; Shrivastava et al., 2017; Tsimpidi et al., 2017).

Particle phase organic nitrates ($pRONO_2$) have recently emerged as a significant component of SOA in areas dominated by biogenic emissions, including the Southeast US (Ayres et al., 2015; Pye et al., 2015; Xu et al., 2015b; Fisher et al., 2016; Lee et al., 2016; Zare et al., 2019), in the Rocky Mountains (Fry et al., 2013), across Europe (Kiendler-Scharr et al., 2016), in the boreal forest (Hao et al., 2014), in the California Central Valley (Rollins et al., 2012; Rollins et al., 2013), and in rural areas of both northern and southern China (Zhu et al., 2016; Xu et al., 2021; Zhu et al., 2021). A number of studies have also found significant contributions of $pRONO_2$ to SOA in regions of oil and gas production, including the Alberta Oil Sands (Lee et al., 2019) and in the Uintah Basin (Lee et al., 2015). Recent observations have shown that organic nitrates are a significant contributor to OA in Chinese cities (Zhang et al., 2016; Yu et al., 2019). Specifically, Yu et al. (2019) found that organic nitrates make up $9 - 25\%$ of OA during spring - autumn in urban Shenzhen, and the dominant precursors to $pRONO_2$ included both biogenic (α-pinene, limonene, and camphene)

and anthropogenic (styrene) VOCs.

Organic nitrates are produced from the oxidation of VOCs in the presence of NO_x, as shown in Figure 4.1. During the daytime when photochemistry is active, OH oxidation of VOCs generates RO_2 radicals (R32). The minor product (branching ratio α) of the reaction of NO with RO_2 radicals are gas-phase organic nitrates (gRONO$_2$, R33). In the nocturnal residual layer away from fresh NO emissions, NO_3 radicals can add to the double bonds of alkenes to generate gRONO$_2$ (R34) (e.g., Fry et al., 2018).

$$RH + OH \rightarrow RO_2 + H_2O \tag{R32}$$

$$RO_2 + NO \xrightarrow{\alpha} RONO_2 \tag{R33}$$

$$NO_3 + R_1{=}R_2 \rightarrow R_1(ONO_2){-}R_2 \tag{R34}$$
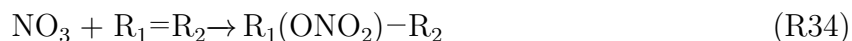
If the RONO$_2$ generated from either the OH-initiated or NO$_3$-initiated reaction pathways have sufficiently low volatility, they may partition into the aerosol phase as particle-phase organic nitrates, pRONO$_2$ (Figure 4.1). The addition of a nitrate functional group reduces the saturation concentration of a given molecule by approximately 2.5 orders of magnitude (Pankow and Asher, 2008), thereby generating a lower volatility compound that may condense to form SOA.

In this study, we examine the contribution of pRONO$_2$ to OA in Seoul, Korea. As a megacity, Seoul has a complex mixture of urban emissions, including from a number of chemical facilities and from transport of emissions from China, that contribute to the aerosol burden (Nault et al., 2018; Jordan et al., 2020), though Nault et al. (2018) determined that the dominant precursors for SOA production in Seoul were locally emitted VOCs. To better understand the sources of SOA in Seoul, here we aim to quantify the contribution of pRONO$_2$ to the total OA mass and determine the precursors and processes that control the production of pRONO$_2$ in Korea using observations from the 2016 Korea-United States Air Quality (KORUS-AQ) measurement campaign.

4.2   Methods

Here, we introduce the KORUS-AQ campaign, the TD-LIF measurements of pRONO$_2$ and tRONO$_2$, the CU-AMS measurements of pRONO$_2$ and OA, and our CMAQ simulations of RONO$_2$ over Northeast Asia during the time period of the KORUS-AQ campaign.

KORUS-AQ

The KORUS-AQ campaign took place during May and June 2016 over the Korean peninsula and the Yellow Sea. Seoul, Korea is bordered to the west by the Yellow Sea and Gyeonggi Bay and bordered to the north, east, and south by forested and mountainous regions (Park et al., 2017). During KORUS-AQ, winds were typically from the west or northwest, meaning
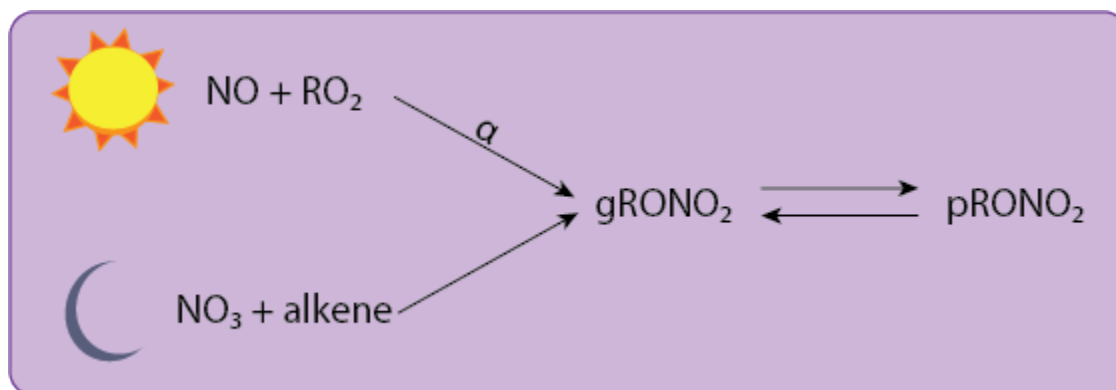
Figure 4.1: Schematic of $RONO_2$ production and phase partitioning.

that air over the Yellow Sea can be considered 'background' air for Seoul (Kim et al., 2017). There are a number of large industrial facilities along the Northwest coast of South Korea, including the Daesan petrochemical complex which produces large amounts of VOC emissions (Fried et al., 2020).

This analysis uses observations from the NASA DC-8 which flew 20 research flights out of Pyeongtaek, South Korea ($\approx$ 60 km south of Seoul). Flights typically began around 08:00 LT (KST). During a typical flight, three missed approaches were performed over the Seoul Air Base (within 15 km of Seoul city center): one soon after takeoff around 08:00 LT, one around 12:00 LT, and one prior to landing around 15:00 LT. Each missed approach included 15-45 minutes of observations within the boundary layer in the Seoul Metropolitan Area. Flights also consisted of transects west of Seoul over the Yellow Sea, south of Seoul to Jeju, and/or southeast of Seoul to Busan at varying altitudes, as shown in Figure 4.2.

TD-LIF measurements of $tRONO_2$ and $pRONO_2$

Measurements of $tRONO_2$ (gas + particle) were made using the UC Berkeley thermal dissociation laser induced fluoresence (TD-LIF) instrument (Day et al., 2002; Wooldridge et al., 2010). Briefly, one channel of the instrument measures NO_2 by laser induced fluorescence (LIF). Two other channels first flow air through a heated quartz oven. One channel is set at 180°C, the temperature at which peroxy nitrates (RO_2NO_2) dissociate into RO_2 and NO_2. The second is set at 360°C, the temperature at which $RONO_2$ dissociate into $RO + NO_2$. The difference in NO_2 detected in adjacent channels gives the mixing ratio for each class of compounds: the RO_2NO_2 mixing ratio corresponds to the difference between the 180°C channel and the unheated channel, and the $RONO_2$ mixing ratio corresponds to the difference between the 360°C channel and the 180°C channel.

$pRONO_2$ concentrations were measured using a fourth channel configured as described in Rollins et al. (2010). Before entering the heated section of the instrument, air passes

through a 10 cm long activated carbon honeycomb denuder with an inner diameter of 2 cm which removes gas-phase compounds. The particles that remain are then rapidly heated to vaporize the aerosols and dissociate the $RONO_2$ molecules present into RO and NO_2. NO_2 is then detected via LIF, giving a measurement of $pRONO_2$. We estimate a limit of detection of 20 ppt of $pRONO_2$, or 0.055 $\mu g\,m^{-3}$ of NO_3. Though inorganic nitrate compounds will also be vaporized, volatile inorganic nitrate salts form HNO_3 when vaporized (Womack et al., 2017) and will therefore not interfere in this measurement. Empirical and theoretical studies confirm that NO_2, HNO_3, and gas-phase organic nitrates are all removed at nearly 100% efficiency in the charcoal denuder, while particles greater than 100 nm in diameter are transmitted with over 95% efficiency (Rollins et al., 2010). Furthermore, during KORUS-AQ the denuder could be bypassed with a pair of 3-way valves, as shown in Figure C.1. When bypassed, the NO_2 calibration mixture reached the $pRONO_2$ LIF cell. When not bypassed, the NO_2 calibration events served as checks for NO_2 breaking through the denuder. No breakthrough was detectable throughout the deployment.

KORUS-AQ is the first time $pRONO_2$ measurements have been made with TD-LIF on aircraft. Previous ground-based measurements of $pRONO_2$ by the TD-LIF were made in the Rocky Mountains during BEACHON-RoMBAS (Fry et al., 2013), in the Uintah Basin (Lee et al., 2015), in the Southeast US during SOAS (Lee et al., 2016), and in the California Central Valley during CalNex (Rollins et al., 2013).

We apply a small correction for the loss of charged particles to TD-LIF measurements of $tRONO_2$ and $pRONO_2$. In the TD-LIF inlet configuration during KORUS-AQ, air for all channels goes through 10 - 20 cm of PFA Teflon before heating. We performed a series of laboratory experiments (detailed in Section C.1) to determine the loss of charged particles in these lengths of PFA Teflon tubing. Taking into account the ambient distribution of charged particles (Wiedensohler, 1988) and the observed aerosol size distribution during KORUS-AQ, there is less than 20% loss for charged particles with diameters less than 280 nm in the TD-LIF inlet.

We also apply a correction for inertial losses of particles in the TD-LIF inlet. We model the inertial losses on the two bends (90° and 98°) in the inlet (see Section C.1) for varying particle sizes. We apply the size-dependent modeled losses to the aerosol volume distribution measured by laser aerosol spectrometer (LAS, Langley LARGE group). On average, we estimate that the TD-LIF observes $\approx$ 60% of the particles observed by LAS. We apply both particle loss corrections (charged and inertial) to both the $pRONO_2$ and $tRONO_2$ TD-LIF measurements.

CU-AMS measurements of $pRONO_2$

A second measurement of $pRONO_2$ was made by the University of Colorado-Boulder high-resolution time-of-flight aerosol mass spectrometer (CU-AMS, Aerodyne Research, Inc.). The CU-AMS also measured organic aerosol (OA) concentrations. A description of the CU-AMS aircraft sampling can be found in DeCarlo et al. (2006) and Nault et al. (2018).

The CU-AMS uses NO_x ion ratios (NO_2^+/NO^+) to differentiate between inorganic nitrate (NH_4NO_3) and organic nitrate ($pRONO_2$) (Fry et al., 2013), described further in Section C.2. Uncertainties in this method are greatest when $pRONO_2 < 20\%$ of the measured nitrate; those measurements have been removed from this analysis.

The high NH_4NO_3 loadings during KORUS-AQ create uncertainty for the CU-AMS measurement of $pRONO_2$, and though we applied a series of corrections for particle loss in the TD-LIF inlet (described in Section 4.2), we could not entirely reconcile the differences between the two measurements. Since the two measurements may be prone to larger uncertainties under different aerosol size and composition conditions, we conduct the following analyses using both the TD-LIF and CU-AMS $pRONO_2$ measurements separately and treat them as upper and lower bounds. A comparison of the TD-LIF and CU-AMS measurements, both before and after corrections, can be seen in Figure C.9.

Because the TD-LIF and CU-AMS $pRONO_2$ measurements do not agree perfectly, we also use a CU-AMS-adjusted $tRONO_2$ to ensure a consistent comparison. In the following calculations that use CU-AMS $pRONO_2$, we subtract the TD-LIF $pRONO_2$ measurement from the TD-LIF $tRONO_2$ measurement to give an estimate of the gas-phase $RONO_2$ measured by the TD-LIF ($gRONO_2$). We then add the CU-AMS $pRONO_2$ to the estimated TD-LIF $gRONO_2$ to generate the CU-AMS-adjusted $tRONO_2$.

CMAQ modeling of $RONO_2$ chemistry and phase partitioning

We ran the Community Multiscale Air Quality Modeling System (CMAQ) model v5.2 (Wyat Appel et al., 2018; Kelly et al., 2019) with the RACM2_Berkeley2.1 chemical mechanism (Zare et al., 2018; Zare et al., 2019) over Northeast Asia with a 15-km horizontal grid and 27 vertical layers. Meteorological fields were generated by WRF v3.8.1 and processed for use in CMAQ by MCIP v4.5 (Otte and Pleim, 2010). The simulation period was April 17, 2016 - June 12, 2016, with the first 14 days as a spin-up period to minimize the impact of initial conditions.

We used the KORUSv5.0 anthropogenic emissions inventory developed at Konkuk University based on the CREATE emission inventory (Woo et al., 2020), MEGANv2.1 biogenic emissions (Guenther et al., 2012), and FINNv1.5 fire emissions (Wiedinmyer et al., 2011), all processed through the Sparse Matrix Operator Kernel Emissions (SMOKE) system (Houyoux et al., 2000). The KORUSv5.0 emissions inventory was prepared using the SAPRC07T AERO6 mechanism, which we then converted to RACM2_Berkeley2.1 (detailed in Table C.1).

We made a few adjustments to the emissions inventory informed by a series of comparisons between CMAQ modeled VOC concentrations and aircraft VOC measurements made with whole air samples (WAS) analyzed with multi-column gas chromatography (Simpson et al., 2020). We increased monoterpene emissions by a factor of three to improve the magnitude agreement between modeled and observed concentrations of monoterpenes (see Figure C.12). Note we expect monoterpenes in Korea to have both biogenic as well as anthropogenic sources (McDonald et al., 2018; Gkatzelis et al., 2021).

Comparison between modeled and observed BTEX (benzene, toluene, ethyl benzene, and xylenes) indicated that these species were also underestimated in the emissions inventory (see Figure C.12). We updated BTEX emissions over the Daesan petrochemical complex to match emission fluxes calculated from observations using a mass balance approach by Fried et al. (2020). Elsewhere, we note that the spatial pattern of modeled TOL (defined as toluene and less reactive aromatics, for measurement comparison purposes we approximate as the sum of toluene and ethyl benzene) corresponds well to the spatial pattern of the sum of measured toluene and ethyl benzene (see Figure C.10). However, without any emissions corrections, the model underestimates boundary layer TOL by a factor of 1.4. We also note that measurements of other reactive aromatics (xylenes and 1,2,4-trimethyl benzene) correlate well with the sum of measured toluene and ethyl benzene (see Figure C.11). As such, we scale TOL emissions by 1.4 and define the emissions of the other reactive aromatics based on their measured ratios to the sum of toluene and ethyl benzene. We use measured o-xylene as a proxy for model species XYO, the sum of measured m-xylene and 1,2,4-trimethyl benzene as a proxy for model species XYM, and measured p-xylene as a proxy for model species XYP. This method results in defining XYO as $0.05\times$ TOL, XYM as $0.08\times$ TOL, and XYP as $0.07\times$ TOL.

We use the default initial conditions and boundary conditions from the initial condition (ICON) and boundary condition (BCON) processors in CMAQ v5.2. However, measurements of isoprene-derived nitrates by Caltech's Chemical Ionization Mass Spectrometer (CIT-CIMS) (Crounse et al., 2006) indicated that longer-lived propanone nitrate and ethanal nitrate were underestimated in CMAQ. Consequently, we increased the boundary and initial condition concentrations of propanone nitrate and ethanal nitrate to match the CIT-CIMS observations of both nitrates over the Yellow Sea (propanone nitrate = 21.5 ppt; ethanal nitrate = 4.1 ppt).

The original RACM2 (Regional Atmospheric Chemistry Mechanism) mechanism (Goliff, Stockwell, and Lawson, 2013) is available in CMAQ v5.0.2 and later versions (Sarwar et al., 2013). Browne et al. (2014) modified the mechanism to RACM2_Berkeley to expand the organic nitrate chemistry. New species, along with their corresponding oxidation rates and branching ratios, were added to further classify anthropogenic nitrates (Carter and Atkinson, 1989; Middleton, Stockwell, and Carter, 1990; Arey et al., 2001) and to represent monoterpene nitrates (Jenkin, Saunders, and Pilling, 1997; Saunders et al., 2003; Leungsakul, Jeffries, and Kamens, 2005; Spittler et al., 2006). The parameterization of OH-initiated isoprene oxidation was also updated (Paulot et al., 2009a; Paulot et al., 2009b; Crounse et al., 2011). RACM2_Berkeley was evaluated using aircraft observations over the Canadian boreal forest (Browne et al., 2014).

RACM2_Berkeley was updated to RACM2_Berkeley2 in Zare et al. (2018) to reflect recent advances in the representation of OH- and NO_3- initiated BVOC oxidation under both low- and high-NO_x conditions, with a focus on a detailed representation of nitrates derived from NO_3-initiated oxidation of isoprene and on the fate of the most important individual biogenically-derived organic nitrates. Deposition rates were also updated.

Zare et al. (2019) revised RACM2_Berkeley2 to RACM2_Berkeley2.1 to include an ex-

plicit representation of multi-phase organic nitrate formation and loss, including vapor-pressure driven partitioning into organic aerosol, aqueous-phase uptake, and condensed-phase reactions. Further updates were also done to explicitly represent isoprene nitrates from NO_3 oxidation that are subject to reactive uptake to the aerosol phase. As such, the RACM2_Berkeley2.1 mechanism represents our current understanding of $RONO_2$ chemistry and phase partitioning. Zare et al. (2019) evaluated this mechanism (implemented in CMAQ) using observations from the Southern Oxidant and Aerosol Study (SOAS) campaign in the Southeast US during summer 2013. Inclusion of the particle-phase pathways for $RONO_2$ improved the model-measurement agreement for $tRONO_2$, and the modeled fraction of $tRONO_2$ in the particle phase (F_p) was within the range of observed F_p.

To compare modeled and measured concentrations, we sample CMAQ coincidentally in time (hourly resolution) and horizontal space with each observation. All comparisons in the following analysis use boundary layer measurements ($< 1,000$ m) and the average of the bottom three model layers.

4.3   Results

Maps of average TD-LIF measured and CMAQ modeled $tRONO_2$ used in the following analysis are shown in Figure 4.2. Both the measurements and model indicate that $tRONO_2$ concentrations are highest in and around Seoul. However, the model consistently underpredicts $tRONO_2$ concentrations throughout the region. For reference, CMAQ predicts that $> 95\%$ of $pRONO_2$ are derived from vapor-pressure dependent partitioning into organic aerosol, whereas $< 5\%$ of $pRONO_2$ enter the particle phase through aqueous pathways, similar to what Zare et al. (2019) found for the Southeast US.

$RONO_2$ partition into the aerosol phase and can be a significant contribution to SOA

We explore the average phase partitioning behavior of $RONO_2$ during KORUS-AQ in Figure 4.3. Our observations from both the TD-LIF and CU-AMS indicate that, on average, 1/4 of $tRONO_2$ is in the condensed phase and therefore contributes to the OA burden. We also consider a line, drawn above most measurement means, that represents a reasonable upper limit of 35% for the fraction of $tRONO_2$ in the particle phase.

To quantify the contribution of $pRONO_2$ to total OA concentrations, we assume an average molecular weight for $pRONO_2$ of 300 $g\,mol^{-1}$ (Rollins et al., 2013). We expect condensable $RONO_2$ to be highly oxidized, contain at least one nitrate group (molecular weight = 62 $g\,mol^{-1}$) and to therefore have relatively high masses. With this assumption, we estimate that $\approx 15\%$ of the OA mass can be attributed to $pRONO_2$, as shown in Figure 4.3. We again consider a reasonable upper limit, drawn above most measurement means, to estimate that a maximum of 40% of OA can be attributed to $pRONO_2$. This is within the range of $pRONO_2$ contributions to OA mass measured across Europe (42%) (Kiendler-Scharr
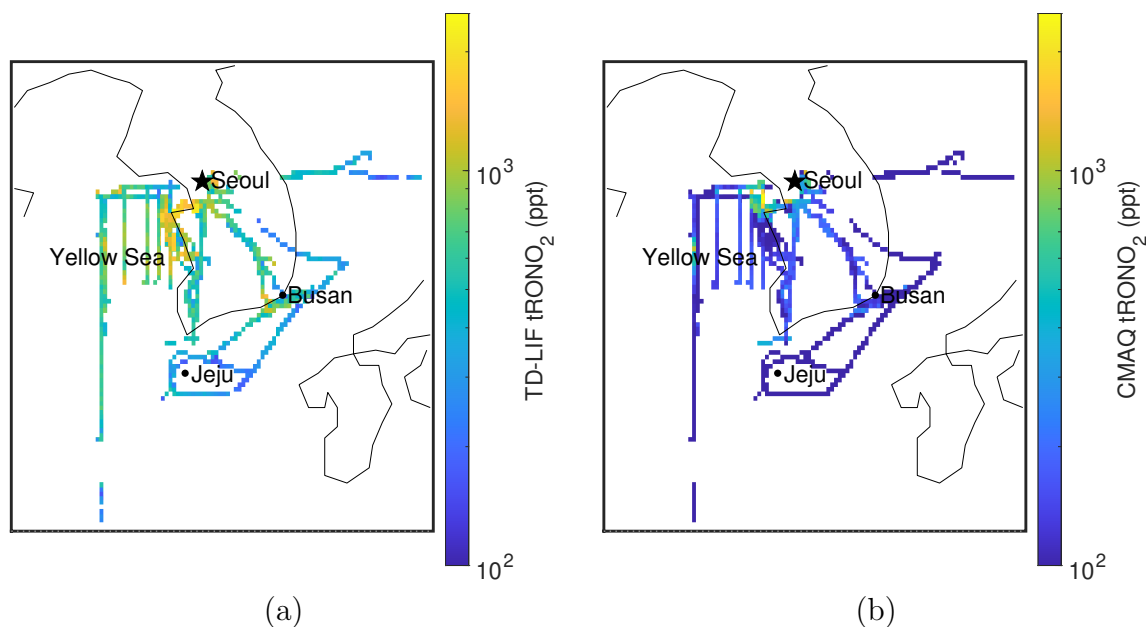
Figure 4.2: Maps of average (a) TD-LIF measured and (b) CMAQ modeled tRONO$_2$ on a log scale, gridded to 0.1°. Seoul, Jeju, Busan, and the Yellow Sea are labeled for reference.

et al., 2016), in a suite of studies across the eastern US, western US and Europe (5-73%) (Ng et al., 2017), and in recent studies in urban and rural China (9-28%) (Yu et al., 2019; Xu et al., 2021).

Observations indicate RONO$_2$ phase partitioning is controlled by absorptive partitioning into OA

Previous studies have shown that vapor pressure controls the phase of organic nitrates (Rollins et al., 2013; Zare et al., 2019). This equilibrium absorptive partitioning follows Raoult's Law: the fraction of RONO$_2$ in the particle phase increases with increasing mass of the absorbing or solvating aerosol, namely total organic aerosol (Donahue et al., 2006; Pankow, 1994). Accordingly, the equilibrium fraction of an individual RONO$_2$ species i in the particle phase ($F_{p,i}$) is given by

$$F_{p,i} = \frac{C_{p,i}}{C_i} = \frac{C_{OA}/C_i^*(T)}{1 + C_{OA}/C_i^*(T)} = \left(1 + \frac{C_i^*(T)}{C_{OA}}\right)^{-1} \tag{4.1}$$

Here, $C_{p,i}$ and C_i are the particle phase and total concentrations of species i, respectively. $C_i^*(T)$ is the temperature-dependent saturation concentration ($\mu g\,m^{-3}$) of species i, and C_{OA} is the concentration of total OA.
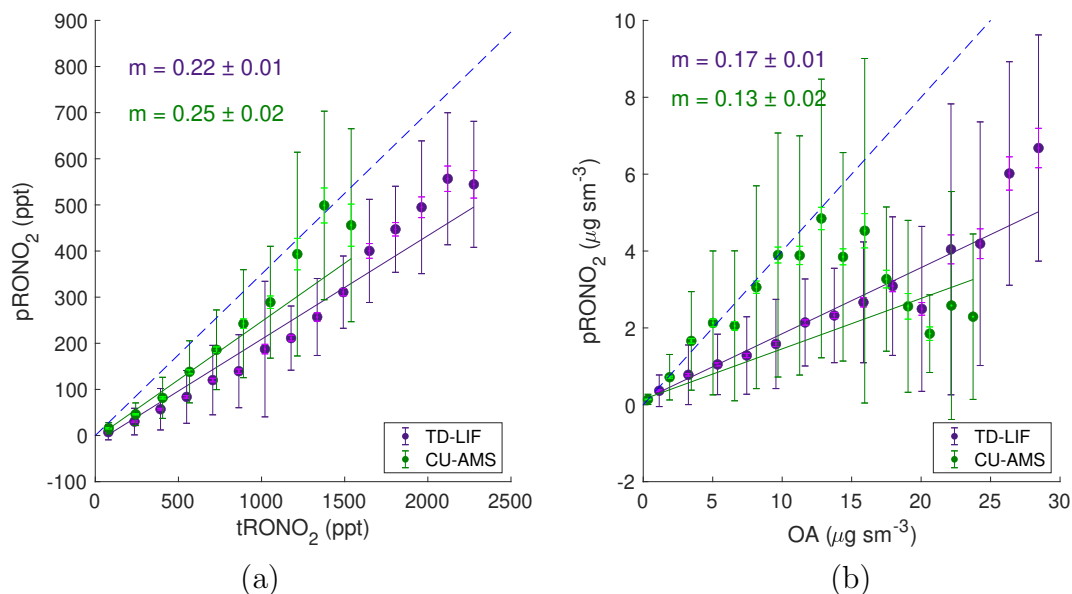
Figure 4.3: (a) Plot of pRONO$_2$ versus tRONO$_2$ mixing ratios as measured by TD-LIF and CU-AMS. Data are binned by tRONO$_2$ mixing ratio, and the average pRONO$_2$ in each bin is plotted. The York fit shown corresponds to the average fraction of RONO$_2$ in the particle phase (F_p). We draw an estimated upper limit ($\approx$35%) for the fraction of RONO$_2$ in the particle phase, as shown in the blue dashed line, drawn above the mean of most measurements. (b) Plot of pRONO$_2$ mass concentration (using an estimated average molecular weight of 300 g mol^{-1}) versus OA mass concentration. Data are binned by OA concentration, and the average pRONO$_2$ in each bin is plotted. The York fit shown corresponds to the average fraction OA mass that can be attributed to pRONO$_2$. Again, we draw an estimated upper limit ($\approx$40%) for the fraction of OA mass attributable to pRONO$_2$, as shown in the blue dashed line, drawn above most measurement means. We do not understand why AMS data above 15 μg m^{-3} deviates so strongly from the trend measured at lower OA concentrations. In both plots, the larger, dark colored error bars correspond to the standard deviation of measurements within each bin to represent observed variability; the smaller, light colored error bars correspond to the standard error of measurements within each bin to represent measurement uncertainty. We apply a threshold requirement of 20 observations per bin to include in plot.

For both the TD-LIF and CU-AMS measurements of $pRONO_2$, the fraction of $RONO_2$ in the particle phase (F_p) increases with increasing OA concentration and increases with decreasing temperature, as shown in Figure 4.4. Assuming the speciation of $RONO_2$ is invariant with temperature, these relationships between F_p, OA, and temperature indicate that the phase partitioning of $RONO_2$ during KORUS-AQ is indeed controlled by equilibrium absorptive partitioning.

To determine the volatility distribution of $RONO_2$ observed during KORUS-AQ, we define a saturation concentration basis set of $\{C_j^*\} = \{3, 30, 300\}$ $\mu g\,m^{-3}$, following the convention of Donahue et al. (2006). Though we expect some $RONO_2$ species to have volatilities outside of this range, because the OA concentrations we observe during KORUS-AQ do not exceed 40 $\mu g\,m^{-3}$ we cannot reasonably constrain volatilities outside of this defined basis set. Given this basis set, the total fraction of organic nitrates in the particle phase ($F_{p,tot}$) can be represented as

$$F_{p,tot} = \frac{\Sigma_i C_i F_{p,i}}{\Sigma_i C_i} = \sum_{j=1}^{n} f_j \left(1 + \frac{C_j^*}{C_{OA}}\right)^{-1} \tag{4.2}$$

Here, f_j is the fraction of organic nitrates that can be classified as having saturation concentration C_j^*, and $n = 3$ for the basis set defined earlier.

We solve for each f_j, the fraction of organic nitrates that can be represented as having saturation concentration C_j^*, in Equation 4.2 using our observations of $F_{p,tot}$ (= $pRONO_2$ / $RONO_2$) and organic aerosol concentrations (C_{OA}). Moreover, because saturation concentration is dependent on temperature, we separate the observations into a series of temperature bins and solve for fitting parameters f_j in each temperature bin, as shown in Figure 4.4 for both TD-LIF and CU-AMS observations. As expected, organic nitrates become less volatile at lower temperatures. At all temperatures, 10-39% of organic nitrates can be represented with $C^* \leq 3\mu g\,m^{-3}$, meaning they will dominantly be condensed at the average observed organic aerosol concentrations of ≈ 9.8 $\mu g\,m^{-3}$. At high temperatures (≈ 300 K), 73-76% of organic nitrates can be represented with $C^* \geq 300$ $\mu g\,m^{-3}$, meaning that they will dominantly remain in the gas phase at observed OA concentrations. At low temperatures (≈ 286 K), the TD-LIF measurements suggest that 67% of organic nitrates can be represented with $C^* \geq 300$ $\mu g\,m^{-3}$ and the CU-AMS measurements suggest 61% of organic nitrates can be represented with $C^* \geq 30$ $\mu g\,m^{-3}$.

We also fit the data to Equation 4.2 using an empirical relationship between C^* and ΔH_{vap} from Epstein, Riipinen, and Donahue (2010) to examine the variation of $RONO_2$ volatilities observed at different temperatures but referenced to 300 K. Figure C.15 shows the distribution of $C^*(300$ K) for $RONO_2$ during KORUS-AQ.

CMAQ modeling misses a large source of semivolatile, anthropogenically-derived $RONO_2$

Our CMAQ simulation underpredicts measured $tRONO_2$ concentrations by a factor of ≈ 3, as shown by the slopes reported in Table 4.1 and plotted in Figure C.14. Moreover, our
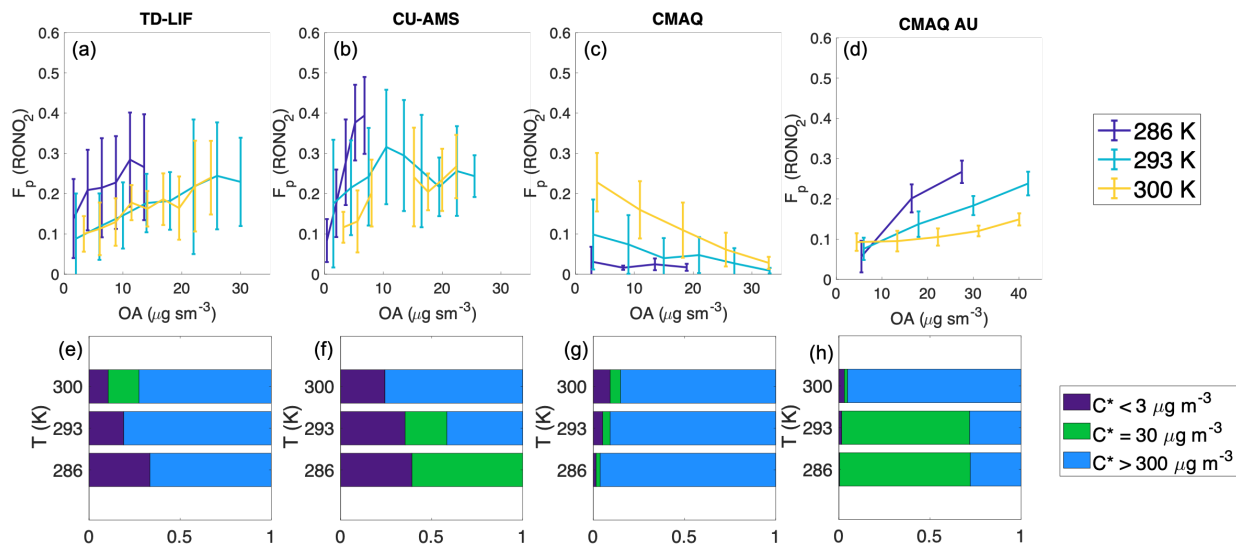
Figure 4.4: [Top] Plots of the fraction of $RONO_2$ in the particle phase (F_p) versus OA concentration. Data were separated into three temperature bins (centered at 286, 293, and 300 K) and binned by OA concentration. The average F_p in each OA bin is plotted, and error bars represent the standard deviation of F_p in each bin. As suggested by absorptive partitioning theory, measured F_p increases with increasing available solvating aerosol (in this case, OA). [Bottom] Temperature-dependent fractional distribution (f_j) of saturation concentrations (C_j^*) fit to a volatility basis set. Each set of plots is shown for the TD-LIF measurements (a,e), the CU-AMS measurements (b,f), unmodified CMAQ output (c,g), and CMAQ output with an unknown source of $RONO_2$ added (d,h).

CMAQ simulation underpredicts measured $pRONO_2$ concentrations by a factor of ≈ 10, indicating that the $RONO_2$ in CMAQ are too volatile. These underpredictions for both $tRONO_2$ and $pRONO_2$ indicate that our simulation is missing a large source of condensable $RONO_2$.

To help determine the origin of the missing source of $RONO_2$, we examine the correlation between the model-measurement $RONO_2$ difference ($RONO_{2,diff}$) and measurements of various VOC classes. We find $R^2 < 0.05$ for the correlation between $RONO_{2,diff}$ and both isoprene and α-pinene, whereas there are relatively stronger correlations between $RONO_{2,diff}$ and anthropogenic alkanes ($R^2 = 0.15$), alkenes ($R^2 = 0.12$), aromatics ($R^2 = 0.23$), and aldehydes ($R^2 = 0.67$). The weak correlations between the $RONO_{2,diff}$ and VOCs of biogenic origin and the relatively stronger correlations between $RONO_{2,diff}$ and VOCs of anthropogenic origin suggest that the missing source of condensable $RONO_2$ is derived from anthropogenic VOCs.

Furthermore, the RACM2_Berkeley2.1 mechanism was initially tested and validated on a regional scale over the Southeast US, an area dominated by biogenic emissions (Zare et al.,

2018; Zare et al., 2019). Additionally, as described in Section 2.4, we adjusted the emissions of monoterpenes to improve the model-measurement agreement for biogenic VOCs. Though we expect some change in the oxidation product distribution between low-NO_x environments (e.g., Southeast US) and high-NO_x environments (e.g., Seoul), we are reasonably confident that our CMAQ simulation is accurately capturing the production and fate of $RONO_2$ derived from biogenic VOCs. We therefore attribute the missing source of $RONO_2$ in our simulations to $RONO_2$ of anthropogenic origin. This previous work evaluating RACM2_Berkeley2.1 in the Southeast US (Zare et al., 2018; Zare et al., 2019) did not look at urban $RONO_2$ in the US, but we have no reason to suspect that this missing source of condensable $RONO_2$ is not a general phenomenon.

The relationship between CMAQ-modeled $F_p(RONO_2)$, OA, and temperature is shown in Figure 4.4c. In contrast to the observations (Figure 4.4a,b) and in contrast with absorptive partitioning theory, the modeled F_p increases with increasing temperature and decreases with increasing OA. Exploration of the speciated distribution of modeled $RONO_2$ (shown in Figure C.16) indicates that the increase in modeled F_p with temperature is driven largely by a temperature-dependent change in the $RONO_2$ speciation. The phase partitioning of each $RONO_2$ species is controlled by absorptive partitioning, meaning the fraction of an individual $RONO_2$ species in the particle phase increases with decreasing temperature. However, the modeled increase in the total concentration of low-volatility monoterpene nitrates (HONIT) with temperature is larger than the modeled change in concentration of other higher-volatility nitrates with temperature. As a result, the concentration of $pRONO_2$ increases with increasing temperature faster than the concentration of $gRONO_2$ increases with temperature, causing the total F_p to increase with increasing temperature. This modeled relationship between F_p and temperature stands in stark disagreement with the observations and therefore indicates that the species distribution of $RONO_2$ over Korea is incorrectly captured in our CMAQ simulation.

To test and quantify our hypothesis that our CMAQ simulation is missing a large source of condensable, anthropogenic $RONO_2$, we test the effect of adding an additional source of $RONO_2$. Because our CMAQ simulation underpredicts measured $tRONO_2$ concentrations by a factor of ≈ 3 (Table 4.1), we assign this additional source to have double the concentration of the existing simulated $RONO_2$. To determine the average volatility of this missing source of $RONO_2$, we iteratively vary its assigned C^* by order of magnitude (e.g., $C^* = 30, 300, 3000$ $\mu g\,m^{-3}$) and use an empirical relationship between C^* and ΔH_{vap} from Epstein, Riipinen, and Donahue (2010). We find the best agreement between modeled and measured $pRONO_2$ and F_p with $C^* = 300$ $\mu g\,m^{-3}$ as shown in Table C.2. Though comparison between modeled and measured $RONO_2$ remains relatively scattered (see Figure C.14) and the missing source likely includes a variety of molecules with a range of volatilities, adding this missing semivolatile $RONO_2$ source improves the magnitude of the model-measurement agreement for $tRONO_2$, $pRONO_2$, and F_p, as shown in Table 4.1. Moreover, as shown in Figure 4.4, addition of this unknown source of relatively condensable $RONO_2$ results in an increase in F_p with decreasing temperature and increasing OA concentration. This relationship between F_p, temperature, and OA is in agreement with the observations and with equilibrium absorptive partitioning

Table 4.1: Comparison of the York fit slopes between measured (TD-LIF and CU-AMS) and CMAQ modeled concentrations of tRONO$_2$, pRONO$_2$, and F_p. Comparison is shown for both the unmodified CMAQ output and CMAQ output with an unknown source of condensable RONO$_2$ added. Scatter plots of these comparisons can be seen in Figure C.14.

	tRONO$_2$		pRONO$_2$		F_p	
	TD-LIF	CU-AMS	TD-LIF	CU-AMS	TD-LIF	CU-AMS
CMAQ	0.30	0.35	0.12	0.09	0.56	0.35
CMAQ add unknown	0.88	0.98	0.92	0.79	0.61	0.44

theory.

4.4 Discussion

The RACM2_Berkeley2.1 mechanism represents our state-of-the-science understanding of RONO$_2$ chemistry, where the only sources of semi-volatile RONO$_2$ are biogenic. However, this mechanism only captures one third of the RONO$_2$ production over the Korean peninsula. Moreover, the unknown source of organic nitrates consists of RONO$_2$ that are lower volatility than most of the existing RONO$_2$ in the model. Consequently, our current understanding of RONO$_2$ chemistry is missing pathways for semivolatile RONO$_2$ production as a result of either missing oxidation pathways (first- or multi-generation, bimolecular or unimolecular) or an underestimation of RONO$_2$ yields.

Because the known chemistry can only account for one third of the observed RONO$_2$, the missing source is approximately double in magnitude to the known sources. During KORUS-AQ, the average reactivity of all measured VOCs with OH was 2.4 s^{-1}, and the effective average RONO$_2$ yield (α), weighted by reactivity, was 1.3%. If the unknown source of RONO$_2$ has a low α of 1%, the missing reactivity must be ≈ 3 s^{-1}. On the other hand, if the unknown source of RONO$_2$ has a higher α of 20%, the missing reactivity must be ≈ 0.15 s^{-1}. For reference, during KORUS-AQ the average isoprene reactivity was 0.051 s^{-1} and the average toluene reactivity was 0.054 s^{-1}.

We hypothesize three potential missing sources of semivolatile RONO$_2$: (1) missing source(s) of semi- and intermediate-volatility organic compounds (S/IVOCs) that are oxidized to RONO$_2$; (2) unrepresented autoxidation mechanisms that produce highly oxygenated organic peroxy radicals (RO$_2$) which could react with NO to form RONO$_2$; or (3) more generations of bimolecular oxidation than are currently represented.

S/IVOCs are considered major SOA precursors (e.g., Robinson et al., 2007; Grieshop et al., 2009; Dzepina et al., 2009; Hodzic et al., 2010; Pye and Seinfeld, 2010; Dzepina et al., 2011; Zhao et al., 2014; Hayes et al., 2015; Ortega et al., 2016; Ma et al., 2017; Nault et al., 2018), but their concentrations are challenging to measure in the atmosphere due to condensation within instruments (e.g., Pagonis et al., 2017), and their chemistry is difficult to measure in chamber experiments due to wall loss (e.g., Zhang et al., 2014). Nault et al.

(2018) concluded that, during KORUS-AQ, S/IVOCs and reactive aromatics contributed to 70% of the total SOA over Seoul. Because they are emitted with relatively low volatility, oxidation of S/IVOCs to form $RONO_2$ could contribute to the missing source of semivolatile $RONO_2$. Because the addition of a nitrate group decreases a molecule's volatility by ≈ 2.5 orders of magnitude (Pankow and Asher, 2008), a missing $RONO_2$ source with saturation concentration 300 $\mu g\,m^{-3}$ implies a precursor with $C^* = 10^5$ $\mu g\,m^{-3}$, namely an IVOC. The contribution of S/IVOCs to $pRONO_2$ is not unprecedented; Lee et al. (2019) determined that much of the $pRONO_2$ formation in the Alberta oil sands occurred via photo-oxidation of IVOCs under high-NO_x conditions.

Autoxidation, a mechanism involving an intramolecular hydrogen-shift followed by addition of molecular oxygen in RO_2 radicals, can quickly (in seconds) generate highly oxygenated molecules, or HOMs (Crounse et al., 2013; Bianchi et al., 2019 and references therein). Because of their high oxygen content, HOMs have significantly reduced volatility compared to their parent VOCs (e.g., Tröstl et al., 2016; Ehn et al., 2014; Mutzel et al., 2015. While most previous studies of HOMs have focused on autoxidation of RO_2 derived from biogenic VOCs, theoretical calculations by Wang et al. (2017) indicate that substituted benzenes, which were measured in high abundance during KORUS-AQ (Simpson et al., 2020; Fried et al., 2020), may also produce HOMs through autoxidation of bicyclic peroxy radicals. Although autoxidation becomes relatively more competitive with bimolecular oxidation pathways as NO_x decreases, absolute rates of autoxidation increase with increasing NO_x due to increased oxidant availability (Pye et al., 2019). In Korea's high-NO_x environment, autoxidation may generate highly oxidized RO_2 which could produce $RONO_2$ via reaction with NO (R33).

Additionally, multiple recent studies have suggested that multi-generation OH oxidation of aromatics can lead to highly oxygenated oxidation products, many of which, particularly under high-NO_x conditions, contain nitrogen (e.g., Tsiligiannis et al., 2019; Garmash et al., 2020; Cheng et al., 2021). Some of these nitrogen-containing products are likely organic nitrates, but the nitrogen-containing product distribution also includes peroxy nitrates and nitro aromatics. Because aromatics are a large contributor to total VOCs over Korea (Simpson et al., 2020; Fried et al., 2020), there could be significant production of semivolatile, multi-functional, oxygenated organic nitrates from multi-generation oxidation of aromatic VOCs.

4.5 Conclusions

Exploration of the phase partitioning of $RONO_2$ over the Korean peninsula using our aircraft-based measurements of $pRONO_2$ and $tRONO_2$ during KORUS-AQ, as an example of urban chemistry, indicate that organic nitrates contribute $\approx 15\%$ of the total OA. This significant contribution of organic nitrates to the OA burden, as has been observed elsewhere, reinforces the notion that a better understanding of the processes that control the production, loss, and phase partitioning of $RONO_2$ are crucial for understanding the processes that control SOA production and loss. Our current understanding of $RONO_2$ chemistry can only explain

one third of the observed $RONO_2$ in Korea and is therefore missing a source of semi-volatile, anthropogenically-derived $RONO_2$ in and around Seoul. We recommend further laboratory and field research to determine the source VOCs and mechanisms that drive the production of this missing source of organic nitrates.

Chapter 5

Conclusion

5.1 Summary

The work presented here leverages data from four aircraft experiments in conjunction with modeling to provide new constraints on the lifetime and fate of NO_x in urban environments. I focus particularly on the importance of nighttime chemistry and condensed phase chemistry.

In Chapter 2, I showed that the wintertime lifetime of NO_x in the Northeast US is controlled by nocturnal multiphase chemistry. The dominant wintertime sink of NO_x in this environment is HNO_3 formed via heterogeneous hydrolysis of N_2O_5, resulting in a nighttime NO_x lifetime of ≈ 6 hours. Daytime NO_x loss in this environment is much slower, with a NO_x lifetime of 29 hours.

In Chapter 3, I showed that nocturnal, NO_3-initiated production of $RONO_2$ is competitive with daytime OH-initiated $RONO_2$ production in three distinct chemical environments: the rural Southeast US, the Colorado Front Range, and the mega-city of Seoul, South Korea. Though nocturnal NO_3-initiated $RONO_2$ production has typically been assumed negligible in urban environments, I show that nighttime $RONO_2$ production is similar in magnitude to daytime production in all three of these regions.

Finally, in Chapter 4 I examined the contribution of condensed $RONO_2$ to the organic aerosol budget in Seoul, South Korea. I find that $\approx 15\%$ of the organic aerosol mass can be attributed to $RONO_2$, similar in magnitude to recent observations in other areas of the world. However, our current understanding of $RONO_2$ chemistry can only explain half of the observed $RONO_2$.

5.2 Predictions about future urban NO_x chemistry

Over the past few decades, US cities have enacted emission controls on VOCs which have been particularly effective for temperature-independent VOC sources. As a result, much of the remaining VOC abundance is emitted from temperature-dependent sources via evaporation or biogenic processes. Recent studies have shown that VOC concentrations in Los Angeles

are now steeply temperature dependent, causing both O_3 and organic aerosol to also be temperature dependent (Nussbaumer and Cohen, 2020; Nussbaumer and Cohen, 2021). In the nearby San Joaquin Valley, Pusede et al. (2014) found that a large fraction of VOC emissions are temperature dependent, causing O_3 exceedances to also depend strongly on temperature.

As the proportion of electric cars and trucks increases, we expect further reductions in urban NO_x and VOC emissions. As cities continue to shift to low-NO_x chemical regimes with VOC reactivity (VOCR) controlled primarily by temperature, the emission patterns and dominant chemical reactions change. For example, Romer Present, Zare, and Cohen (2020) showed that recent changes in NO_x and VOC emissions have led to an increase in the importance of $RONO_2$ as a loss pathway for NO_x and a corresponding decrease in the importance of HNO_3 as a sink of NO_x.

We set up a simple steady-state model to predict how $RONO_2$ chemistry will change as urban NO_x emissions continue to decrease and as VOC emissions become more strongly temperature-dependent. For daytime photochemistry, we adopt the steady-state approximations detailed in Murphy et al. (2006b). For nighttime dark reactions, we use the steady-state approximations detailed in Chapter 2 of this dissertation. Nussbaumer and Cohen (2021) found that, in Los Angeles, VOC concentrations increase by a factor of ≈ 2.5 from 20°C to 40°C. As an illustrative model, we adopt this temperature dependence and assign a hypothetical VOCR increase from 3 to 7.5 s^{-1} from 20°C to 40°C. Further, we estimate that the $RONO_2$ in this hypothetical urban scenario can be described by a volatility basis set with $C^* = \{5 \times 10^0,\ 5 \times 10^2,\ 5 \times 10^4\}$ μg m^{-3} with an enthalphy of vaporization of 80 kJ mol^{-1}. We also adopt the temperature dependence of organic aerosol in Los Angeles determined in Nussbaumer and Cohen (2021) and assume it to be invariant with NO_x. Our daytime steady-state model assumes a constant P(HO$_x$) of 6.25×10^6 molec cm^{-3} s^{-1}, a constant NO_2:NO ratio of 4, and a constant branching ratio α of 0.04. Our nighttime steady-state model assumes a constant O_3 mixing ratio of 40 ppb, a constant heterogeneous uptake coefficient of N_2O_5 ($\gamma_{N_2O_5}$) of 0.04, and a constant aerosol surface area of 100 μm^2 cm^{-3}.

We predict how the balance of NO_x sinks will change under low-NO_x regimes when VOC emissions are highly temperature dependent, as shown in Figure 5.1. We predict that the fraction of NO_x lost as $RONO_2$ increases as NO_x decreases during both day and night. We also predict that the fraction of NO_x lost as $RONO_2$ will increase with temperature, but that this increase will be steeper for nocturnal chemistry than for photochemistry.

In this scenario, the contribution of p$RONO_2$ to the organic aerosol mass will change as NO_x emissions continue to decrease and as VOC emissions continue to be highly temperature dependent. As shown in Figure 5.1, the contribution of photochemically-produced p$RONO_2$ to OA peaks at intermediate NO_x concentrations and low temperatures. The contribution of $RONO_2$ produced from NO_3 chemistry decreases with decreasing NO_x concentration and is relatively invariant with temperature. However, these predictions could be complicated by changes in the $RONO_2$ product distribution (and thus $RONO_2$ vapor pressure distribution) as NO_x concentrations change, including by changes in the relative importance of autoxidation mechanisms with changes in NO_x concentrations. The steady-state model used here does
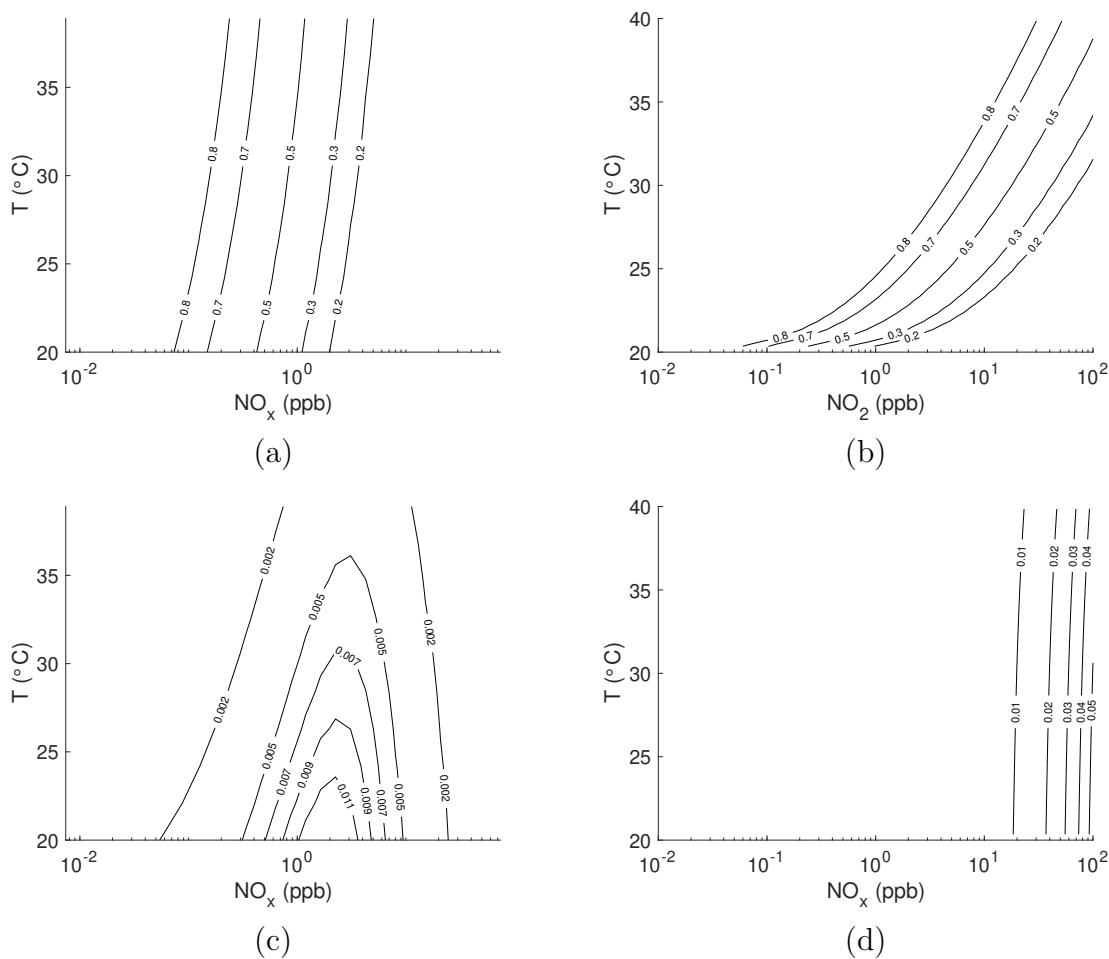
Figure 5.1: Plots of the fraction of NO_x lost as $RONO_2$ during (a) daytime photochemistry and (b) nocturnal chemistry, and plots of the fraction of OA attributable to one hour of $RONO_2$ production during (c) daytime photochemistry and (d) nocturnal chemistry, as a function of temperature and NO_x concentration. Parameterized temperature dependence includes changes in VOCR with temperature, changes in N_2O_5 equilibrium with temperature (for nighttime calculations), and changes in saturation concentration with temperature (for aerosol calculations). Calculations were done with a steady-state model.

not account for these possible changes.

5.3 Questions about the future of NO_x chemistry

The work presented here raises a number of further questions about the future of NO_x chemistry. Here I offer a number of questions to guide further research in this area.

- As urban areas shift to low-NO_x chemical regimes with VOC emissions largely temperature dependent, are the predictions outlined in Section 5.2 correct? The steady-state model used in our predictions does not account for changes in oxidation product distributions as NO_x concentrations change. What effect will possible changes in product distributions have on NO_x lifetime and organic aerosol production?

- Chapter 3 discusses the importance of nocturnal $RONO_2$ production for NO_x loss in a rural area, an area with both urban and oil/gas emissions, and a megacity. Are there other environments in which NO_3-initiated production of $RONO_2$ is important for understanding the NO_x lifetime?

- Chapter 4 discusses the contribution of $pRONO_2$ to OA in Seoul. Is the contribution similar in other cities? How does this understanding of a substantial contribution of $pRONO_2$ to OA mass influence our understanding of aerosol lifetime?

- Autoxidation becomes a more important process in lower NO_x regimes. What role do autoxidation mechanisms play in the production of $RONO_2$? A combination of further laboratory and field studies will be important for characterizing these mechanisms.

- Are semi- and intermediate-volatility organic compounds (S/IVOCs) important precursors of $RONO_2$? Measurement capabilities of S/IVOCs are currently limited. Further research into measurement techniques, oxidation mechanisms, and $RONO_2$ yields of S/IVOCs could lead to important insights related to production of condensable $RONO_2$.

Bibliography

[1]   Mattias Aldener et al. "Reactivity and loss mechanisms of NO3 and N2O5 in a polluted marine environment: Results from in situ measurements during New England Air Quality Study 2002". In: *Journal of Geophysical Research: Atmospheres* 111.23 (2006), D23S73. ISSN: 01480227. DOI: 10.1029/2006JD007252. URL: http://doi.wiley.com/10.1029/2006JD007252.

[2]   B Alexander et al. "Quantifying atmospheric nitrate formation pathways based on a global model of the oxygen isotopic composition (O) of atmospheric nitrate". In: *Atmospheric Chemistry and Physics* 9.2 (2009), pp. 5043–5056. ISSN: 1680-7324. DOI: 10.5194/acp-9-5043-2009. URL: www.atmos-chem-phys.net/9/5043/2009/.

[3]   M J Alvarado et al. "Nitrogen oxides and PAN in plumes from boreal fires during ARCTAS-B and their impact on ozone: an integrated analysis of aircraft and satellite observations". In: *Atmospheric Chemistry and Physics* 10 (2010), pp. 9739–9760. DOI: 10.5194/acp-10-9739-2010. URL: www.atmos-chem-phys.net/10/9739/2010/.

[4]   Eric C. Apel et al. "Upper tropospheric ozone production from lightning NOx-impacted convection: Smoke ingestion case study from the DC3 campaign". In: *Journal of Geophysical Research: Atmospheres* 120 (2015), pp. 2505–2523. DOI: 10.1002/2014JD022121.

[5]   Cristina L. Archer et al. "On the predominance of unstable atmospheric conditions in the marine boundary layer offshore of the U.S. northeastern coast". In: *Journal of Geophysical Research* 121.15 (2016), pp. 8869–8885. ISSN: 21562202. DOI: 10.1002/2016JD024896.

[6]   Janet Arey et al. "Alkyl Nitrate, Hydroxyalkyl Nitrate, and Hydroxycarbonyl Formation from the NOx - Air Photooxidations of C5-C8 w-ALkanes". In: *Journal of Physical Chemistry A* 105.6 (2001), pp. 1020–1027. ISSN: 10895639. DOI: 10.1021/jp003292z.

[7]   R Atkinson et al. "Evaluated kinetic and photochemical data for atmospheric chemistry: Volume II - gas phase reactions of organic species". In: *Atmos. Chem. Physics* 6.11 (2006), pp. 3625–4055. ISSN: 1680-7316. DOI: 10.5194/acp-6-3625-2006. URL: http://www.atmos-chem-phys.net/6/3625/2006/.

[8]   B. R. Ayres et al. "Organic nitrate aerosol formation via NO3 + biogenic volatile organic compounds in the southeastern United States". In: *Atmospheric Chemistry and Physics* 15.23 (2015), pp. 13377–13392. ISSN: 16807324. DOI: 10.5194/acp-15-13377-2015.

[9]   George A. Ban-Weiss et al. "Long-term changes in emissions of nitrogen oxides and particulate matter from on-road gasoline and diesel vehicles". In: *Atmospheric Environment* 42.2 (2008), pp. 220–232. ISSN: 13522310. DOI: 10.1016/j.atmosenv.2007.09.049.

[10]   T H Bertram and J A Thornton. "Toward a general parameterization of N2O5 reactivity on aqueous particles: the competing effects of particle liquid water, nitrate and chloride". In: *Atmospheric Chemistry and Physics* 9 (2009), pp. 8351–8363. URL: www.atmos-chem-phys.net/9/8351/2009/.

[11]   Isabelle Bey et al. "Global modeling of tropospheric chemistry with assimilated meteorology: Model description and evaluation". In: *Journal of Geophysical Research: Atmospheres* 106.D19 (2001), pp. 23073–23095. ISSN: 01480227. DOI: 10.1029/2001JD000807. URL: http://doi.wiley.com/10.1029/2001JD000807.

[12]   Huisheng Bian et al. *Investigation of global particulate nitrate from the AeroCom phase III experiment.* Vol. 17. 2017, pp. 12911–12940. ISBN: 1712911201. DOI: 10.5194/acp-17-12911-2017.

[13]   Federico Bianchi et al. "Highly Oxygenated Organic Molecules (HOM) from Gas-Phase Autoxidation Involving Peroxy Radicals: A Key Contributor to Atmospheric Aerosol". In: *Chemical Reviews* 119.6 (2019), pp. 3472–3509. ISSN: 15206890. DOI: 10.1021/acs.chemrev.8b00395.

[14]   Gary A. Bishop and Donald H. Stedman. "A decade of on-road emissions measurements". In: *Environmental Science and Technology* 42.5 (2008), pp. 1651–1656. ISSN: 0013936X. DOI: 10.1021/es702413b.

[15]   C Bloss et al. "Development of a detailed chemical mechanism (MCMv3.1) for the atmospheric oxidation of aromatic hydrocarbons". In: *Atmos. Chem. Phys* 5 (2005), pp. 641–664. URL: www.atmos-chem-phys.org/acp/5/641/.

[16]   Steven S. Brown et al. "Budgets for nocturnal VOC oxidation by nitrate radicals aloft during the 2006 Texas Air Quality Study". In: *Journal of Geophysical Research Atmospheres* 116.24 (2011), pp. 1–15. ISSN: 01480227. DOI: 10.1029/2011JD016544.

[17]   Steven S. Brown et al. "Cavity enhanced spectroscopy for measurement of nitrogen oxides in the Anthropocene: Results from the Seoul tower during MAPS 2015". In: *Faraday Discussions* 200 (2017), pp. 529–557. ISSN: 13645498. DOI: 10.1039/c7fd00001d.

[18]   Steven S. Brown et al. "Nighttime removal of NOx in the summer marine boundary layer". In: *Geophysical Research Letters* 31.7 (2004). ISSN: 00948276. DOI: 10.1029/2004GL019412.

[19] Steven S. Brown et al. "Nocturnal odd-oxygen budget and its implications for ozone loss in the lower troposphere". In: *Geophysical Research Letters* 33.8 (2006). ISSN: 00948276. DOI: 10.1029/2006GL025900.

[20] Steven S. Brown et al. "Reactive uptake coefficients for N2O5 determined from aircraft measurements during the Second Texas Air Quality Study: Comparison to current model parameterizations". In: *Journal of Geophysical Research* 114.D7 (2009), pp. 1–16. ISSN: 0148-0227. DOI: 10.1029/2008JD011679. URL: http://www.agu.org/pubs/crossref/2009/2008JD011679.shtml.

[21] E. C. Browne et al. "Observations of total RONO2 over the boreal forest: NOx sinks and HNO3 sources". In: *Atmospheric Chemistry and Physics* 13.9 (2013), pp. 4543–4562. ISSN: 16807316. DOI: 10.5194/acp-13-4543-2013.

[22] E C Browne et al. "On the role of monoterpene chemistry in the remote continental boundary layer". In: *Atmospheric Chemistry and Physics* 14 (2014), pp. 1225–1238. DOI: 10.5194/acp-14-1225-2014.

[23] J B Burkholder et al. *Chemical Kinetics and Photochemical Data for Use in Atmospheric Studies, Evaluation No. 18*. Tech. rep. Pasadena: Jet Propulsion Laboratory, 2015. URL: https://jpldataeval.jpl.nasa.gov.

[24] M.R. Canagaratna et al. "Chemical and Microphysical Characterization of Ambien Aerosols with the Aerodyne Aerosol Mass Spectrometer". In: *Mass Spectrometry Reviews* 26 (2007), pp. 185–222.

[25] William P.L. Carter. "Development of a database for chemical mechanism assignments for volatile organic emissions". In: *Journal of the Air and Waste Management Association* 65.10 (2015), pp. 1171–1184. ISSN: 21622906. DOI: 10.1080/10962247.2015.1013646. URL: http://dx.doi.org/10.1080/10962247.2015.1013646.

[26] William P.L. Carter and Roger Atkinson. "Alkyl Nitrate Formation from the Atmospheric Photooxidation of Alkanes; a Revised Estimation Method". In: *Journal of Atmospheric Chemistry* 8 (1989), pp. 165–173.

[27] Xi Cheng et al. "Highly Oxygenated Organic Molecules Produced by the Oxidation of Benzene and Toluene in a Wide Range of OH Exposure and NOx Conditions". In: *Atmospheric Chemistry and Physics Discussions* 2 (2021).

[28] I. Colbeck and Roy M. Harrison. "Dry deposition of ozone: some measurements of deposition velocity and of vertical profiles to 100 metres". In: *Atmospheric Environment (1967)* 19.11 (1985), pp. 1807–1818. ISSN: 00046981. DOI: 10.1016/0004-6981(85)90007-1.

[29] J. J. Colman et al. "Description of the analysis of a wide range of volatile organic compounds in whole air samples collected during PEM-Tropics A and B". In: *Analytical Chemistry* 73.15 (2001), pp. 3723–3731. ISSN: 00032700. DOI: 10.1021/ac010027g.

[30] John D. Crounse et al. "Autoxidation of organic compounds in the atmosphere". In: *Journal of Physical Chemistry Letters* 4.20 (2013), pp. 3513–3520. ISSN: 19487185. DOI: 10.1021/jz4019207.

[31] John D. Crounse et al. "Measurement of gas-phase hydroperoxides by chemical ionization mass spectrometry". In: *Analytical Chemistry* 78.19 (2006), pp. 6726–6732. ISSN: 00032700. DOI: 10.1021/ac0604235.

[32] John D Crounse et al. "Peroxy radical isomerization in the oxidation of isoprene". In: *Physical Chemistry Chemical Physics* (2011), pp. 13607–13613. DOI: 10.1039/c1cp21330j.

[33] John N. Crowley et al. "Variable lifetimes and loss mechanisms for NO3 and N2O5 during the DOMINO campaign: Contrasts between marine, urban and continental air". In: *Atmospheric Chemistry and Physics* 11.21 (2011), pp. 10853–10870. ISSN: 16807316. DOI: 10.5194/acp-11-10853-2011.

[34] Timothy R. Dallmann and Robert A. Harley. "Evaluation of mobile source emission trends in the United States". In: *Journal of Geophysical Research Atmospheres* 115.14 (2010), pp. 1–12. ISSN: 01480227. DOI: 10.1029/2010JD013862.

[35] J M Davis, P V Bhave, and K M Foley. "Parameterization of N2O5 reaction probabilities on the surface of particles containing ammonium, sulfate, and nitrate". In: *Atmospheric Chemistry and Physics* 8 (2008), pp. 5295–5311. URL: www.atmos-chemphys.net/8/5295/2008/.

[36] Douglas A. Day et al. "A thermal dissociation laser-induced fluorescence instrument for in situ detection of NO2, peroxy nitrates, alkyl nitrates, and HNO3". In: *Journal of Geophysical Research: Atmospheres* 107.D6 (Mar. 2002), pp. 4–1. ISSN: 01480227. DOI: 10.1029/2001JD000779. URL: http://doi.wiley.com/10.1029/2001JD000779.

[37] Douglas A Day et al. "On alkyl nitrates, O3, and the "missing NOy"". In: *J. Geophys. Res.* 108.D16 (2003), JD003685. ISSN: 0148-0227. DOI: 10.1029/2003JD003685. URL: http://doi.wiley.com/10.1029/2003JD003685.

[38] Peter F. DeCarlo et al. "Field-deployable, high-resolution, time-of-flight aerosol mass spectrometer". In: *Analytical Chemistry* 78.24 (2006), pp. 8281–8289. ISSN: 00032700. DOI: 10.1021/ac061249n.

[39] J. A. deGouw et al. "Validation of proton transfer reaction-mass spectrometry (PTR-MS) measurements of gas-phase organic compounds in the atmosphere during the New England Air Quality Study (NEAQS) in 2002". In: *Journal of Geophysical Research D: Atmospheres* 108.21 (2003), pp. 1–18. ISSN: 01480227. DOI: 10.1029/2003jd003863.

[40] Mary Angelique G. Demetillo et al. "Observing nitrogen dioxide air pollution inequality using high-spatial-resolution remote sensing measurements in Houston, Texas". In: *Environmental Science and Technology* 54.16 (2020), pp. 9882–9895. ISSN: 15205851. DOI: 10.1021/acs.est.0c01864.

[41]   Frank J. Dentener and Paul J. Crutzen. "Reaction of N2O5 on tropospheric aerosols: Impact on the global distributions of NOx , O3, and OH". In: *Journal of Geophysical Research* 98.D4 (1993), p. 7149. ISSN: 0148-0227. DOI: 10.1029/92JD02979. URL: http://doi.wiley.com/10.1029/92JD02979.

[42]   Jack E. Dibb, R W Talbot, and E M Scheuer. "Composition and distribution of aerosols over the North Atlantic during the Subsonic Assessment Ozone and Nitrogen Oxide Experiment (SONEX)". In: *Journal of Geophysical Research* 105.D3 (2000), pp. 3709–3717. ISSN: 0148-0227. DOI: 10.1029/1999JD900424.

[43]   Jack E. Dibb et al. "Aerosol chemical composition and distribution during the Pacific Exploratory Mission (PEM) Tropics". In: *Journal of Geophysical Research* 104.D5 (1999), p. 5785. ISSN: 0148-0227. DOI: 10.1029/1998JD100001.

[44]   M. B. Dillon et al. "Chemical evolution of the Sacramento urban plume: Transport and oxidation". In: *Journal of Geophysical Research: Atmospheres* 107.D5 (2002), pp. 3–1. ISSN: 01480227. DOI: 10.1029/2001JD000969. URL: http://doi.wiley.com/10.1029/2001JD000969.

[45]   Xiang Ding et al. "Spatial and seasonal trends in biogenic secondary organic aerosol tracers and water-soluble organic carbon in the Southeastern United States". In: *Environmental Science and Technology* 42.14 (2008), pp. 5171–5176. ISSN: 0013936X. DOI: 10.1021/es7032636.

[46]   N. M. Donahue et al. "Coupled partitioning, dilution, and chemical aging of semivolatile organics". In: *Environmental Science and Technology* 40.8 (2006), pp. 2635–2643. ISSN: 0013936X. DOI: 10.1021/es052297c.

[47]   William P. Dubé et al. "Aircraft instrument for simultaneous, in situ measurement of NO3 and N2O5 via pulsed cavity ring-down spectroscopy". In: *Review of Scientific Instruments* 77.3 (2006). ISSN: 00346748. DOI: 10.1063/1.2176058.

[48]   E. J. Dunlea et al. "Evolution of Asian aerosols during transpacific transport in INTEX-B". In: *Atmospheric Chemistry and Physics* 9.19 (2009), pp. 7257–7287. ISSN: 16807324. DOI: 10.5194/acp-9-7257-2009.

[49]   K. Dzepina et al. "Evaluation of recently-proposed secondary organic aerosol models for a case study in Mexico City". In: *Atmospheric Chemistry and Physics* 9.15 (2009), pp. 5681–5709. ISSN: 16807324. DOI: 10.5194/acp-9-5681-2009.

[50]   Katja Dzepina et al. "Modeling the multiday evolution and aging of secondary organic aerosol during MILAGRO 2006". In: *Environmental Science and Technology* 45.8 (2011), pp. 3496–3503. ISSN: 0013936X. DOI: 10.1021/es103186f.

[51]   Peter M. Edwards et al. "Ozone photochemistry in an oil and natural gas extraction region during winter: Simulations of a snow-free season in the Uintah Basin, Utah". In: *Atmospheric Chemistry and Physics* 13.17 (2013), pp. 8955–8971. ISSN: 16807316. DOI: 10.5194/acp-13-8955-2013.

[52] Peter M. Edwards et al. "Transition from high- to low-NO$_x$ control of night-time oxidation in the southeastern US". In: *Nature Geoscience* 10.7 (2017), pp. 490–495. ISSN: 17520908. DOI: `10.1038/ngeo2976`.

[53] Mikael Ehn et al. "A large source of low-volatility secondary organic aerosol". In: *Nature* 506.7489 (2014), pp. 476–479. ISSN: 00280836. DOI: `10.1038/nature13032`.

[54] Scott A. Epstein, Ilona Riipinen, and Neil M. Donahue. "A semiempirical correlation between enthalpy of vaporization and saturation concentration for organic aerosol". In: *Environmental Science and Technology* 44.2 (2010), pp. 743–748. ISSN: 0013936X. DOI: `10.1021/es902497z`.

[55] B. Ervens, B. J. Turpin, and R. J. Weber. "Secondary organic aerosol formation in cloud droplets and aqueous particles (aqSOA): A review of laboratory, field and model studies". In: *Atmospheric Chemistry and Physics* 11.21 (2011), pp. 11069–11102. ISSN: 16807316. DOI: `10.5194/acp-11-11069-2011`.

[56] Mat J. Evans and Daniel J. Jacob. "Impact of new laboratory studies of N2O5 hydrolysis on global model budgets of tropospheric nitrogen oxides, ozone, and OH". In: *Geophysical Research Letters* 32.9 (2005), p. L09813. ISSN: 0094-8276. DOI: `10.1029/2005GL022469`. URL: `http://doi.wiley.com/10.1029/2005GL022469`.

[57] D. K. Farmer et al. "Impact of organic nitrates on urban ozone production". In: *Atmospheric Chemistry and Physics* 11.9 (2011), pp. 4085–4094. ISSN: 16807316. DOI: `10.5194/acp-11-4085-2011`.

[58] D. K. Farmer et al. "Response of an aerosol mass spectrometer to organonitrates and organosulfates and implications for atmospheric chemistry". In: *Proceedings of the National Academy of Sciences of the United States of America* 107.15 (2010), pp. 6670–6675. ISSN: 00278424. DOI: `10.1073/pnas.0912340107`.

[59] Dorothy L. Fibiger et al. "Wintertime overnight NOx removal in a Southeastern United States coal-fired power plant plume: a model for understanding winter NOx processing and its implications". In: *Journal of Geophysical Research: Atmospheres* (2018), pp. 1–14. ISSN: 2169897X. DOI: `10.1002/2017JD027768`. URL: `http://doi.wiley.com/10.1002/2017JD027768`.

[60] Jenny A. Fisher et al. "Organic nitrate chemistry and its implications for nitrogen budgets in an isoprene- and monoterpene-rich atmosphere : constraints from aircraft (SEAC^{4}RS) and ground-based (SOAS) observations in the Southeast US". In: *Atmospheric Chemistry and Physics* 16 (2016), pp. 5969–5991. DOI: `10.5194/acp-16-5969-2016`.

[61] Frank Flocke et al. "Air Quality in the Northern Colorado Front Range Metro Area: The Front Range Air Pollution and Photochemistry Éxperiment (FRAPPÉ)". In: *Journal of Geophysical Research: Atmospheres* 125.2 (2020). ISSN: 21698996. DOI: `10.1029/2019JD031197`.

[62] Alan Fried et al. "Airborne formaldehyde and volatile organic compound measurements over the Daesan petrochemical complex on Korea's northwest coast during the Korea-United States Air Quality study". In: *Elementa: Science of the Anthropocene* 8.1 (2020), pp. 1–28. ISSN: 2325-1026. DOI: `10.1525/elementa.2020.121`.

[63] Gregory J. Frost et al. "Effects of changing power plant NOx emissions on ozone in the eastern United States: Proof of concept". In: *Journal of Geophysical Research Atmospheres* 111.12 (2006), pp. 1–19. ISSN: 01480227. DOI: `10.1029/2005JD006354`.

[64] J. L. Fry et al. "Observations of gas- and aerosol-phase organic nitrates at BEACHON-RoMBAS 2011". In: *Atmospheric Chemistry and Physics* 13.17 (2013), pp. 8585–8605. ISSN: 16807316. DOI: `10.5194/acp-13-8585-2013`.

[65] J L Fry et al. "Organic nitrate and secondary organic aerosol yield from NO3 oxidation of β-pinene evaluated using a gas-phase kinetics/aerosol partitioning model". In: *Atmospheric Chemistry and Physics* 9.3 (2009), pp. 1431–1449.

[66] Juliane L. Fry et al. "Secondary Organic Aerosol Formation and Organic Nitrate Yield from NO3 Oxidation of Biogenic Hydrocarbons". In: *Environmental Science & Technology* 48.20 (2014), pp. 11944–11953. ISSN: 0013-936X. DOI: `10.1021/es502204x`. URL: `http://pubs.acs.org/doi/10.1021/es502204x`.

[67] Juliane L. Fry et al. "Secondary organic aerosol (SOA) yields from NO3 radical + isoprene based on nighttime aircraft power plant plume transects". In: *Atmospheric Chemistry and Physics* 18.16 (2018), pp. 11663–11682. ISSN: 16807324. DOI: `10.5194/acp-18-11663-2018`.

[68] Hendrik Fuchs et al. "A Sensitive and Versatile Detector for Atmospheric NO2 and NOx Based on Blue Diode Laser Cavity Ring-Down Spectroscopy". In: *Environmental Science & Technology* 43.20 (2009), pp. 7831–7836. ISSN: 0013-936X. DOI: `10.1021/es902067h`. URL: `http://pubs.acs.org/doi/abs/10.1021/es902067h`.

[69] Hendrik Fuchs et al. "Determination of Inlet Transmission and Conversion Efficiencies for in Situ Measurements of the Nocturnal Nitrogen Oxides, NO3, N2O5 and NO2, via Pulsed Cavity Ring-Down Spectroscopy". In: *Journal of Geophysical Research* 80.15 (2008), pp. 6010–6017. DOI: `10.1021/ac8007253`.

[70] Olga Garmash et al. "Multi-generation OH oxidation as a source for highly oxygenated organic molecules from aromatics". In: *Atmospheric Chemistry and Physics* 20.1 (2020), pp. 515–537. ISSN: 16807324. DOI: `10.5194/acp-20-515-2020`.

[71] Christoph Gerbig et al. "An improved fast-response vacuum-UV resonance fluorescence CO instrument". In: *Journal of Geophysical Research* 104 (1999), pp. 1699–1704. ISSN: 0148-0227. DOI: `10.1029/1998JD100031`.

[72] Georgios I. Gkatzelis et al. "Identifying Volatile Chemical Product Tracer Compounds in U.S. Cities". In: *Environmental Science and Technology* 55.1 (2021), pp. 188–199. ISSN: 15205851. DOI: `10.1021/acs.est.0c05467`.

[73] Allen. H. Goldstein and Ian E. Galbally. "Known and Unexplored Organic Constituents in the Earth's Atmosphere". In: *Environmental Science & Technology* (2007), pp. 1515–1521. DOI: 10.1021/es072476p.

[74] Wendy S. Goliff, William R. Stockwell, and Charlene V. Lawson. "The regional atmospheric chemistry mechanism, version 2". In: *Atmospheric Environment* 68 (2013), pp. 174–185. ISSN: 13522310. DOI: 10.1016/j.atmosenv.2012.11.038.

[75] J A de Gouw et al. "Budget of organic carbon in a polluted atmosphere : Results from the New England Air Quality Study in 2002". In: *Journal of Geophysical Research* 110.D16305 (2005), pp. 1–22. DOI: 10.1029/2004JD005623.

[76] J A de Gouw et al. "Sources of particulate matter in the northeastern United States in summer: 1 . Direct emissions and secondary formation of organic matter in urban plumes". In: *Journal of Geophysical Research* 113 (2008), pp. 1–19. DOI: 10.1029/2007JD009243.

[77] A. P. Grieshop et al. "Laboratory investigation of photochemical oxidation of organic aerosol from wood fires 1: Measurement and simulation of organic aerosol evolution". In: *Atmospheric Chemistry and Physics* 9.4 (2009), pp. 1263–1277. ISSN: 16807324. DOI: 10.5194/acp-9-1263-2009.

[78] A B Guenther et al. "Model Development The Model of Emissions of Gases and Aerosols from Nature version 2.1 (MEGAN2. 1): an extended and updated framework for modeling biogenic emissions". In: *Geoscientific Model Development* 5 (2012), pp. 1471–1492. DOI: 10.5194/gmd-5-1471-2012.

[79] Hongyu Guo et al. "Fine particle pH and the partitioning of nitric acid during winter in the northeastern United States". In: *Journal of Geophysical Research* 121.17 (2016), pp. 10355–10376. ISSN: 21562202. DOI: 10.1002/2016JD025311.

[80] M Hallquist et al. "The formation , properties and impact of secondary organic aerosol : current and emerging issues". In: *Atmospheric Chemistry and Physics* 9 (2009), pp. 5155–5236.

[81] L. Q. Hao et al. "Atmospheric submicron aerosol composition and particulate organic nitrate formation in a boreal forestland-urban mixed region". In: *Atmospheric Chemistry and Physics* 14.24 (2014), pp. 13483–13495. ISSN: 16807324. DOI: 10.5194/acp-14-13483-2014.

[82] P L Hayes et al. "Modeling the formation and aging of secondary organic aerosols in Los Angeles during CalNex 2010". In: *Atmospheric Chemistry and Physics* 15 (2015), pp. 5773–5801. DOI: 10.5194/acp-15-5773-2015.

[83] Colette L Heald et al. "A large organic aerosol source in the free troposphere missing from current models". In: *Geophysical Research Letters* 32.L18809 (2005), pp. 1–4. DOI: 10.1029/2005GL023831.

[84] Colette L Heald et al. "A simplified description of the evolution of organic aerosol composition in the atmosphere". In: *Geophysical Research Letters* 37.L08803 (2010), pp. 1–5. DOI: 10.1029/2010GL042737.

[85] W Hinds. *Aerosol Technology: Properties, Behavior, and Measurement of Airborne Particles.* New York: Wiley-Interscience, 1998.

[86] A. Hodzic et al. "Modeling organic aerosols in a megacity: Potential contribution of semi-volatile and intermediate volatility primary organic compounds to secondary organic aerosol formation". In: *Atmospheric Chemistry and Physics* 10.12 (2010), pp. 5491–5514. ISSN: 16807316. DOI: 10.5194/acp-10-5491-2010.

[87] Alma Hodzic et al. "Characterization of organic aerosol across the global remote troposphere: A comparison of ATom measurements and global chemistry models". In: *Atmospheric Chemistry and Physics* 20.8 (2020), pp. 4607–4635. ISSN: 16807324. DOI: 10.5194/acp-20-4607-2020.

[88] Larry W. Horowitz et al. "Observational constraints on the chemistry of isoprene nitrates over the eastern United States". In: *Journal of Geophysical Research Atmospheres* 112.12 (2007), pp. 1–13. ISSN: 01480227. DOI: 10.1029/2006JD007747.

[89] Marc R. Houyoux et al. "Emission inventory development and processing for the Seasonal Model for Regional Air Quality (SMRAQ) project". In: *Journal of Geophysical Research Atmospheres* 105.D7 (2000), pp. 9079–9090. ISSN: 01480227. DOI: 10.1029/1999JD900975.

[90] Wei Huang et al. "Chemical Characterization of Highly Functionalized Organonitrates Contributing to Night-Time Organic Aerosol Mass Loadings and Particle Growth". In: *Environmental Science and Technology* 53.3 (2019), pp. 1165–1174. ISSN: 15205851. DOI: 10.1021/acs.est.8b05826.

[91] R. C. Hudman et al. "Steps towards a mechanistic model of global soil nitric oxide emissions: Implementation and space based-constraints". In: *Atmospheric Chemistry and Physics* 12.16 (2012), pp. 7779–7795. ISSN: 16807316. DOI: 10.5194/acp-12-7779-2012.

[92] M E Jenkin, J C Young, and A R Rickard. "The MCM v3.3.1 degradation scheme for isoprene". In: *Atmos. Chem. Phys* 15 (2015), pp. 11433–11459. DOI: 10.5194/acp-15-11433-2015. URL: www.atmos-chem-phys.net/15/11433/2015/.

[93] M E Jenkin et al. "Protocol for the development of the Master Chemical Mechanism, MCM v3 (Part B): tropospheric degradation of aromatic volatile organic compounds". In: *Atmospheric Chemistry and Physics* 3 (2003), pp. 181–193. URL: www.atmos-chem-phys.org/acp/3/181/.

[94] Michael E Jenkin, Sandra M Saunders, and Michael J Pilling. "The tropospheric degradation of volatile organic compounds: a protocol for mechanism development". In: *Atmospheric Environment* 31.1 (1997), pp. 81–104.

[95] J L Jimenez et al. "Evolution of Organic Aerosols in the Atmosphere". In: *Science* 326 (2009), pp. 1525–1530.

[96] Carolyn E. Jordan et al. "Investigation of factors controlling PM2.5 variability across the South Korean Peninsula during KORUS-AQ". In: *Elementa: Science of the Anthropocene* 8 (2020). ISSN: 2325-1026. DOI: `10.1525/elementa.424`.

[97] James T. Kelly et al. "Assessing PM2.5 model performance for the conterminous U.S. with comparison to model performance statistics from 2007-2015". In: *Atmospheric Environment* 214.May (2019), p. 116872. ISSN: 18732844. DOI: `10.1016/j.atmosenv.2019.116872`. URL: `https://doi.org/10.1016/j.atmosenv.2019.116872`.

[98] Hannah S. Kenagy et al. "NOx Lifetime and NOy Partitioning During WINTER". In: *Journal of Geophysical Research: Atmospheres* 123.17 (2018), pp. 9813–9827. ISSN: 21698996. DOI: `10.1029/2018JD028736`.

[99] J P Kercher, T P Riedel, and J A Thornton. "Chlorine activation by N2O5: simultaneous, in situ detection of ClNO2 and N2O5 by chemical ionization mass spectrometry". In: *Atmos. Meas. Tech* 2 (2009), pp. 193–204. URL: `www.atmos-meas-tech.net/2/193/2009/`.

[100] A. Kiendler-Scharr et al. "Ubiquity of organic nitrates from nighttime chemistry in the European submicron aerosol". In: *Geophysical Research Letters* 43.14 (2016), pp. 7735–7744. ISSN: 19448007. DOI: `10.1002/2016GL069239`.

[101] Hyun Cheol Kim et al. "Regional contributions to particulate matter concentration in the Seoul metropolitan area , South Korea : seasonal variation and sensitivity to meteorology and emissions inventory". In: *Atmospheric Chemistry and Physics* 17 (2017), pp. 10315–10332.

[102] Si Wan Kim et al. "Satellite-observed U.S. power plant NOx emission reductions and their impact on air quality". In: *Geophysical Research Letters* 33.22 (2006), pp. 1–5. ISSN: 00948276. DOI: `10.1029/2006GL027749`.

[103] Jesse H. Kroll et al. "Chamber studies of secondary organic aerosol growth by reactive uptake of simple carbonyl compounds". In: *Journal of Geophysical Research Atmospheres* 110.23 (2005), pp. 1–10. ISSN: 01480227. DOI: `10.1029/2005JD006004`.

[104] R. von Kuhlmann et al. "Sensitivities in global scale modeling of isoprene". In: *Atmospheric Chemistry and Physics* 4 (2004), pp. 1–17. DOI: `10.5194/acp-4-1-2004`.

[105] A. J. Kwan et al. "Peroxy radical chemistry and OH radical production during the NO3-initiated oxidation of isoprene". In: *Atmospheric Chemistry and Physics* 12.16 (2012), pp. 7499–7515. ISSN: 16807316. DOI: `10.5194/acp-12-7499-2012`.

[106] B. W. LaFranchi et al. "Closing the peroxy acetyl (PA) radical budget: observations of acyl peroxy nitrates (PAN, PPN, and MPAN) during BEARPEX 2007". In: *Atmospheric Chemistry and Physics* 9.2 (2009), pp. 9879–9926. ISSN: 1680-7375. DOI: `10.5194/acpd-9-9879-2009`. URL: `http://www.atmos-chem-phys-discuss.net/9/9879/2009/`.

[107] Joshua L. Laughner and Ronald C. Cohen. "Direct observation of changing NOx lifetime in North American cities". In: *Science* 366 (2019), pp. 723–727.

[108] Alex K. Y. Lee et al. "A Large Contribution of Anthropogenic Organo-Nitrates to Secondary Organic Aerosol in the Alberta Oil Sands". In: *Atmospheric Chemistry and Physics* 19 (2019), pp. 12209–12219. ISSN: 1680-7375. DOI: 10.5194/acp-19-12209-2019.

[109] Ben H Lee et al. "An Iodide-Adduct High-Resolution Time-of-Flight Chemical-Ionization Mass Spectrometer: Application to Atmospheric Inorganic and Organic Compounds". In: *Environmental Science and Technology* 48 (2014), pp. 6309–6317. DOI: 10.1021/es500362a. URL: http://pubs.acs.org/doi/pdf/10.1021/es500362a.

[110] Ben H. Lee et al. "Highly functionalized organic nitrates in the southeast United States: Contribution to secondary organic aerosol and reactive nitrogen budgets". In: *Proceedings of the National Academy of Sciences* 113.6 (2016), pp. 1516–1521. ISSN: 0027-8424. DOI: 10.1073/pnas.1508108113. URL: http://www.pnas.org/lookup/doi/10.1073/pnas.1508108113.

[111] L. Lee et al. "Low temperatures enhance organic nitrate formation: Evidence from observations in the 2012 Uintah Basin Winter Ozone Study". In: *Atmospheric Chemistry and Physics* 14.22 (2014), pp. 12441–12454. ISSN: 16807324. DOI: 10.5194/acp-14-12441-2014.

[112] L Lee et al. "Particulate organic nitrates observed in an oil and natural gas production region during wintertime". In: *Atmos. Chem. Phys* 15 (2015), pp. 9313–9325. DOI: 10.5194/acp-15-9313-2015. URL: www.atmos-chem-phys.net/15/9313/2015/.

[113] J. Lelieveld et al. "The contribution of outdoor air pollution sources to premature mortality on a global scale". In: *Nature* 525.7569 (2015), pp. 367–371. ISSN: 14764687. DOI: 10.1038/nature15371.

[114] D. H. Lenschow, R. Pearson, and B. B. Stankov. "Estimating the ozone budget in the boundary layer by use of aircraft measurements of ozone eddy flux and mean concentration". In: *Journal of Geophysical Research* 86.8 C (1981), pp. 7291–7297. ISSN: 01480227. DOI: 10.1029/jc086ic08p07291.

[115] Sirakarn Leungsakul, Harvey E. Jeffries, and Richard M. Kamens. "A kinetic mechanism for predicting secondary aerosol formation from the reactions of d-limonene in the presence of oxides of nitrogen and natural sunlight". In: *Atmospheric Environment* 39.37 (2005), pp. 7063–7082. ISSN: 13522310. DOI: 10.1016/j.atmosenv.2005.08.024.

[116] Jonathan Liebmann et al. "Alkyl nitrates in the boreal forest: Formation via the NO3, OH and O3 induced oxidation of BVOCs and ambient lifetimes". In: *Atmospheric Chemistry and Physics* 19 (2019), pp. 10391–10403. ISSN: 1680-7324. DOI: 10.5194/acp-19-10391-2019.

[117] Jonathan Liebmann et al. "Direct measurement of NO3 radical reactivity in a boreal forest". In: *Atmospheric Chemistry and Physics* 3 (2018), pp. 1–34. ISSN: 1680-7375. DOI: 10.5194/acp-2017-975. URL: https://www.atmos-chem-phys-discuss.net/acp-2017-975/.

[118] Jonathan M. Liebmann et al. "Direct measurements of NO3 reactivity in and above the boundary layer of a mountaintop site: Identification of reactive trace gases and comparison with OH reactivity". In: *Atmospheric Chemistry and Physics* 18.16 (2018), pp. 12045–12059. ISSN: 16807324. DOI: 10.5194/acp-18-12045-2018.

[119] Prettiny K Ma et al. "Evaluating the impact of new observational constraints on P-S/IVOC emissions, multi-generation oxidation, and chamber wall losses on SOA modeling for Los Angeles, CA". In: *Atmospheric Chemistry and Physics* 17 (2017), pp. 9237–9259. DOI: 10.5194/acp-17-9237-2017.

[120] Juliana Maantay. "Asthma and air pollution in the Bronx: Methodological and data considerations in using GIS for environmental justice and health research". In: *Health and Place* 13.1 (2007), pp. 32–56. ISSN: 13538292. DOI: 10.1016/j.healthplace.2005.09.009.

[121] H.L. Macintyre and M.J. Evans. "Sensitivity of a global model to the uptake of N2O5 by tropospheric aerosol". In: *Atmospheric Chemistry and Physics* 10 (2010), pp. 7409–7414. DOI: 10.5194/acp-10-7409-2010. URL: https://www.atmos-chem-phys.net/10/7409/2010/acp-10-7409-2010.pdf.

[122] J. Mao et al. "Chemistry of hydrogen oxide radicals (HOx) in the Arctic troposphere in spring". In: *Atmospheric Chemistry and Physics* 10.13 (2010), pp. 5823–5838. ISSN: 16807316. DOI: 10.5194/acp-10-5823-2010.

[123] Brian C. McDonald et al. "Volatile chemical products emerging as largest petrochemical source of urban organic emissions". In: *Science* 359.6377 (2018), pp. 760–764. ISSN: 10959203. DOI: 10.1126/science.aaq0524.

[124] Erin E. McDuffie et al. "Heterogeneous N2O5 Uptake During Winter: Aircraft Measurements During the 2015 WINTER Campaign and Critical Evaluation of Current Parameterizations". In: *Journal of Geophysical Research: Atmospheres* 123 (2018), pp. 1–28. DOI: 10.1002/2018JD028336.

[125] Cameron S. McNaughton et al. "Results from the DC-8 inlet characterization experiment (DICE): Airborne versus surface sampling of mineral dust and sea salt aerosols". In: *Aerosol Science and Technology* 41.2 (2007), pp. 136–159. ISSN: 02786826. DOI: 10.1080/02786820601118406.

[126] A. K. Mebust and Ronald C. Cohen. "Space-based observations of fire NOx emission coefficients: A global biome-scale comparison". In: *Atmospheric Chemistry and Physics* 14.5 (2014), pp. 2509–2524. ISSN: 16807316. DOI: 10.5194/acp-14-2509-2014.

[127] Keren Mezuman, Susanne E. Bauer, and Kostas Tsigaridis. "Evaluating secondary inorganic aerosols in three dimensions". In: *Atmospheric Chemistry and Physics* 16.16 (2016), pp. 10651–10669. ISSN: 16807324. DOI: `10.5194/acp-16-10651-2016`.

[128] Paulette Middleton, William R. Stockwell, and William P.L. Carter. "Aggregation and analysis of volatile organic compound emissions for regional modeling". In: *Atmospheric Environment Part A, General Topics* 24.5 (1990), pp. 1107–1133. ISSN: 09601686. DOI: `10.1016/0960-1686(90)90077-Z`.

[129] Dev E. Millstein and Robert A. Harley. "Effects of retrofitting emission control systems on in-use heavy diesel vehicles". In: *Environmental Science and Technology* 44.13 (2010), pp. 5042–5048. ISSN: 0013936X. DOI: `10.1021/es1006669`.

[130] Marie Lynn Miranda et al. "Making the environmental justice grade: The relative burden of air pollution exposure in the United States". In: *International Journal of Environmental Research and Public Health* 8.6 (2011), pp. 1755–1771. ISSN: 16604601. DOI: `10.3390/ijerph8061755`.

[131] Andrea Molod et al. *The GEOS-5 atmospheric general circulation model: Mean climate and development from MERRA to Fortuna.* Ed. by M.J. Suarez. Vol. 28. Goddard Space Flight Center, Greenbelt, MD: National Aeronautics and Space Administration, 2012. ISBN: 2012104606. URL: `http://gmao.gsfc.nasa.gov/pubs/docs/tm28.pdf`.

[132] D M Murphy et al. "Single-particle mass spectrometry of tropospheric aerosol particles". In: *Journal of Geophysical Research* 111.D23S32 (2006), pp. 1–15. DOI: `10.1029/2006JD007340`.

[133] J G Murphy et al. "Observations of the diurnal and seasonal trends in nitrogen oxides in the western Sierra Nevada". In: *Atmos. Chem. Phys. Atmospheric Chemistry and Physics* 6 (2006), pp. 5321–5338. URL: `www.atmos-chem-phys.net/6/5321/2006/`.

[134] Anke Mutzel et al. "Highly Oxidized Multifunctional Organic Compounds Observed in Tropospheric Particles: A Field and Laboratory Study". In: *Environmental Science and Technology* 49.13 (2015), pp. 7754–7761. ISSN: 15205851. DOI: `10.1021/acs.est.5b00885`.

[135] Benjamin A Nault et al. "Secondary organic aerosol production from local emissions dominates the organic aerosol budget over Seoul, South Korea, during KORUS-AQ". In: *Atmospheric Chemistry and Physics* 18 (2018), pp. 17769–17800. DOI: `10.5194/acp-18-17769-2018`.

[136] J. Andy Neuman et al. "Reactive nitrogen transport and photochemistry in urban plumes over the North Atlantic Ocean". In: *Journal of Geophysical Research Atmospheres* 111.23 (2006), pp. 1–11. ISSN: 01480227. DOI: `10.1029/2005JD007010`.

[137] N. L. Ng et al. "Secondary organic aerosol (SOA) formation from reaction of isoprene with nitrate radicals (NO3)". In: *Atmospheric Chemistry and Physics* 8.14 (2008), pp. 4117–4140. ISSN: 16807324. DOI: `10.5194/acp-8-4117-2008`.

[138] Nga Lee Ng et al. "Nitrate radicals and biogenic volatile organic compounds: Oxidation, mechanisms, and organic aerosol". In: *Atmospheric Chemistry and Physics* 17.3 (2017), pp. 2103–2162. ISSN: 16807324. DOI: 10.5194/acp-17-2103-2017.

[139] L. J. Nunnermacker et al. "NOy lifetimes and O3 production efficiencies in urban and power plant plumes: Analysis of field data". In: *Journal of Geophysical Research* 105 (2000), p. 9165. ISSN: 0148-0227. DOI: 10.1029/1999JD900753.

[140] Clara M. Nussbaumer and Ronald C. Cohen. "Impact of OA on the Temperature Dependence of PM 2.5 in the Los Angeles Basin". In: *Environmental Science & Technology* 55.6 (2021), pp. 3549–3558. ISSN: 0013-936X. DOI: 10.1021/acs.est.0c07144.

[141] Clara M. Nussbaumer and Ronald C. Cohen. "The Role of Temperature and NOx in Ozone Trends in the Los Angeles Basin". In: *Environmental Science and Technology* 54.24 (2020), pp. 15652–15659. ISSN: 15205851. DOI: 10.1021/acs.est.0c04910.

[142] Amber M. Ortega et al. "Real-time measurements of secondary organic aerosol formation and aging from ambient air in an oxidation flow reactor in the Los Angeles area". In: *Atmospheric Chemistry and Physics* 16.11 (2016), pp. 7411–7433. ISSN: 16807324. DOI: 10.5194/acp-16-7411-2016.

[143] T. L. Otte and J. E. Pleim. "The Meteorology-Chemistry Interface Processor (MCIP) for the CMAQ modeling system: Updates through MCIPv3.4.1". In: *Geoscientific Model Development* 3.1 (2010), pp. 243–256. ISSN: 19919603. DOI: 10.5194/gmd-3-243-2010.

[144] Demetrios Pagonis et al. "Effects of gas-wall partitioning in Teflon tubing and instrumentation on time-resolved measurements of gas-phase organic compounds". In: *Atmospheric Measurement Techniques* 10.12 (2017), pp. 4687–4696. ISSN: 18678548. DOI: 10.5194/amt-10-4687-2017.

[145] J. F. Pankow and W. E. Asher. "SIMPOL.1: A simple group contribution method for predicting vapor pressures and enthalpies of vaporization of multifunctional organic compounds". In: *Atmospheric Chemistry and Physics* 8.10 (2008), pp. 2773–2796. ISSN: 16807324. DOI: 10.5194/acp-8-2773-2008.

[146] James F. Pankow. "An absorption model of the gas/aerosol partitioning involved in the formation of secondary organic aerosol". In: *Atmospheric Environment* 28.2 (1994), pp. 189–193. ISSN: 13522310. DOI: 10.1016/j.atmosenv.2007.10.060.

[147] Moon-soo Park et al. "High-resolution urban observation network for user-specific meteorological information service in the Seoul Metropolitan Area , South Korea". In: *Atmospheric Measurement Techniques* 10 (2017), pp. 1575–1594. DOI: 10.5194/amt-10-1575-2017.

[148] J. P. Parrella et al. "Tropospheric bromine chemistry: Implications for present and pre-industrial ozone and mercury". In: *Atmospheric Chemistry and Physics* 12.15 (2012), pp. 6723–6740. ISSN: 16807316. DOI: 10.5194/acp-12-6723-2012.

[149] David D. Parrish et al. "Air quality progress in North American megacities: A review". In: *Atmospheric Environment* 45.39 (2011), pp. 7015–7025. ISSN: 13522310. DOI: 10.1016/j.atmosenv.2011.09.039. URL: http://dx.doi.org/10.1016/j.atmosenv.2011.09.039.

[150] Fabien Paulot et al. "Isoprene photooxidation: new insights into the production of acids and organic nitrates". In: *Atmospheric Chemistry and Physics* 9 (2009), pp. 1479–1501. URL: www.atmos-chem-phys.net/9/1479/2009/.

[151] Fabien Paulot et al. "Unexpected Epoxide Formation in the Gas-Phase Photooxidation of Isoprene". In: *Science* 325 (2009), pp. 730–734. DOI: 10.1126/science.1172910.

[152] A. E. Perring, S. E. Pusede, and Ronald C. Cohen. "An Observational Perspective on the Atmospheric Impacts of Alkyl and Multifunctional Nitrates on Ozone and Secondary Organic Aerosol". In: *Chemical Reviews* 113.8 (Aug. 2013), pp. 5848–5870. ISSN: 0009-2665. DOI: 10.1021/cr300520x. URL: http://pubs.acs.org/doi/abs/10.1021/cr300520x.

[153] A E Perring et al. "Airborne observations of total RONO2 : new constraints on the yield and lifetime of isoprene nitrates". In: 9 (2009), pp. 1451–1463.

[154] A. E. Perring et al. "The production and persistence of ΣRONO2 in the Mexico City plume". In: *Atmospheric Chemistry and Physics* 10.15 (2010), pp. 7215–7229. ISSN: 16807316. DOI: 10.5194/acp-10-7215-2010. URL: http://www.atmos-chem-phys.net/10/7215/2010/acp-10-7215-2010.pdf.

[155] C. Arden Pope, Majid Ezzati, and Douglas W. Dockery. "Fine-Particulate Air Pollution and Life Expectancy in the United States". In: *New England Journal of Medicine* 360.4 (2009), pp. 376–386. ISSN: 0028-4793. DOI: 10.1056/nejmsa0805646.

[156] S. E. Pusede et al. "On the temperature dependence of organic reactivity, nitrogen oxides, ozone production, and the impact of emission controls in San Joaquin Valley, California". In: *Atmospheric Chemistry and Physics* 14.7 (2014), pp. 3373–3395. ISSN: 16807324. DOI: 10.5194/acp-14-3373-2014.

[157] H. O.T. Pye and J. H. Seinfeld. "A global perspective on aerosol from low-volatility organic compounds". In: *Atmospheric Chemistry and Physics* 10.9 (2010), pp. 4377–4401. ISSN: 16807316. DOI: 10.5194/acp-10-4377-2010.

[158] Havala O.T. Pye et al. "Anthropogenic enhancements to production of highly oxygenated molecules from autoxidation". In: *Proceedings of the National Academy of Sciences of the United States of America* 116.14 (2019), pp. 6641–6646. ISSN: 10916490. DOI: 10.1073/pnas.1810774116.

[159] Havala O.T. Pye et al. "Modeling the Current and Future Roles of Particulate Organic Nitrates in the Southeastern United States". In: *Environmental Science and Technology* 49.24 (2015), pp. 14195–14203. ISSN: 15205851. DOI: 10.1021/acs.est.5b03738.

[160] B A Ridley et al. "Distributions of NO, NOx, NOy, and O3 to 12 km altitude during the summer monsoon season over New Mexico". In: *Journal of Geophysical Research: Atmospheres* 99.D12 (1994), pp. 25519–25534. ISSN: 0148-0227. DOI: 10.1029/94JD02210. URL: http://dx.doi.org/10.1029/94JD02210.

[161] Theran P. Riedel et al. "Chlorine activation within urban or power plant plumes: Vertically resolved ClNO2 and Cl2 measurements from a tall tower in a polluted continental setting". In: *Journal of Geophysical Research Atmospheres* 118.15 (2013), pp. 8702–8715. ISSN: 21698996. DOI: 10.1002/jgrd.50637.

[162] M.M. Rienecker et al. "The GEOS-5 Data Assimilation System - Documentation of Versions 5.01, 5.1.0, and 5.2.0". In: *NASA Technical Report Series on Global Modeling and Data Assimilation* 27 (2008), p. 101. URL: http://gmao.gsfc.nasa.gov/pubs/docs/tm28.pdf.

[163] Allen L. Robinson et al. "Rethinking organic aerosols: Semivolatile emissions and photochemical aging". In: *Science* 315.5816 (2007), pp. 1259–1262. ISSN: 00368075. DOI: 10.1126/science.1133061.

[164] Andrew W. Rollins et al. "Evidence for NOx Control over Nighttime SOA Formation". In: *Science* 337.6099 (2012), pp. 1210–1212. DOI: 10.1126/science.1221520. URL: http://science.sciencemag.org/content/sci/337/6099/1210.full.pdf.

[165] Andrew W. Rollins et al. "Gas/particle partitioning of total alkyl nitrates observed with TD-LIF in Bakersfield". In: *Journal of Geophysical Research Atmospheres* 118.12 (2013), pp. 6651–6662. ISSN: 21698996. DOI: 10.1002/jgrd.50522.

[166] Andrew W. Rollins et al. "Isoprene oxidation by nitrate radical: Alkyl nitrate and secondary organic aerosol yields". In: *Atmospheric Chemistry and Physics* 9.18 (2009), pp. 6685–6703. ISSN: 16807324. DOI: 10.5194/acp-9-6685-2009.

[167] Andrew W. Rollins et al. "Real time in situ detection of organic nitrates in atmospheric aerosols." In: *Environmental science & technology* 44.14 (2010), pp. 5540–5545. ISSN: 0013-936X. DOI: 10.1021/es100926x.

[168] Paul S. Romer et al. "Constraints on Aerosol Nitrate Photolysis as a Potential Source of HONO and NOx". In: *Environmental Science and Technology* 52.23 (2018), pp. 13738–13746. ISSN: 15205851. DOI: 10.1021/acs.est.8b03861.

[169] Paul S. Romer et al. "The lifetime of nitrogen oxides in an isoprene-dominated forest". In: *Atmospheric Chemistry and Physics* 16.12 (2016), pp. 7623–7637. ISSN: 16807324. DOI: 10.5194/acp-16-7623-2016.

[170] Paul S. Romer Present, Azimeh Zare, and Ronald C. Cohen. "The changing role of organic nitrates in the removal and transport of NOx". In: *Atmospheric Chemistry and Physics* 20 (2020), pp. 267–279. DOI: 10.5194/acp-20-267-2020.

[171] R. S. Rosen et al. "Observations of total alkyl nitrates during Texas Air Quality Study 2000: Implications for O3 and alkyl nitrate photochemistry". In: *Journal of Geophysical Research: Atmospheres* 109.7 (2004), pp. 1–15. ISSN: 01480227. DOI: 10.1029/2003jd004227.

[172] A R Russell, L C Valin, and Ronald C. Cohen. "Trends in OMI NO2 observations over the United States: effects of emission control technology and the economic recession". In: 12 (2012), pp. 12197–12209. DOI: 10.5194/acp-12-12197-2012.

[173] T. B. Ryerson. "Effect of petrochemical industrial emissions of reactive alkenes and NOx on tropospheric ozone formation in Houston, Texas". In: *Journal of Geophysical Research* 108.D8 (2003), p. 4249. ISSN: 0148-0227. DOI: 10.1029/2002JD003070. URL: http://doi.wiley.com/10.1029/2002JD003070.

[174] T. B. Ryerson, E. J. Williams, and F. C. Fehsenfeld. "An efficient photolysis system for fast-response NO2 measurements". In: *Journal of Geophysical Research Atmospheres* 105.D21 (2000), pp. 26447–26461. ISSN: 01480227. DOI: 10.1029/2000JD900389.

[175] T. B. Ryerson et al. "Emissions lifetimes and ozone formation in power plant plumes". In: *Journal of Geophysical Research* 103.D17 (1998), pp. 22569–22583. ISSN: 0148-0227. DOI: 10.1029/98JD01620.

[176] Thomas B. Ryerson et al. "Design and initial characterization of an inlet for gas-phase NOy measurements from aircraft". In: *Journal of Geophysical Research* 104.D5 (1999), pp. 5483–5492.

[177] G Sarwar et al. "A comparison of atmospheric composition using the Carbon Bond and Regional Atmospheric Chemistry Mechanisms". In: *Atmospheric Chemistry and Physics* 13 (2013), pp. 9695–9712. DOI: 10.5194/acp-13-9695-2013.

[178] S M Saunders et al. "Protocol for the development of the Master Chemical Mechanism, MCM v3 (Part A): tropospheric degradation of non-aromatic volatile organic compounds". In: *Atmospheric Chemistry and Physics* 3 (2003), pp. 161–180. URL: www.atmos-chem-phys.org/acp/3/161/.

[179] Manfred Schneider et al. "C1-C15 alkyl nitrates, benzyl nitrate, and bifunctional nitrates: Measurements in California and South Atlantic air and global comparison using C2Cl4 and CHBr3 as marker molecules". In: *Environmental Science and Technology* 32.20 (1998), pp. 3055–3062. ISSN: 0013936X. DOI: 10.1021/es980132g.

[180] Jason C. Schroder et al. "Sources and Secondary Production of Organic Aerosols in the Northeastern US during WINTER". In: *Journal of Geophysical Research: Atmospheres* submitted (2018).

[181] U. Schumann and H. Huntrieser. "The global lightning-induced nitrogen oxides source". In: *Atmospheric Chemistry and Physics* 7.14 (2007), pp. 3823–3907. ISSN: 16807324. DOI: 10.5194/acp-7-3823-2007.

[182] Dian J. Seidel et al. "Climatology of the planetary boundary layer over the continental United States and Europe". In: *Journal of Geophysical Research: Atmospheres* 117.D17106 (2012). ISSN: 01480227. DOI: 10.1029/2012JD018143. URL: http://doi.wiley.com/10.1029/2012JD018143.

[183] Manish Shrivastava et al. "Recent advances in understanding secondary organic aerosol: Implications for global climate forcing". In: *Reviews of Geophysics* 55 (2017), pp. 509–559. DOI: 10.1002/2016RG000540.

[184] Isobel J Simpson et al. "Boreal forest fire emissions in fresh Canadian smoke plumes: C1-C10 volatile organic compounds (VOCs), CO2, CO, NO2, NO, HCN, and CH3CH". In: *Atmos. Chem. Phys* 11 (2011), pp. 6445–6463. DOI: 10.5194/acp-11-6445-2011.

[185] Isobel J. Simpson et al. "Characterization, sources and reactivity of volatile organic compounds (VOCs) in Seoul and surrounding regions during KORUS-AQ". In: *Elementa: Science of the Anthropocene* 8 (2020). ISSN: 2325-1026. DOI: 10.1525/elementa.434.

[186] Nicolas Sobanski et al. "Day- and Night-time Formation of Organic Nitrates at a Forested Mountain-site in South West Germany". In: *Atmospheric Chemistry and Physics* 17 (2017), pp. 4115–4130. DOI: 10.5194/acp-17-4115-2017.

[187] M. Spittler et al. "Reactions of NO3 radicals with limonene and α-pinene: Product and SOA formation". In: *Atmospheric Environment* 40.3 (2006), pp. 116–127. ISSN: 13522310. DOI: 10.1016/j.atmosenv.2005.09.093.

[188] T. K. Starn et al. "Nighttime isoprene chemistry at an urban-impacted forest site". In: *Journal of Geophysical Research Atmospheres* 103.D17 (1998), pp. 22437–22447. ISSN: 01480227. DOI: 10.1029/98JD01201.

[189] D. Stone et al. "Radical chemistry at night: Comparisons between observed and modelled HOx, NO3 and N2O5 during the RONOCO project". In: *Atmospheric Chemistry and Physics* 14.3 (2014), pp. 1299–1321. ISSN: 16807316. DOI: 10.5194/acp-14-1299-2014.

[190] J. Walter Strapp, W. R. Leaitch, and P. S. K. Liu. "Hydrated and Dried Aerosol-Size-Distribution Measurements from the Particle Measuring Systems FSSP-300 Probe and the Deiced PCASP-100X Probe". In: *Journal of Atmospheric and Oceanic Technology* 9.5 (1992), pp. 548–555. ISSN: 0739-0572. DOI: 10.1175/1520-0426(1992)009<0548:HADASD>2.0.CO;2.

[191] A G Sutugin and N A Fuchs. "Formation of condensation aerosols under rapidly changing environmental conditions: theory and method of calculation". In: *Aerosol Science* (1970), pp. 287–293.

[192] Alexander P. Teng, John D. Crounse, and Paul O. Wennberg. "Isoprene Peroxy Radical Dynamics". In: *Journal of the American Chemical Society* 139.15 (2017), pp. 5367–5377. ISSN: 15205126. DOI: 10.1021/jacs.6b12838.

[193] J. Thieser et al. "A two-channel thermal dissociation cavity ring-down spectrometer for the detection of ambient NO2, RO2NO2 and RONO2". In: *Atmospheric Measurement Techniques* 9.2 (2016), pp. 553–576. ISSN: 18678548. DOI: `10.5194/amt-9-553-2016`.

[194] Owen B. Toon et al. "Planning, implementation, and scientific goals of the Studies of Emissions and Atmospheric Composition, Clouds and Climate Coupling by Regional Surveys (SEAC4RS) field mission". In: *Journal of Geophysical Research: Atmospheres* 121 (2016), pp. 4967–5009. DOI: `10.1002/2015JD024297`.

[195] Katherine R. Travis et al. "Why do models overestimate surface ozone in the Southeast United States?" In: *Atmospheric Chemistry and Physics* 16.21 (2016), pp. 13561–13577. ISSN: 16807324. DOI: `10.5194/acp-16-13561-2016`.

[196] Jasmin Tröstl et al. "The role of low-volatility organic compounds in initial particle growth in the atmosphere". In: *Nature* 533.7604 (2016), pp. 527–531. ISSN: 14764687. DOI: `10.1038/nature18271`.

[197] Epameinondas Tsiligiannis et al. "Effect of NOx on 1,3,5-trimethylbenzene (TMB) oxidation product distribution and particle formation". In: *Atmospheric Chemistry and Physics* 19 (2019), pp. 15073–15086. ISSN: 1680-7316. DOI: `10.5194/acp-19-15073-2019`.

[198] Alexandra P Tsimpidi et al. "Global-scale combustion sources of organic aerosols : sensitivity to formation and removal mechanisms". In: *Atmospheric Chemistry and Physics* 17 (2017), pp. 7345–7364. DOI: `10.5194/acp-17-7345-2017`.

[199] G. S. Tyndall et al. "Atmospheric chemistry of small organic peroxy radicals". In: *Journal of Geophysical Research* 106.D11 (2001), pp. 12157–12182. ISSN: 0148-0227. DOI: `10.1029/2000JD900746`. URL: `http://doi.wiley.com/10.1029/2000JD900746`.

[200] L. C. Valin, A. R. Russell, and Ronald C. Cohen. "Variations of OH radical in an urban plume inferred from NO2 column measurements". In: *Geophysical Research Letters* 40.9 (2013), pp. 1856–1860. ISSN: 00948276. DOI: `10.1002/grl.50267`.

[201] Rainer Volkamer et al. "Secondary organic aerosol formation from anthropogenic air pollution : Rapid and higher than expected". In: *Geophysical Research Letters* 33.L17811 (2006), pp. 1–4. DOI: `10.1029/2006GL026899`.

[202] S. L. Von Der Weiden, F. Drewnick, and S. Borrmann. "Particle Loss Calculator - A new software tool for the assessment of the performance of aerosol inlet systems". In: *Atmospheric Measurement Techniques* 2.2 (2009), pp. 479–494. ISSN: 18678548. DOI: `10.5194/amt-2-479-2009`.

[203] N. L. Wagner et al. "The sea breeze/land breeze circulation in Los Angeles and its influence on nitryl chloride production in this region". In: *Journal of Geophysical Research Atmospheres* 117.22 (2012), pp. 1–15. ISSN: 01480227. DOI: `10.1029/2012JD017810`.

[204] Nicholas L. Wagner et al. "Diode laser-based cavity ring-down instrument for NO3, N2O5, NO, NO2 and O3 from aircraft". In: *Atmos. Meas. Tech* 4 (2011), pp. 1227–1240. DOI: 10.5194/amt-4-1227-2011. URL: www.atmos-meas-tech.net/4/1227/2011/.

[205] Nicholas L. Wagner et al. "N2O5 uptake coefficients and nocturnal NO2 removal rates determined from ambient wintertime measurements". In: *Journal of Geophysical Research Atmospheres* 118.16 (2013), pp. 9331–9350. ISSN: 21698996. DOI: 10.1002/jgrd.50653.

[206] Sainan Wang et al. "Formation of Highly Oxidized Radicals and Multifunctional Products from the Atmospheric Oxidation of Alkylbenzenes". In: *Environmental Science and Technology* 51.15 (2017), pp. 8442–8449. ISSN: 15205851. DOI: 10.1021/acs.est.7b02374.

[207] R. A. Washenfelder et al. "Measurement of atmospheric ozone by cavity ring-down spectroscopy". In: *Environmental Science & Technology* 45 (2011), pp. 2938–2944. ISSN: 1520-5851. DOI: 10.1021/es103340u. URL: http://www.ncbi.nlm.nih.gov/pubmed/21366216.

[208] Rodney J Weber et al. "A study of secondary organic aerosol formation in the anthropogenic-influenced southeastern United States". In: *Journal of Geophysical Research* 112.D13302 (2007), pp. 1–13. DOI: 10.1029/2007JD008408.

[209] A. J. Weinheimer et al. "Meridional distributions of NOx, NOy, and other species in the lower stratosphere and upper troposphere during AASE II". In: *Geophysical Research Letters* 21.23 (1994), pp. 2583–2586. ISSN: 19448007. DOI: 10.1029/94GL01897.

[210] Paul O. Wennberg et al. "Gas-Phase Reactions of Isoprene and Its Major Oxidation Products". In: *Chemical Reviews* 118.7 (2018), pp. 3337–3390. ISSN: 15206890. DOI: 10.1021/acs.chemrev.7b00439.

[211] Alfred Wiedensohler. "An approximation of the bipolar charge distribution for particles in the submicron size range". In: *Journal of Aerosol Science* 19.3 (1988), pp. 387–389. ISSN: 10970290.

[212] C Wiedinmyer et al. "Model Development The Fire INventory from NCAR (FINN): a high resolution global model to estimate the emissions from open burning". In: *Geoscientific Model Development* 4 (2011), pp. 625–641. DOI: 10.5194/gmd-4-625-2011.

[213] R. J. Wild et al. "Reactive nitrogen partitioning and its relationship to winter ozone events in Utah". In: *Atmospheric Chemistry and Physics* 16.2 (2016), pp. 573–583. ISSN: 16807324. DOI: 10.5194/acp-16-573-2016.

[214] Robert J. Wild et al. "A measurement of total reactive nitrogen, NOy, together with NO2, NO, and O3 via cavity ring-down spectroscopy". In: *Environmental Science and Technology* 48.16 (2014), pp. 9609–9615. ISSN: 15205851. DOI: 10.1021/es501896w.

[215] Edmond W Wilson et al. "Measurement and Estimation of Rate Constants for the Reactions of Hydroxyl Radical with Several Alkanes and Cycloalkanes". In: *Journal of Physical Chemistry A* 110 (2006), pp. 3593–3604. DOI: 10.1021/jp055841c. URL: http://pubs.acs.org/doi/pdf/10.1021/jp055841c.

[216] Caroline C Womack et al. "Evaluation of the accuracy of thermal dissociation CRDS and LIF techniques for atmospheric measurement of reactive nitrogen species". In: *Atmospheric Chemistry and Physics* 2 (2017), pp. 1911–1926. DOI: 10.5194/amt-10-1911-2017.

[217] Jung Hun Woo et al. "Development of the CREATE inventory in support of integrated climate and air quality modeling for Asia". In: *Sustainability (Switzerland)* 12.19 (2020). ISSN: 20711050. DOI: 10.3390/SU12197930.

[218] Matthew C Woody et al. "Understanding sources of organic aerosol during CalNex-2010 using the CMAQ-VBS". In: *Atmospheric Chemistry and Physics* 16 (2016), pp. 4081–4100. DOI: 10.5194/acp-16-4081-2016.

[219] P. J. Wooldridge et al. "Total Peroxy Nitrates (ΣPNs) in the atmosphere: The Thermal Dissociation-Laser Induced Fluorescence (TD-LIF) technique and comparisons to speciated PAN measurements". In: *Atmospheric Measurement Techniques* 3.3 (2010), pp. 593–607. ISSN: 18671381. DOI: 10.5194/amt-3-593-2010.

[220] Andrew S. Wozniak, James E. Bauer, and Rebecca M. Dickhut. "Characteristics of water-soluble organic carbon associated with aerosol particles in the eastern United States". In: *Atmospheric Environment* 46 (2012), pp. 181–188. ISSN: 13522310. DOI: 10.1016/j.atmosenv.2011.10.001. URL: http://dx.doi.org/10.1016/j.atmosenv.2011.10.001.

[221] K. Wyat Appel et al. "Overview and evaluation of the community multiscale air quality (CMAQ) modeling system version 5.2". In: *Springer Proceedings in Complexity* (2018), pp. 69–73. ISSN: 22138692. DOI: 10.1007/978-3-319-57645-9{_}11.

[222] F. Xiong et al. "Observation of isoprene hydroxynitrates in the Southeastern United States and implications for the fate of NOx". In: *Atmospheric Chemistry and Physics* 15 (2015), pp. 11257–11272. DOI: 10.5194/acp-15-11257-2015.

[223] L. Xu et al. "Aerosol characterization over the southeastern United States using high-resolution aerosol mass spectrometry: Spatial and seasonal variation of aerosol composition and sources with a focus on organic nitrates". In: *Atmospheric Chemistry and Physics* 15.13 (2015), pp. 7307–7336. ISSN: 16807324. DOI: 10.5194/acp-15-7307-2015.

[224] Lu Xu et al. "Effects of anthropogenic emissions on aerosol formation from isoprene and monoterpenes in the southeastern United States". In: *Proceedings of the National Academy of Sciences of the United States of America* 112.1 (2015), pp. 37–42. ISSN: 10916490. DOI: 10.1073/pnas.1417609112.

[225]   Weiqi Xu et al. "Estimation of particulate organic nitrates from thermodenuder-aerosol mass spectrometer measurements in the North China Plain". In: *Atmospheric Measurement Techniques* 14 (2021), pp. 3693–3705. ISSN: 18678548. DOI: 10.5194/amt-14-3693-2021.

[226]   Z. N. Xu et al. "Multifunctional products of isoprene oxidation in polluted atmosphere and their contribution to SOA". In: *Geophysical Research Letters* (2020), pp. 1–10. ISSN: 0094-8276. DOI: 10.1029/2020gl089276.

[227]   R. J. Yamartino. "A Comparison of Several "Single-Pass" Estimators of the Standard Deviation of Wind Direction". In: *Journal of Climate and Applied Meteorology* 23 (1984), pp. 1362–1366. DOI: 10.1175/1520-0450(1984)023<1362:ACOSPE>2.0.CO;2.

[228]   Derek York et al. "Unified equations for the slope, intercept, and standard errors of the best straight line". In: *American Journal of Physics* 72.3 (2004), pp. 367–375. ISSN: 0002-9505. DOI: 10.1119/1.1632486. URL: http://aapt.scitation.org/doi/10.1119/1.1632486.

[229]   Kuangyou Yu et al. "Characterization of nighttime formation of particulate organic nitrates based on high-resolution aerosol mass spectrometry in an urban atmosphere in China". In: *Atmospheric Chemistry and Physics* 19.7 (2019), pp. 5235–5249. ISSN: 16807324. DOI: 10.5194/acp-19-5235-2019.

[230]   Azimeh Zare et al. "A comprehensive organic nitrate chemistry: Insights into the lifetime of atmospheric organic nitrates". In: *Atmospheric Chemistry and Physics* 18.20 (2018), pp. 15419–15436. ISSN: 16807324. DOI: 10.5194/acp-18-15419-2018.

[231]   Azimeh Zare et al. "Vapor-Pressure Pathways Initiate but Hydrolysis Products Dominate the Aerosol Estimated from Organic Nitrates". In: *ACS Earth and Space Chemistry* 3 (2019), pp. 1426–1437. DOI: 10.1021/acsearthspacechem.9b00067.

[232]   J. K. Zhang et al. "Characterization of submicron particles during biomass burning and coal combustion periods in Beijing, China". In: *Science of the Total Environment* 562 (2016), pp. 812–821. ISSN: 18791026. DOI: 10.1016/j.scitotenv.2016.04.015.

[233]   Q Zhang et al. "Ubiquity and dominance of oxygenated species in organic aerosols in anthropogenically-influenced Northern Hemisphere midlatitudes". In: *Geophysical Research Letters* 34.L13801 (2007), pp. 1–6. DOI: 10.1029/2007GL029979.

[234]   Xuan Zhang et al. "Influence of vapor wall loss in laboratory chambers on yields of secondary organic aerosol". In: *Proceedings of the National Academy of Sciences of the United States of America* 111.16 (2014), pp. 5802–5807. ISSN: 10916490. DOI: 10.1073/pnas.1404727111.

[235]   Yunliang Zhao et al. "Intermediate-volatility organic compounds: A large source of secondary organic aerosol". In: *Environmental Science and Technology* 48.23 (2014), pp. 13743–13750. ISSN: 15205851. DOI: 10.1021/es5035188.

[236] Qiao Zhu et al. "Atmospheric aerosol compositions and sources at two national background sites in northern and southern China". In: *Atmospheric Chemistry and Physics* 16.15 (2016), pp. 10283–10297. ISSN: 16807324. DOI: 10.5194/acp-16-10283-2016.

[237] Qiao Zhu et al. "Characterization of Organic Aerosol at a Rural Site in the North China Plain Region: Sources, Volatility and Organonitrates". In: *Advances in Atmospheric Sciences* (2021). ISSN: 0256-1530. DOI: 10.1007/s00376-020-0127-2.

Appendix A

Supporting information for "NO_x lifetime and NO_y partitioning during WINTER"

A.1 Daytime production rate calculations

We calculate the daytime production of alkyl nitrates via Reaction R13 as

$$P(\Sigma \, \mathrm{ANs}) = \sum_i \alpha_i f_{\mathrm{NO}_i} k_{\mathrm{OH+RH_i}} [\mathrm{OH}][\mathrm{RH_i}] \tag{A.1}$$

where

$$f_{\mathrm{NO}_i} = \frac{k_{\mathrm{RO_{2i}+NO}}[\mathrm{NO}]}{k_{\mathrm{RO_{2i}+NO}}[\mathrm{NO}] + k_{\mathrm{RO_{2i}+HO_2}}[\mathrm{HO_2}] + k_{\mathrm{RO_{2i}+RO_2}}[\mathrm{RO_2}]} \approx 1 \text{ during WINTER} \tag{A.2}$$

We approximate $f_{\mathrm{NO}} \approx 1$ since $[\mathrm{NO}] \gg [\mathrm{HO_2}]$, $[\mathrm{RO_2}]$ during WINTER. We use the following VOCs: methane, ethane, propane, n-butane, n-pentane, i-butane, i-pentane, 2-methyl pentane, 3-methyl pentane, n-hexane, n-heptane, isoprene, methacrolein, methyl vinyl ketone, α-pinene, β-pinene, butanal, 1-butene, benzene, toluene, o-xylene, m-xylene, p-xylene, ethyl benzene, 1,2,4-trimethyl benzene, and 1,2,3-trimethyl benzene (Perring, Pusede, and Cohen, 2013). All α values were taken from Perring, Pusede, and Cohen (2013). We calculate the daytime production of peroxy nitrates as (LaFranchi et al., 2009)

$$P(\Sigma \, \mathrm{PNs}) = \beta \times \alpha_{\mathrm{CH_3CHO}} \times k_{\mathrm{CH_3CHO}} \times [\mathrm{OH}][\mathrm{CH_3CHO}] \tag{A.3}$$

where

$$\beta = \frac{k_{\text{RC(O)O}_2+\text{NO}_2}[\text{NO}_2]}{k_{\text{RC(O)O}_2+\text{NO}_2}[\text{NO}_2] + k_{\text{RC(O)O}_2+\text{NO}}[\text{NO}] + k_{\text{RC(O)O}_2+\text{HO}_2}[\text{HO}_2] + k_{\text{RC(O)O}_2+\text{RO}_2}[\text{RO}_2]} \tag{A.4}$$

We estimate $[\text{RO}_2]$ as (Browne et al., 2013)

$$[\text{RO}_2] = \frac{-k_{\text{HO}_2+\text{RO}_2}[\text{HO}_2] - k_{\text{NO}+\text{RO}_2}[\text{NO}] + \sqrt{x}}{4 \times k_{\text{RO}_2+\text{RO}_2}} \tag{A.5}$$

where

$$x = (k_{\text{HO}_2+\text{RO}_2}[\text{HO}_2] + k_{\text{NO}+\text{RO}_2}[\text{NO}])^2 + 8 \times k_{\text{RO}_2+\text{RO}_2} \times P(\text{RO}_2) \tag{A.6}$$

We calculate daytime production of nitric acid as

$$P(\text{HNO}_3) = k_{\text{OH}+\text{NO}_2}[\text{OH}][\text{NO}_2] \tag{A.7}$$

A.2 Nighttime production rate calculations

We calculate the average production rate of HNO$_3$ (Eq. A.8) from N$_2$O$_5$ reactions on aerosol surfaces at night as two times the rate of R17 plus the rate of R18 since R17 produces two molecules of nitric acid for each molecule of N$_2$O$_5$ consumed and R18 produces one molecule of nitric acid for each molecule of N$_2$O$_5$ consumed:

$$P(\text{HNO}_3) = \frac{1}{4} \times \bar{c}_{\text{N}_2\text{O}_5} \times \gamma_{\text{N}_2\text{O}_5} \times [\text{N}_2\text{O}_5] \times (2 \times \text{SA} + \text{SA}_{\text{sea salt}}) \tag{A.8}$$

Here $\bar{c}_{\text{N}_2\text{O}_5}$ represents the mean molecular speed of N$_2$O$_5$ and $\gamma_{\text{N}_2\text{O}_5}$ represents the heterogeneous uptake coefficient for N$_2$O$_5$. The rate of R17 is proportional to the wet surface area (SA) of aerosol particles and the rate of R18 is proportional to the surface area of chloride-containing aerosol particles (SA$_{\text{sea salt}}$). This rate is valid for small values of $\gamma_{\text{N}_2\text{O}_5}$ and small particles (i.e., not diffusion-limited regimes) (Sutugin and Fuchs, 1970).

We estimate $\gamma_{\text{N}_2\text{O}_5}$ using our 2-box model described in Sect. 2.4. For simplicity, we use the same $\gamma_{\text{N}_2\text{O}_5}$ for all aerosols regardless of sea salt content, though this coefficient can vary.

Wet aerosol surface area is calculated using the dry aerosol surface area measured by the passive cavity aerosol spectrometer probe corrected for hygroscopic growth. We estimate the wet aerosol surface area by applying growth factors as a function of the measured relative humidity. The growth factors are calculated with the E-AIM model (`http://www.aim.env.uea.ac.uk/aim/aim.php`) assuming that the submicron aerosol is composed of NH$_4$NO$_3$. We use the median wet aerosol surface area over the ocean for SA, though there was variation in the observed aerosol surface area.

We use the average fraction of total aerosol surface area that is attributable to sea salt aerosols as a simple proxy for ClNO$_2$ yield, though chlorine can be displaced from sea spray and repartitioned into smaller aerosol particles, and there are additional factors that contribute to ClNO$_2$ yield (e.g., Bertram and Thornton, 2009; Wagner et al., 2012; Riedel et al.,

2013). To estimate the surface area of sea salt aerosols (SA$_{sea\ salt}$), we assume that sea salt mass is concentrated in the super-micron particle size range. Particles with diameter 1-10 μm (super-micron) contribute an average of 3% ($\pm$ 3%, 1 standard deviation) to the total aerosol surface area at night over the ocean during WINTER, so we define SA$_{sea\ salt}$ = 0.03 $\times$ SA. This approach does not account for any variation in the ClNO$_2$ yield and may underestimate ClNO$_2$ yield because it ignores any contribution of sub-micron chloride-containing aerosols to ClNO$_2$ formation. Sub-micron aerosols dominate urban aerosol surface area and, consequently, dominate N$_2$O$_5$ uptake onto aerosols.

A.3   Uncertainty calculations

We estimate the range of NO$_x$ e-folding lifetimes (τ_{total}, accounting for both physical and chemical loss processes) using the bivariate York fitting method (York et al., 2004) which accounts for variability in both the x and y variables. We assume variability in x (time elapsed from East Coast) is dominated by the variation in wind speed during a given flight. The average fractional 1σ variation in wind speed within each day or night subset of each flight used in this analysis was 30%, so we assign a fractional uncertainty of 30% in x. We estimate variability in y ([NO$_x$]) as the 1σ variation in the observed NO$_x$ concentration in each time bin.

Since HNO$_3$ is the dominant sink of NO$_x$ during both day and night, we assume variability in the chemical lifetime of NO$_x$ ($\tau_{chem.}$) is dominated by variation in the rate of conversion of NO$_x$ to HNO$_3$. We assume the uncertainty in the daytime chemical lifetime of NO$_x$ lost to HNO$_3$ is dominated by uncertainty in modeled OH concentrations which we estimate as 1σ variation in modeled [OH]. We estimate the variability in the nighttime chemical lifetime of NO$_x$ from uncertainties in [NO], [NO$_2$], [N$_2$O$_5$], aerosol surface area, and $\gamma_{N_2O_5}$. We incorporate CL instrument uncertainty for [NO] = 10% (Ridley et al., 1994), TD-LIF instrument uncertainty for [NO$_2$] = 10% (Day et al., 2002), HRToF-CIMS instrument uncertainty for [N$_2$O$_5$] = 30% (Kercher, Riedel, and Thornton, 2009; Lee et al., 2014a), and PCASP uncertainty for aerosol surface area = 41% (Strapp, Leaitch, and Liu, 1992).

We have defined the e-folding lifetime of NO$_x$ and the chemical lifetime of NO$_x$ as first order with respect to the concentration of NO$_x$, but we have defined the mixing lifetime of NO$_x$ as first order with respect to the concentration gradient of NO$_x$ between the boundary layer (BL) and the free troposphere (FT). If we make the assumption that [NO$_x$]$_{FT} \ll$ [NO$_x$]$_{BL}$ such that [NO$_x$]$_{BL}$ - [NO$_x$]$_{FT} \approx$ [NO$_x$]$_{BL}$, then

$$\frac{1}{\tau_{total}} = \frac{1}{\tau_{chem.}} + \frac{1}{\tau_{mix}} \tag{A.9}$$

Accounting for the estimated variability in τ_{total} and $\tau_{chem.}$, we estimate the variability in τ_{mix} to be 8.2 h during the day and 10.7 h at night.

Appendix B

Supporting information for "Evidence of nighttime production of organic nitrates during SEAC^{4}RS, FRAPPÉ, and KORUS-AQ"

Table B.1: Description of instrumentation used in analysis.

Species	Technique	Accuracy	Sampling interval	Reference
NO$_2$, RONO$_2$	TD-LIF[a]	15%	10 s	Day et al., 2002; Wooldridge et al., 2010
O$_3$, NO	CL[b]	3-15%	1 s	Ryerson et al., 1999
				Ryerson, Williams, and Fehsenfeld, 2000
O$_3$, NO	CL[c]	5-10%	1 s	Ridley et al., 1994; Weinheimer et al., 1994
alkenes	WAS[d]	1-5%	30-60 s	Colman et al., 2001; Simpson et al., 2011
alkenes	TOGA[e]	<15%	2 min	Apel et al., 2015

[a] UC Berkeley Thermal Dissociation-Laser Induced Fluorescence
[b] NOAA chemiluminescence, used during SEAC⁴RS
[c] NCAR chemiluminescence, used during FRAPPÉ and KORUS-AQ
[d] UC Irvine Whole Air Sampling with gas chromatography
[e] NCAR Trace Organic Gas Analyzer
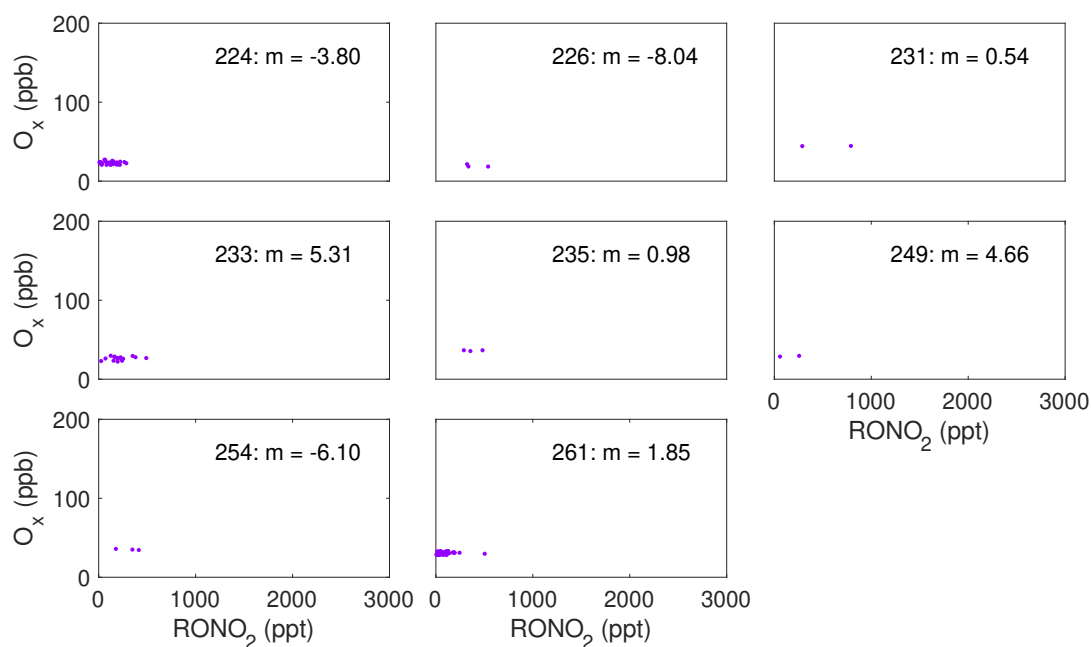
Figure B.1: Plots of O_x vs. $RONO_2$ during SEAC[4]RS during morning (before 11:00 local time) for each flight day. Plots are labeled by flight date (Julian day) and the slope of a York linear fit (m). Only data in the boundary layer (< 1 km) are included.
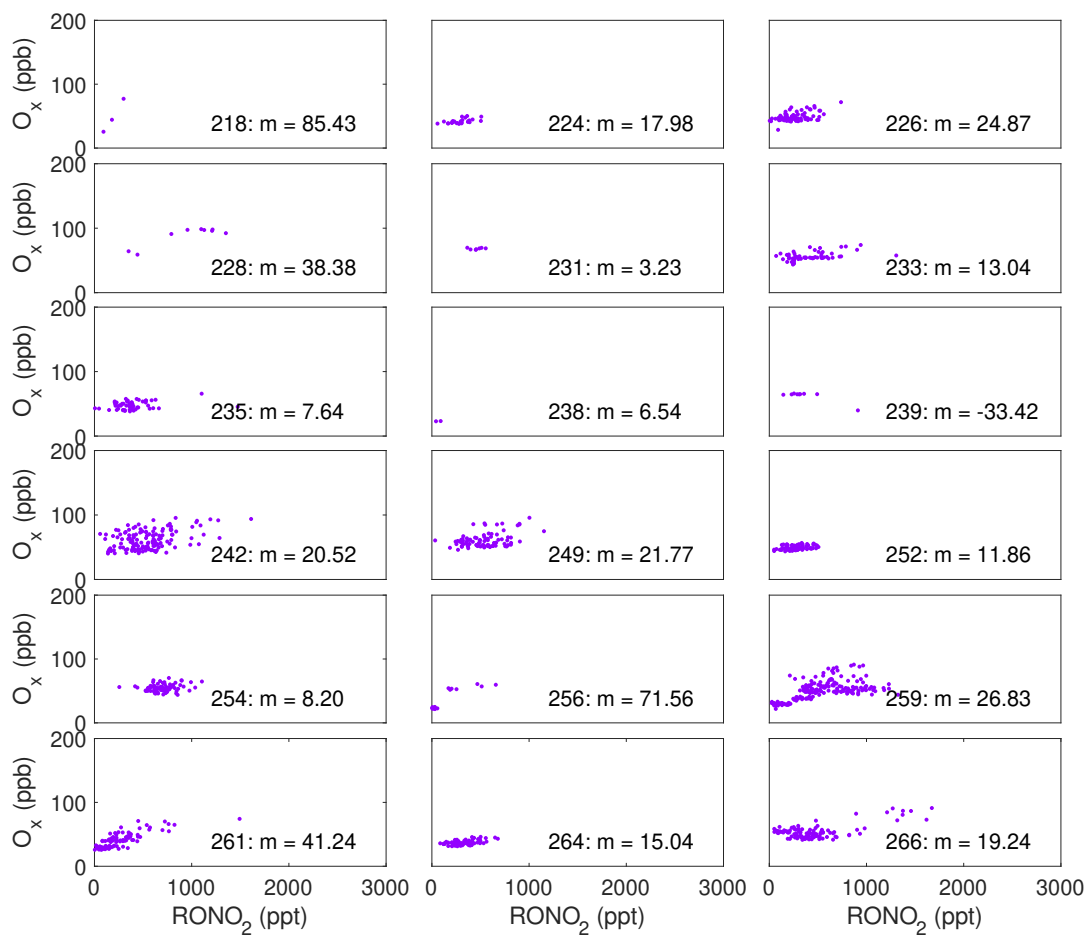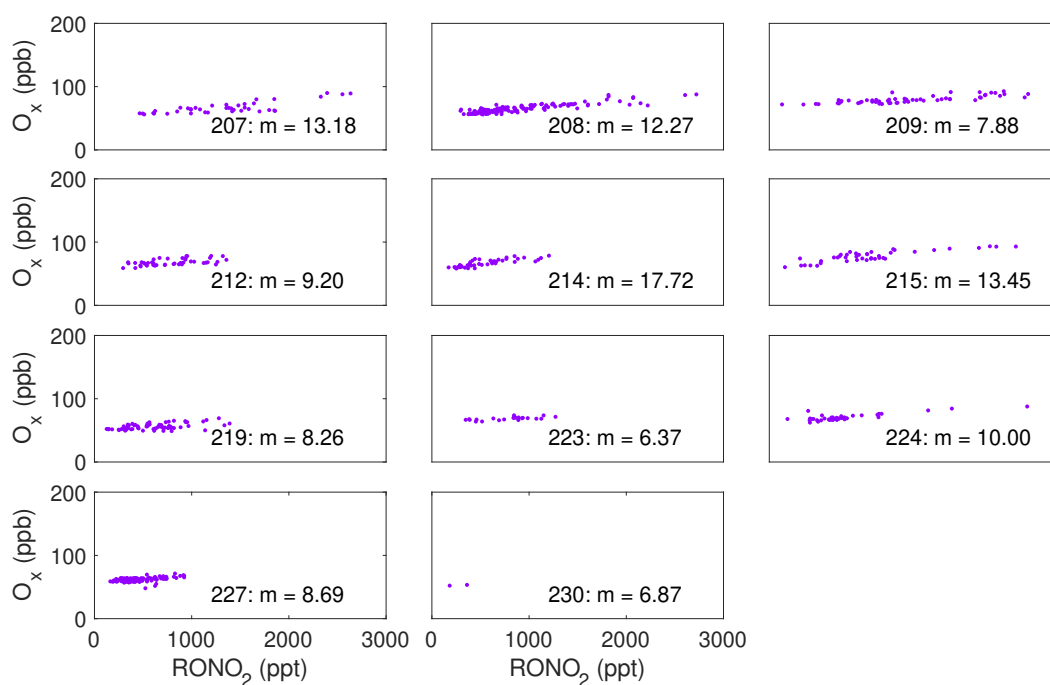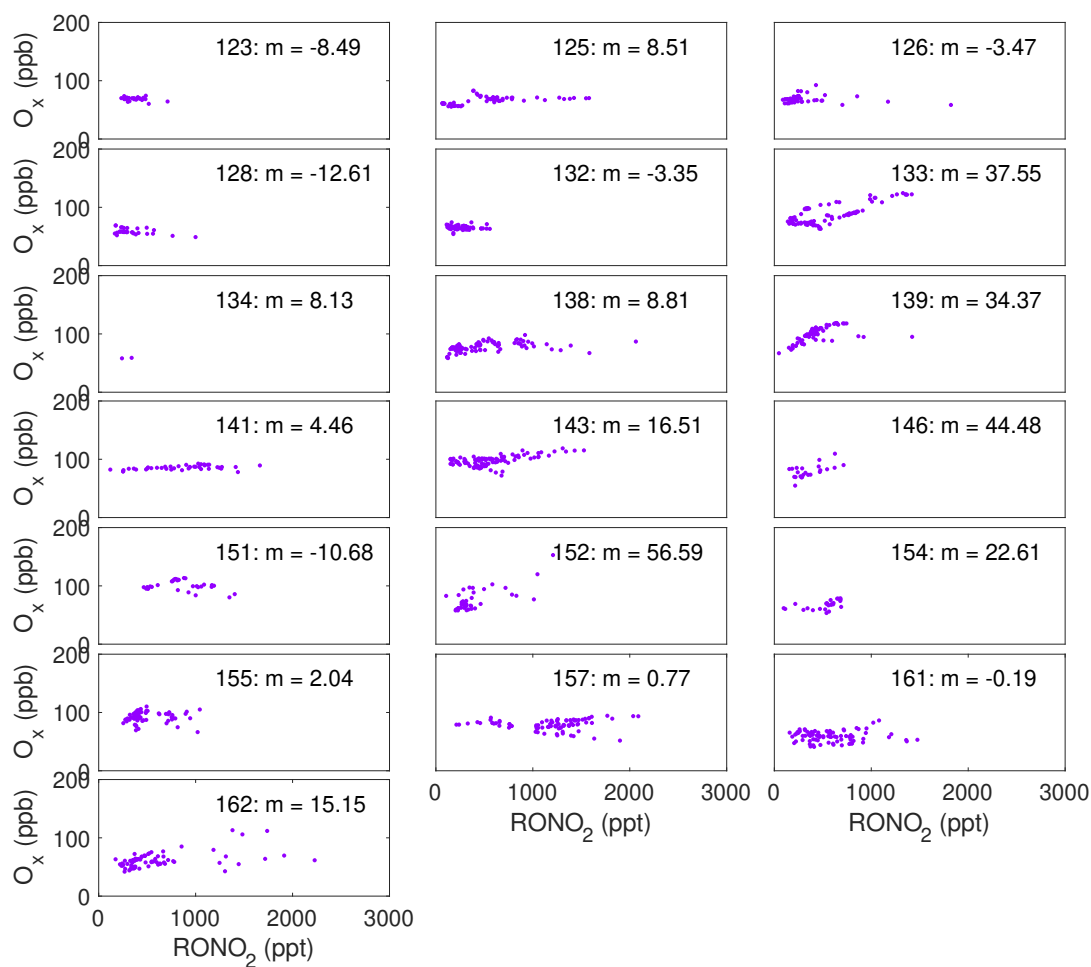
Figure B.2: Plots of O_x vs. $RONO_2$ during SEAC[4]RS during afternoon (13:00 - 19:00 local time) for each flight day. Plots are labeled by flight date (Julian day) and the slope of a York linear fit (m). Only data in the boundary layer (< 1 km) are included.
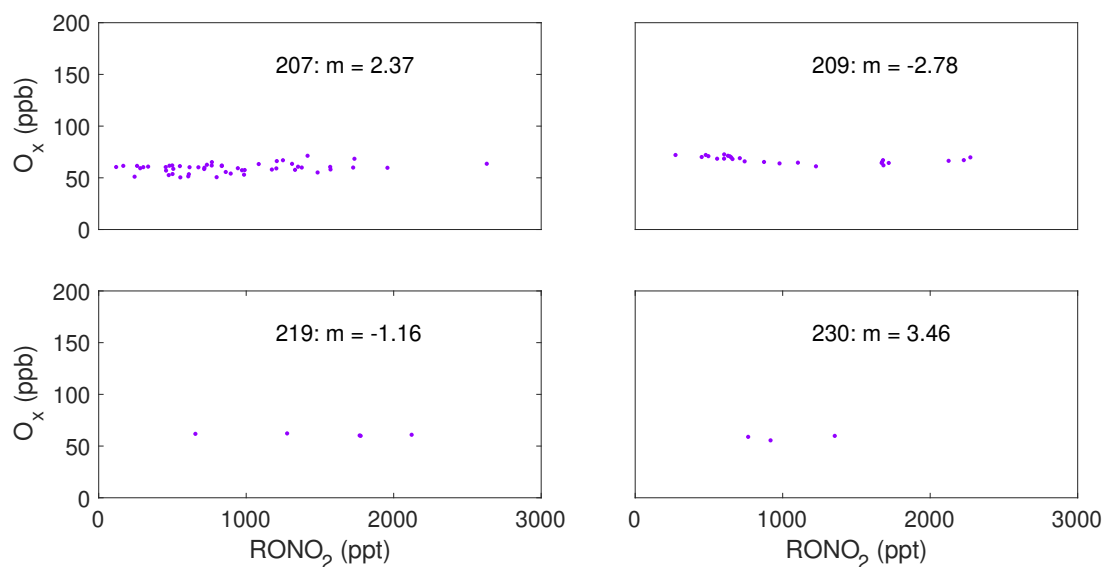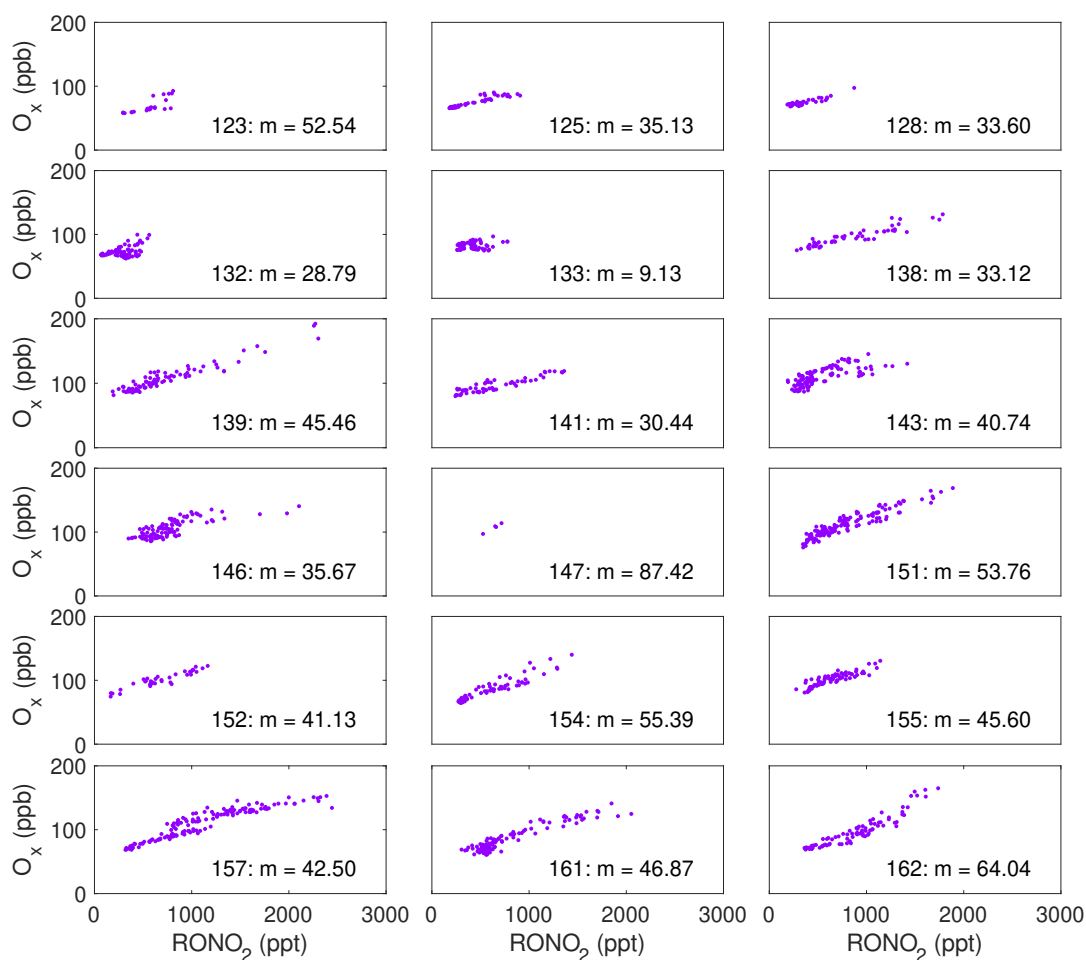
Figure B.3: Plots of O_x vs. $RONO_2$ during FRAPPÉ during morning (before 11:00 local time) for each flight day. Plots are labeled by flight date (Julian day) and the slope of a York linear fit (m). Only data in the boundary layer (< 2 km) are included.

Figure B.4: Plots of O_x vs. $RONO_2$ during FRAPPÉ during afternoon (13:00 - 19:00 local time) for each flight day. Plots are labeled by flight date (Julian day) and the slope of a York linear fit (m). Only data in the boundary layer (< 2 km) are included.

Figure B.5: Plots of O_x vs. $RONO_2$ during KORUS-AQ during morning (before 11:00 local time) for each flight day. Plots are labeled by flight date (Julian day) and the slope of a York linear fit (m). Only data in the boundary layer (< 1 km) are included.

Figure B.6: Plots of O_x vs. $RONO_2$ during KORUS-AQ during afternoon (13:00 - 19:00 local time) for each flight day. Plots are labeled by flight date (Julian day) and the slope of a York linear fit (m). Only data in the boundary layer (< 1 km) are included.
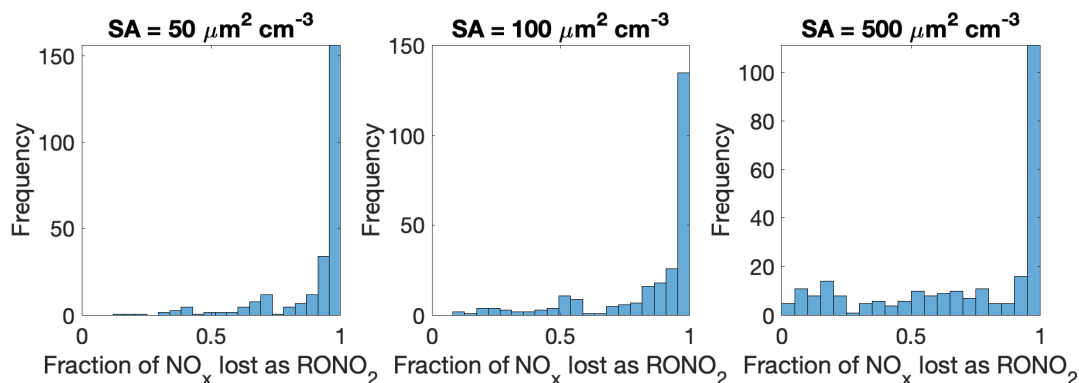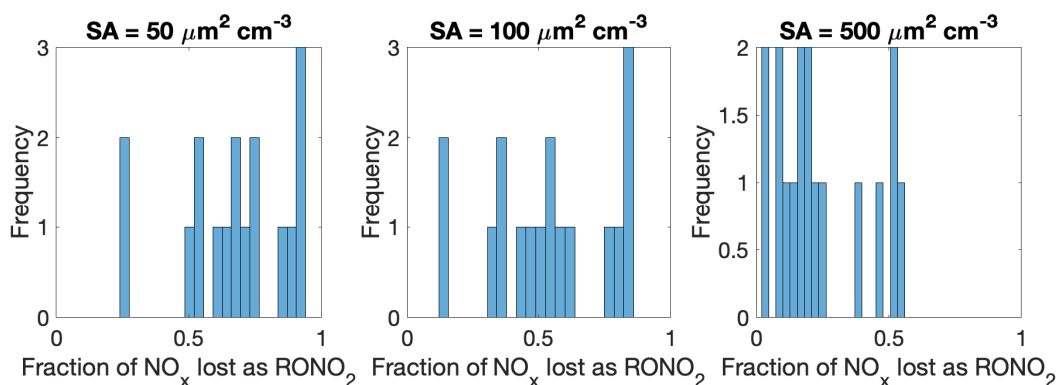
Figure B.7: Histograms of the fraction of NO_x lost as $RONO_2$ (defined as $\frac{P(RONO_2)}{P(RONO_2)+P(HNO_3)}$ overnight) calculated from evening observations (after 16:30) of temperature, pressure, alkenes, NO_2, and O_3 during SEAC⁴RS for three different aerosol surface areas (SA = 50, 100, and 500 $\mu m^2\,cm^{-3}$) assuming $\gamma(N_2O_5) = 0.04$ and NO_3 and N_2O_5 in steady-state.
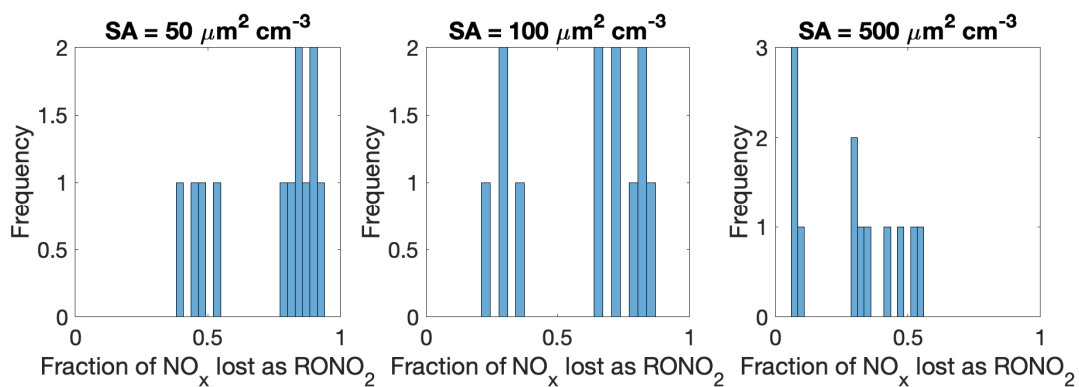

Figure B.8: Histograms of the fraction of NO_x lost as $RONO_2$ (defined as $\frac{P(RONO_2)}{P(RONO_2)+P(HNO_3)}$ overnight) calculated from evening observations (after 16:30) of temperature, pressure, alkenes, NO_2, and O_3 during FRAPPÉ for three different aerosol surface areas (SA = 50, 100, and 500 $\mu m^2\,cm^{-3}$) assuming $\gamma(N_2O_5) = 0.04$ and NO_3 and N_2O_5 in steady-state.

Figure B.9: Histograms of the fraction of NO_x lost as $RONO_2$ (defined as $\frac{P(\mathrm{RONO_2})}{P(\mathrm{RONO_2})+P(\mathrm{HNO_3})}$ overnight) calculated from evening observations (after 16:30) of temperature, pressure, alkenes, NO_2, and O_3 during KORUS-AQ for three different aerosol surface areas (SA = 50, 100, and 500 $\mu m^2\,cm^{-3}$) assuming $\gamma(N_2O_5) = 0.04$ and NO_3 and N_2O_5 in steady-state.

Appendix C

Supporting information for "Contribution of organic nitrates to organic aerosol over South Korea during KORUS-AQ"

C.1 Particle loss corrections applied to TD-LIF measurements

In the TD-LIF inlet (as shown in Figure C.1), air for all four channels goes through 10 cm of 1/4" outer diameter PFA Teflon tubing before heating. In addition to this, the pRONO$_2$ channel has 12 cm of antistatic polyurethane, the denuder, 80 cm of antistatic polyurethane, and 8 cm of PFA before heating, all of which have 1/4" outer diameter.

We conducted particle charge loss experiments with PFA Teflon tubing to determine what particle losses could occur in the TD-LIF inlet. We sampled charged particles through both 10 cm and 20 cm lengths of PFA Teflon; the results were the same between both lengths. During the experiment (as shown in Figure C.2), we size-selected ambient particles (in the laboratory) using a differential mobility analyzer (TSI Inc., Model 3081). We alternately sampled through PFA Teflon for 1-2 minutes, then sampled through stainless steel for the same amount, and finally compared the concentrations of particles sampled through each tubing material with a condensation particle counter (TSI Inc., Model 3075).

We sampled both positively and negatively charged particles, and found that they both behave similarly, though we found larger variability in the loss of negatively charged particles (as shown in Figure C.3). We found that particle loss decreases with increasing aerosol size. This makes sense as the electrophoretic force from the charges on the Teflon wall is the same for all particles that have a single charge (most of the charged particles), but the migration velocity scales inversely with the squared diameter.

Taking into account the ambient distribution of charged particles (Wiedensohler, 1988),
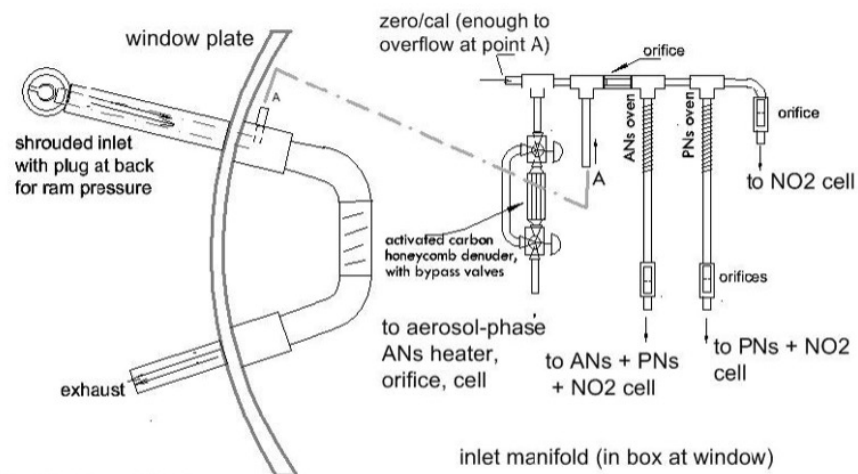
Figure C.1: Inlet diagram for TD-LIF during KORUS-AQ.
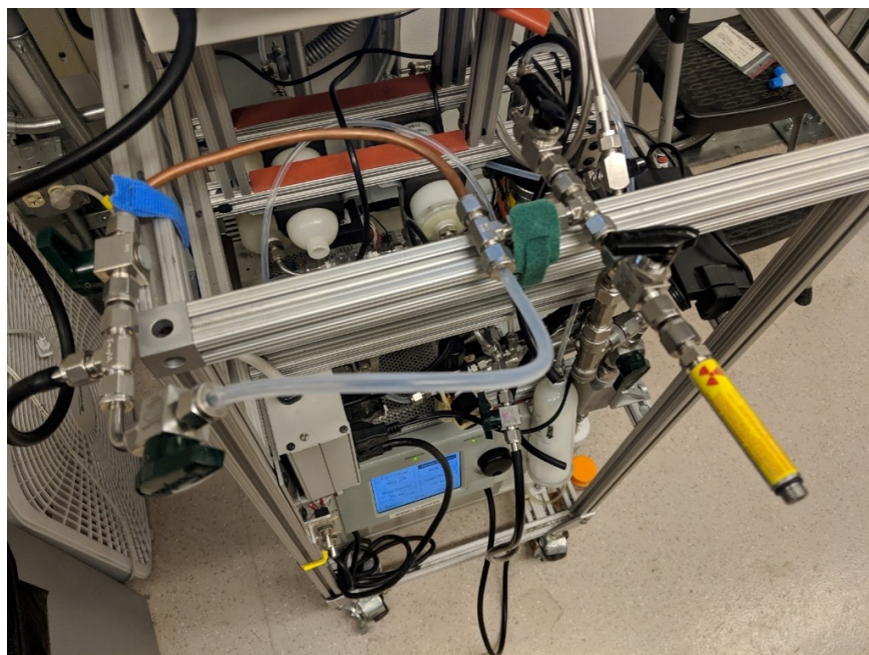

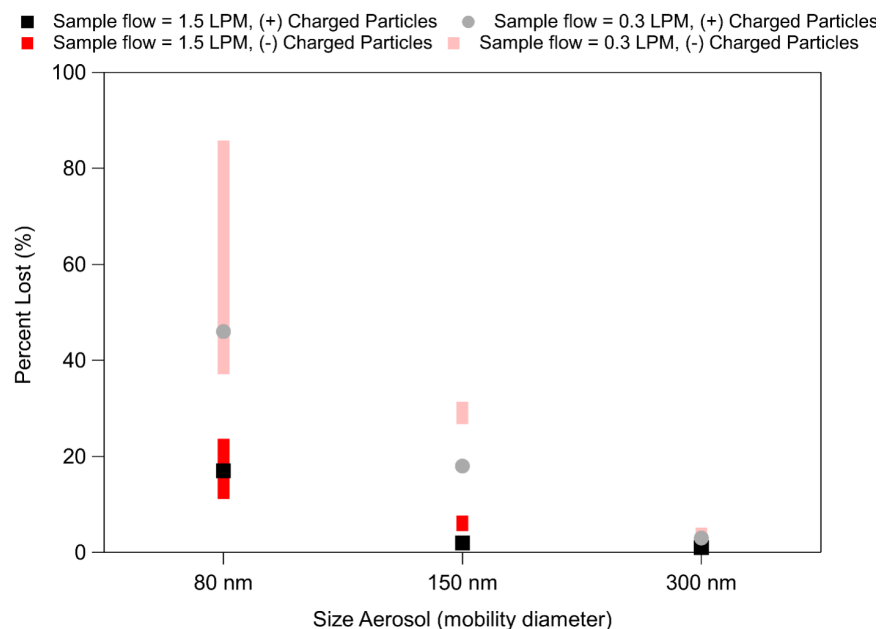Figure C.2: Experimental set-up to investigate charged particle losses.

Figure C.3: The percent loss for all charged particles through 20 cm Teflon tubing at two different flow rates (0.3 and 1.5 LPM) at 3 different particle diameters. There was minimal variability in the positively charged particles; therefore, only showing the mean. However, there was larger variability in the negatively charged particles; therefore, showing the range as a par.

there is < 20% loss for particles with diameters between 20 and 280 nm (Figure C.4). Comparing this with the average mass distribution observed by the CU-AMS (Figure C.3), there is not much observed mass at the diameters where most of the charged particle losses may occur (0 to 100 nm). Thus, losses of charged particles are small for the size distribution of aerosol observed during KORUS-AQ.

We also investigated inertial losses of particles on bends and inlet. The calculations consider non-isokinetic sampling, diffusion, turbulent inertial deposition, inertial deposition in a bend, and inertial deposition in a contraction (Hinds, 1998; McNaughton et al., 2007; Von Der Weiden, Drewnick, and Borrmann, 2009). We calculated particle transmission for two regions of the TD-LIF inlet (Figure C.1): (1) the first bend that is 98°, with a corresponding reduction in velocity by a factor of ≈ 3-4, and a decrease in the inner diameter to 3 cm; and (2) the second bend that is 90°, with a corresponding reduction in velocity by nearly an order of magnitude, and a reduction in inner diameter from 3 to 0.435 cm. These two critical areas lead to a loss of particles to surfaces (< 90% transmission) for particles with diameters > 180 nm (Figure C.4). The diameter where ≈ 50% of particles are detected (d_{50}) is ≈ 335 nm, which corresponds to the CU-AMS observed peak mass distribution (Figure
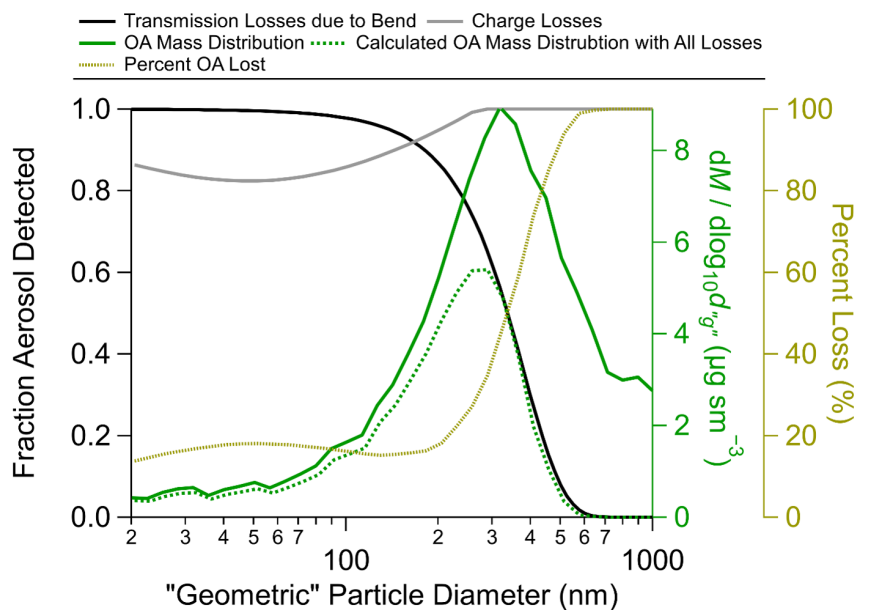
Figure C.4: (Left) Comparisons of particles potentially detected by TD-LIF due to losses of particles by (gray) charge or (black) bends. (Right, green) Average observed mass distribution of organic aerosol for KORUS-AQ (solid) and calculated mass distribution potentially observed by TD-LIF due to losses (dashed). (Right, gold) Percent loss of particles, by size, due to the combined losses from charged particles and bends.

C.4). There is a near-linear increase in the percent of particles lost between 200 and 578 nm (Figure C.4).

To correct the TD-LIF measurements for particle loss, we examined the volume distribution measured by the Langley LARGE group laser aerosol spectrometer (LAS), as shown in Figure C.5. We calculated the fraction of particles lost in the TD-LIF by applying the percent lost (shown in Figure C.4) to the LAS volume distribution (Figure C.5). The resulting fraction of particles observed by the TD-LIF is shown as a time series in Figure C.6. Because the peak in the measured volume distribution is consistently near the TD-LIF d_{50}, on average, the TD-LIF observes $\approx 60\%$ of the particles observed by the LAS. However, the LAS may have been saturated at high volume concentrations (Nault et al., 2018), meaning this correction factor may be an upper limit of particles observed by the TD-LIF. We used this calculated fraction of particles observed by the TD-LIF (shown in Figure C.6) to correct both the $pRONO_2$ and $tRONO_2$ TD-LIF measurements.
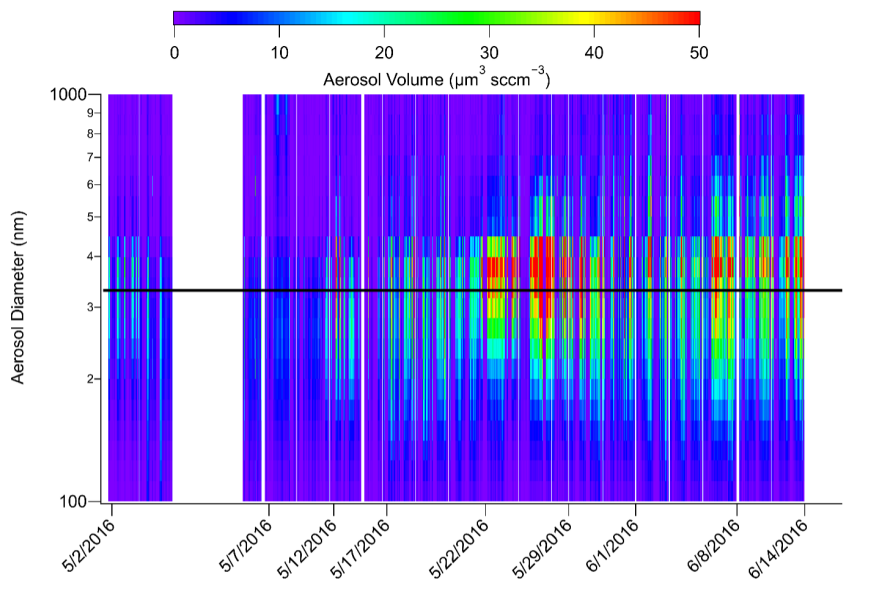
Figure C.5: Time series of the volume distribution, as measured by the Langley LARGE laser aerosol spectrometer, during KORUS-AQ. The black line represents the TD-LIF d_{50} due to inertial particle losses from bends.

C.2 CU-AMS measurements of pRONO$_2$

The CU-AMS distinguishes organic pRONO$_2$ from inorganic NH$_4$NO$_3$ using the measured NO$_x$ ion ratios (NO$_2^+$/NO$^+$). Apportionment was calculated according to the equation introduced by Farmer et al. (2010) (where NO$^+$/NO$_2^+$ ratios were used), but following the formulation using NO$_2^+$/NO$^+$ ratios, as applied in Fry et al. (2013). Figure C.7 shows the measured NO$_x$ ratio vs the NO$_3$ detected by the CU-AMS. NH$_4$NO$_3$ calibrations to determine the NO$_2^+$/NO$^+$ ratio for NH$_4$NO$_3$ showed that this ratio remained very stable at 0.97 during KORUS-AQ. The calibration ratio for pRONO$_2$ is a factor of 2.83 lower, following the "ratio-of-ratio" estimation method first introduced by Fry et al. (2013). At high total NO$_3$ mass concentrations, the NO$_2^+$/NO$^+$ ratio reached the calibration value of 0.97, indicating that this ratio can be reliably used to differentiate the NH$_4$NO$_3$ and pRONO$_2$.

We also performed a series of checks to make sure NaNO$_3$ was not biasing the CU-AMS pRONO$_2$ measurements. When NaNO$_3$ thermally decomposes on the CU-AMS vaporizer, the NO$_2^+$/NO$^+$ ratio is more similar to pRONO$_2$ than NH$_4$NO$_3$. For NaNO$_3$ interference in the CU-AMS to occur, however, particles containing NaNO$_3$ would have to be sufficiently small for the CU-AMS to sample (< 1 μm), which is atypical. To look for evidence of any interference, we calculate 'excess' Na, which is the amount of Na not directly bound with Cl. A comparison of 'excess' Na with the CU-AMS pRONO$_2$ measurement (Figure C.8)
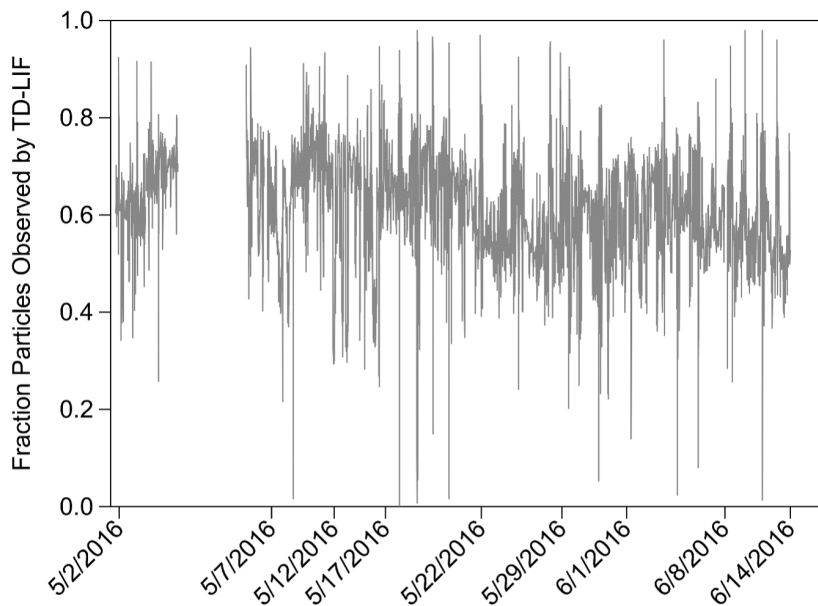
Figure C.6: Time series of the fraction of particles potentially observed by the TD-LIF during KORUS-AQ based on the LAS volume distribution measurements.

shows that, above the limit of detection for Na, there is no correlation of CU-AMS pRONO$_2$ with 'excess' Na. Moreover, NaNO$_3$ mostly comes from fresh NaCl reacting with HNO$_3$ in a large pollution plume, meaning most NaNO$_3$ will occur over the sea or during periods of sea breeze. RF20 sampled a lot of marine air, which could contain NaNO$_3$. As shown in Figure C.8, there is not an anti-correlation between NO$_2^+$/NO$^+$ and Na (R$^2 \approx 0.4$), further confirming that CU-AMS pRONO$_2$ measurements are not biased by NaNO$_3$.

C.3   Comparison of TD-LIF and CU-AMS pRONO$_2$ measurements

We show a comparison of the TD-LIF and CU-AMS measurements of pRONO$_2$ in Figure C.9. Before corrections, on average the CU-AMS pRONO$_2$ measurements are 2.48 times higher than the TD-LIF pRONO$_2$ measurements. After applying corrections to the TD-LIF measurements to account for particle loss and after screening out CU-AMS data where pRONO$_2$ is $< 20\%$ of the total measured aerosol nitrate, the two measurements agree within a factor of two.
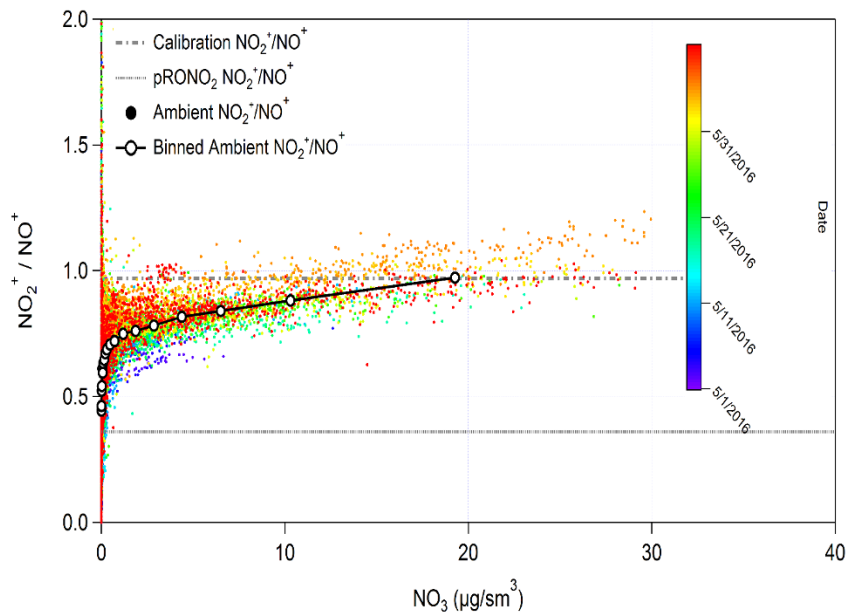
Figure C.7: The NO_2^+/NO^+ ratio versus total NO_3 measured by the CU-AMS, colored by date of measurement. Also shown are the calibration standard ratios for NH_4NO_3 and for $pRONO_2$.

C.4 CMAQ emissions

The KORUSv5.0 emissions inventory was prepared using the SAPRC07T AERO6 mechanism, which we then converted to RACM2_Berkeley2.1, as detailed in Table C.1.

As detailed in the main text, BTEX and monoterpene emissions were updated to better match observations. A comparison between the model-measurement agreement for the unchanged emissions and the altered emissions is shown in Figure C.12.

C.5 Model-measurement comparison

As a test of model efficacy, we show a comparison between measured and modeled trace gas mixing ratios (NO_x,O_3,O_x) and OA concentrations at two of the ground measurement sites during KORUS-AQ in Figure C.13.

Scatter plots comparing modeled and measured $tRONO_2$, $pRONO_2$, and F_p are shown in Figure C.14, for both TD-LIF and CU-AMS measurements and for both unmodified and modified (unknown source added) CMAQ output. Results of iterative tests to determine the volatility of the unknown $RONO_2$ source are shown in Table C.2. The temperature-dependent fractional distribution (f_j) of saturation concentrations at 300 K (C_j(300 K)) fit

Table C.1: Table describing the emissions inventory conversion from SAPRC07T AERO6 to RACM2_Berkeley2.1. Species definitions can be found in the Carter (2015) database. Emissions of species marked with an asterick (*) over the Daesan petrochemical complex were further modified to match emission fluxes calculated from observations using a mass balance approach by Fried et al. (2020).

| SAPRC07T AERO6	RACM2_Berkeley2.1	SAPRC07T AERO6	RACM2_Berkeley2.1
CO	CO	SESQ	SESQ
NO	NO	3 TERP	LIM
NO2	NO2	3 APIN	API
NH3	NH3	BENZ	BEN*
SO2	SO2	1.4 (TOLU + ARO1)	TOL*
HONO	HONO	0.05 (TOLU + ARO1)	XYO*
CH3	CH4	0.08 (TOLU + ARO1)	XYM*
HCL	HCL	0.07 (TOLU + ARO1)	XYP*
CL2	CL2	ACYE	ACE
ACET	ACT	ETOH	EOH
ALK1	ETH	FACD	ORA1
ALK2 + ALK3	HC3	AACD	ORA2
0.9 ALK4	HC5	SULF	SULF
0.1 ALK4	ROH	SOAALK	SOALLK
0.85 ALK5	HC8	NAPH	NAPH
0.05 ALK5	ETEG	NROG	NR
0.10 ALK5	ROH	NVOL	NVOL
BACL + MGLY	MGLY	PEC	PEC
BALD	BALD	PNO3	PNO3
CCHO	ACD	PSO4	PSO4
0.5 CRES	PHEN	POC	POC
0.5 CRES	CSL	PMC	PMC
OLE1 + PRPE	OLT	PCL	PCL
0.85 OLE2	OLI	PNH4	PNH5
0.15 OLE2	DIEN	PNA	PNA
RCHO	ALD	PK	PK
ETHE	ETE	PNCOM	PNCOM
GLY	GLY	PCA	PCA
HCHO	HCHO	PFE	PFE
IPRD	UALD	PAL	PAL
ISOP	ISO	PSI	PSI
MACR + ACRO	MACR	PH2O	PH2O
0.5 MEK	MEK	PMG	PMG
0.5 MEK	HKET	PTI	PTI
PRD2	KET	PMN	PMN
MEOH	MOH	PMOTHR	PMOTHR
MVK	MVK		
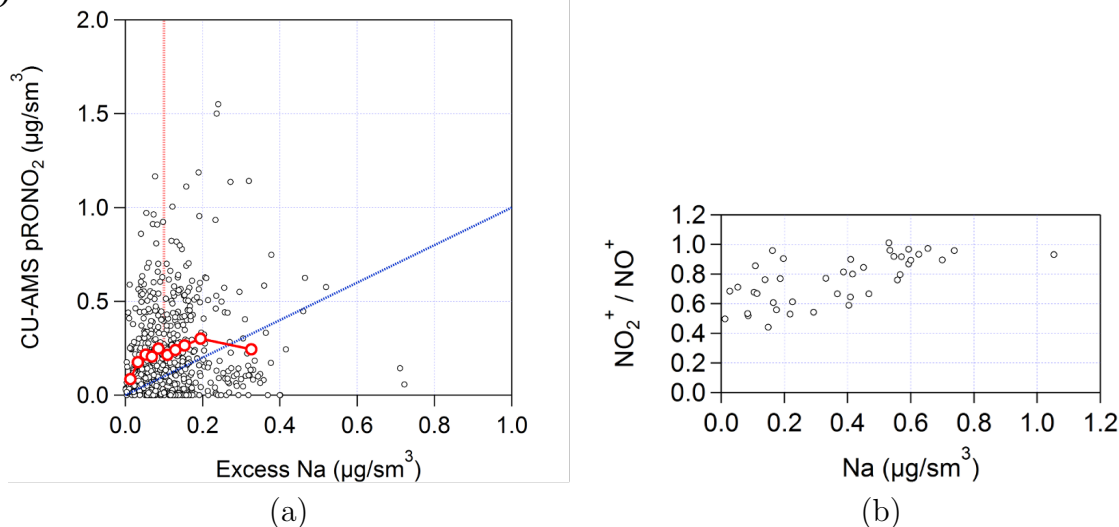
Figure C.8: (a) Plot of CU-AMS measurement of $pRONO_2$ versus 'excess Na' (amount of Na not directly bound with Cl). The blue line is a 1:1 line, the red dashed line indicates the limit of detection (LOD) for filtered Na, and the red circles are deciles. A large fraction of $pRONO_2$ occurs below the Na LOD. Above the LOD, there is no correlation of CU-AMS $pRONO_2$ with excess Na. (b) Plot of NO_2^+/NO^+ ratio versus Na mass concentration during RF20, which included a lot of marine air sampling. There is no anti-correlation between NO_2^+/NO^+ and Na ($R^2 \approx 0.4$).

Table C.2: Comparison of the York fit slopes between measured (TD-LIF and CU-AMS) and CMAQ modeled concentrations of $pRONO_2$ and F_p. Comparison is shown for the unmodified CMAQ output and CMAQ output with an unknown source of condensable $RONO_2$ added, with varied C^* assigned to the unknown $RONO_2$.

	$pRONO_2$		F_p	
	TD-LIF	CU-AMS	TD-LIF	CU-AMS
CMAQ	0.12	0.09	0.54	0.34
CMAQ add unknown with $C^* = 3,000\ \mu g\,m^{-3}$	0.21	0.18	0.23	0.15
CMAQ add unknown with $C^* = 300\ \mu g\,m^{-3}$	0.94	0.81	0.61	0.44
CMAQ add unknown with $C^* = 30\ \mu g\,m^{-3}$	3.62	2.82	2.31	1.66

to a volatility basis set are shown in Figure C.15.

C.6   CMAQ modeled RONO$_2$ speciation

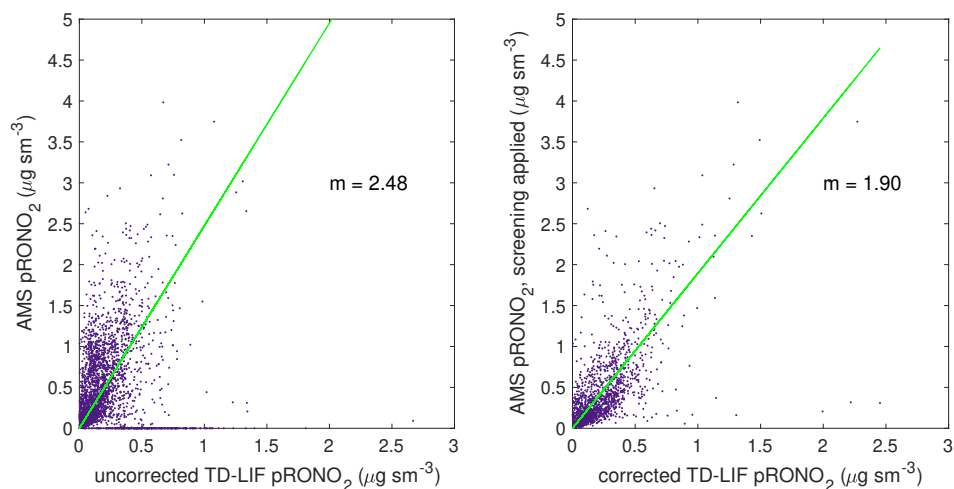The CMAQ modeled speciation of $tRONO_2$ and $pRONO_2$ is shown in Figure C.16.

Figure C.9: Comparison of (left) AMS pRONO$_2$ measurements versus uncorrected TD-LIF pRONO$_2$ measurements and (right) AMS pRONO$_2$ measurements with a screening applied versus corrected TD-LIF pRONO$_2$ measurements. The screening applied to the AMS measurements removes data where pRONO$_2$ is less than 20% of total measured aerosol nitrate since these pRONO$_2$ measurements high uncertainty and high noise.
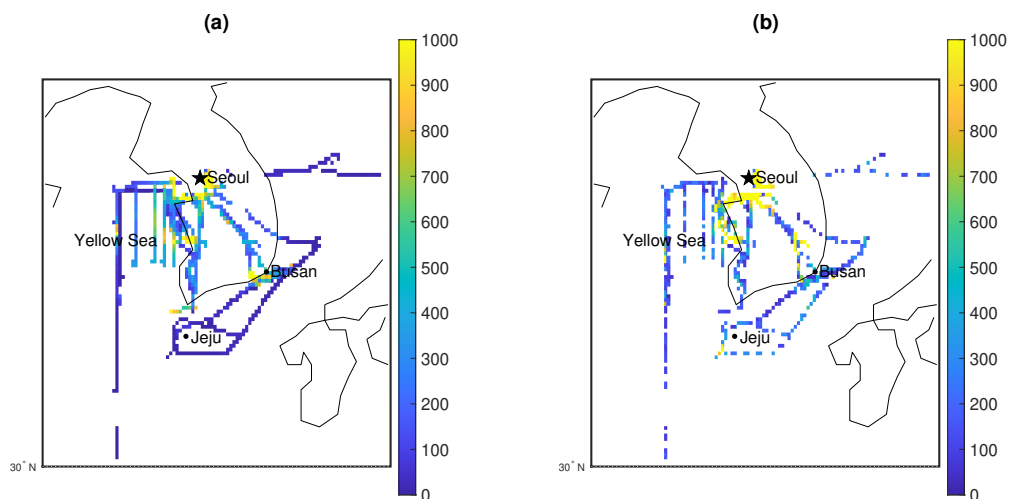

Figure C.10: Maps of (a) modeled TOL (toluene and less reactive aromatics) before emission modifications (ppt) and (b) the sum of WAS measured toluene and ethylbenzene (ppt). In both cases, peak toluene occurs in similar geographic areas.
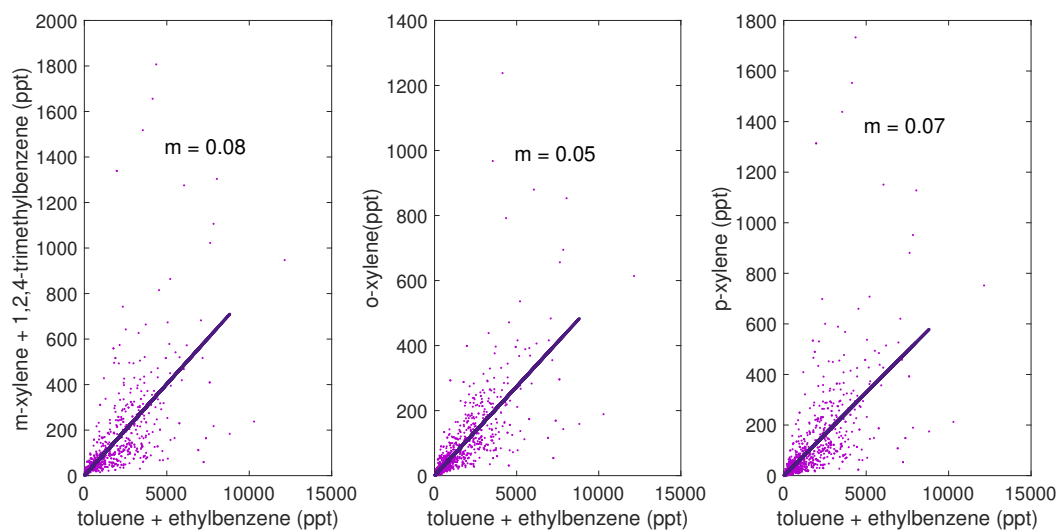
Figure C.11: Plots of WAS measured reactive aromatics (m-xylene, 1,2,4-trimethylbenzene, o-xylene, and p-xylene) versus the sum of WAS measured toluene and ethylbenzene. The slope of a York fit is shown in each plot. We use the slopes between these species to scale the reactive aromatics in the emissions inventory.
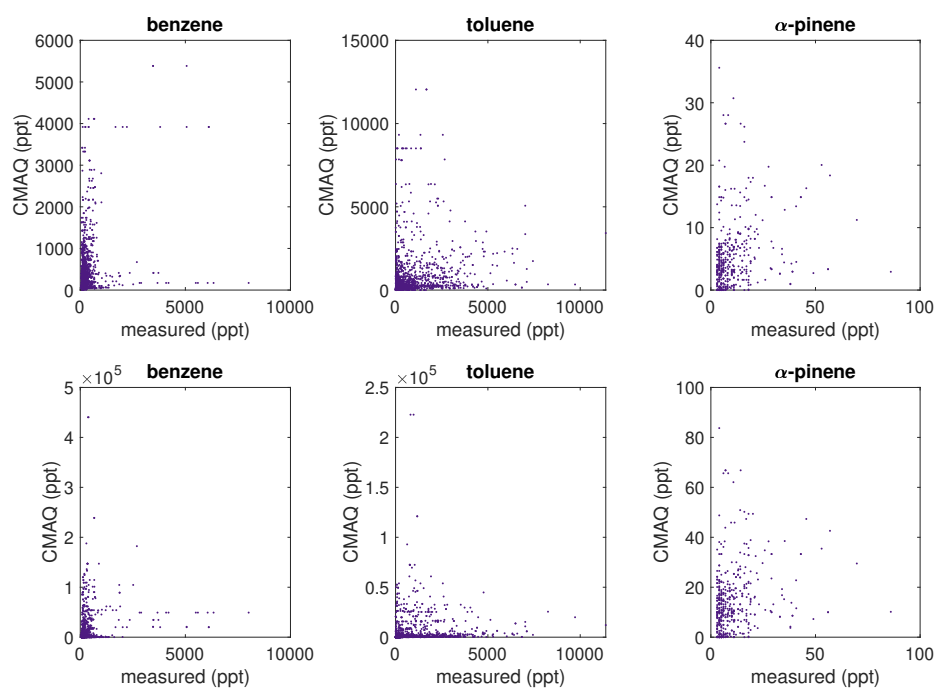
Figure C.12: Model-measurement comparison of benzene, toluene, and α-pinene for (top row) unchanged emissions and (bottom row) updated emissions using whole air sampling (WAS) measurements.
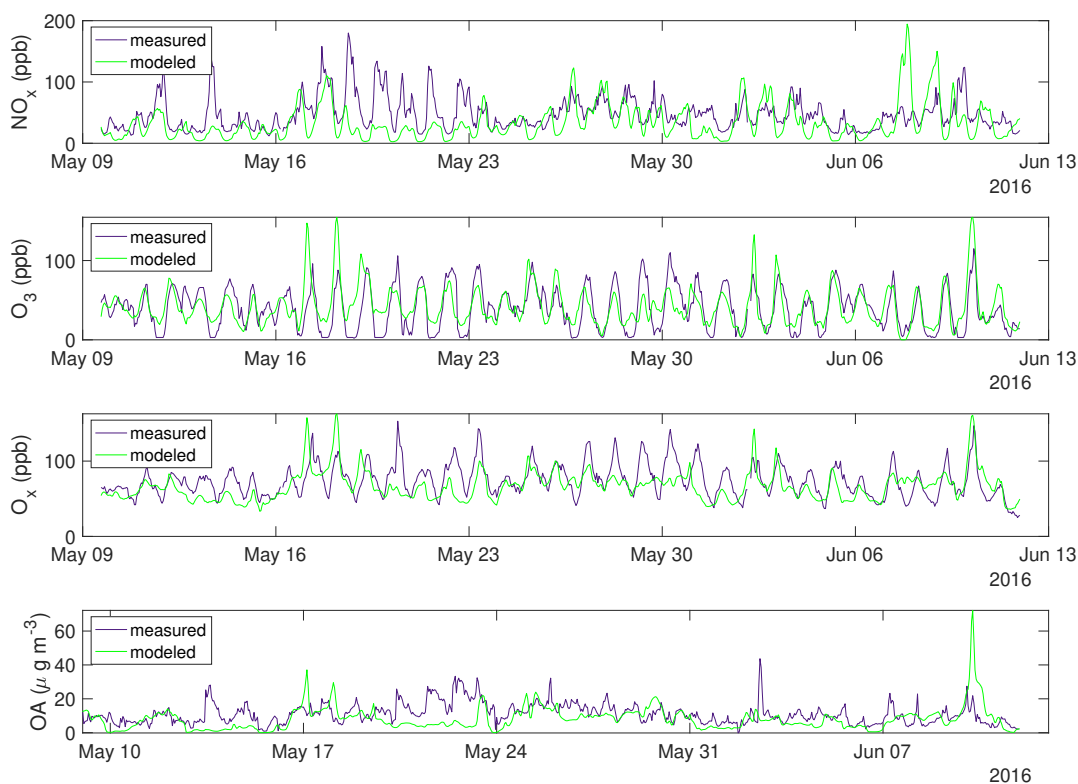
Figure C.13: Comparison between measured and modeled mixing ratios of NO_x, O_3, and O_x ($\equiv O_3 + NO_2$) at the Olympic Park ground site and comparison between measured and modeled concentrations of organic aerosol at KIST during KORUS-AQ as a test of model efficacy. The model is able to successfully capture the diurnal patterns in NO_x and O_3 and the regional OA background concentration.
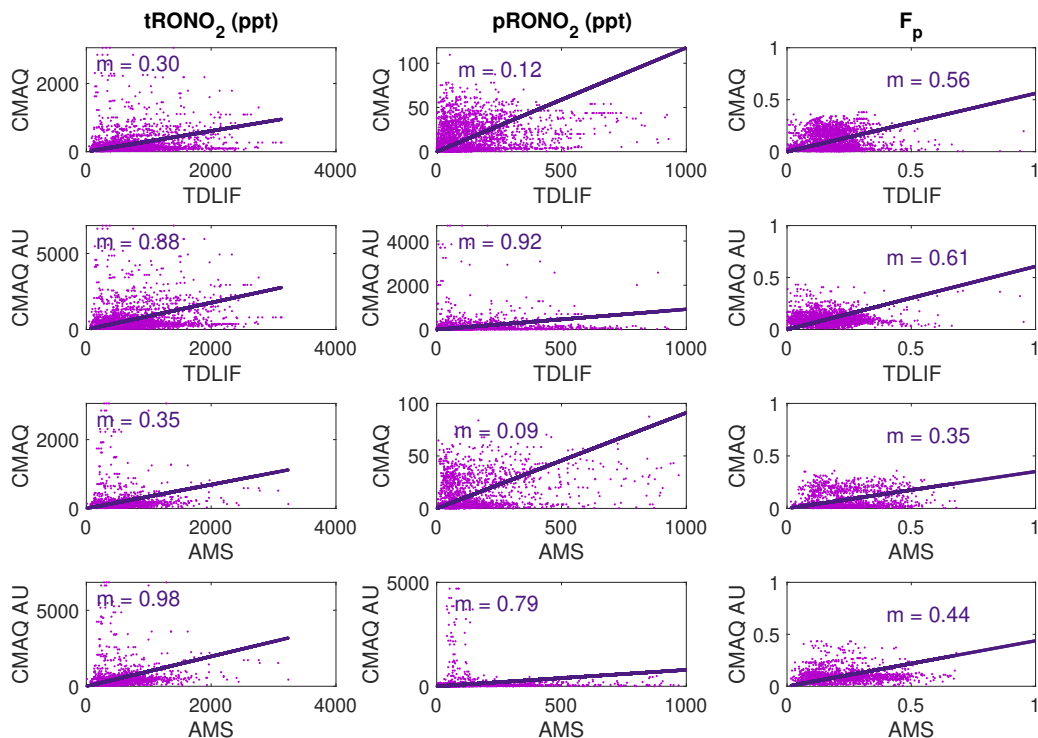
Figure C.14: Plots comparing modeled (CMAQ) and measured (TD-LIF and CU-AMS) tRONO$_2$ mixing ratios (left column, ppt), pRONO$_2$ mixing ratios (middle column, ppt), and F_p (right column, unitless). The top row compares TD-LIF measurements with unmodified CMAQ output, the second row compares TD-LIF measurements with modified (add unknown, AU) CMAQ output, the third row compares AMS measurements with unmodified CMAQ output, and the bottom row compares AMS measurements with modified (add unknown, AU) CMAQ output.
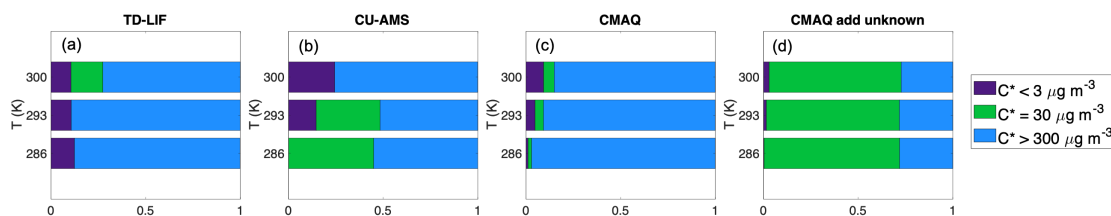
Figure C.15: Temperature-dependent fractional distribution (f_j) of saturation concentrations at 300 K $(C_j^*(300 \text{ K}))$ fit to a volatility basis set. C_j^* at ambient temperatures were converted to $C_j^*(300 \text{ K})$ using the empirical relationship between ΔH and C^* and the Clausius-Clapeyron equation. Each plot is shown for the TD-LIF measurements, the CU-AMS measurements, unmodified CMAQ output, and CMAQ output with an unknown source of $RONO_2$ added.
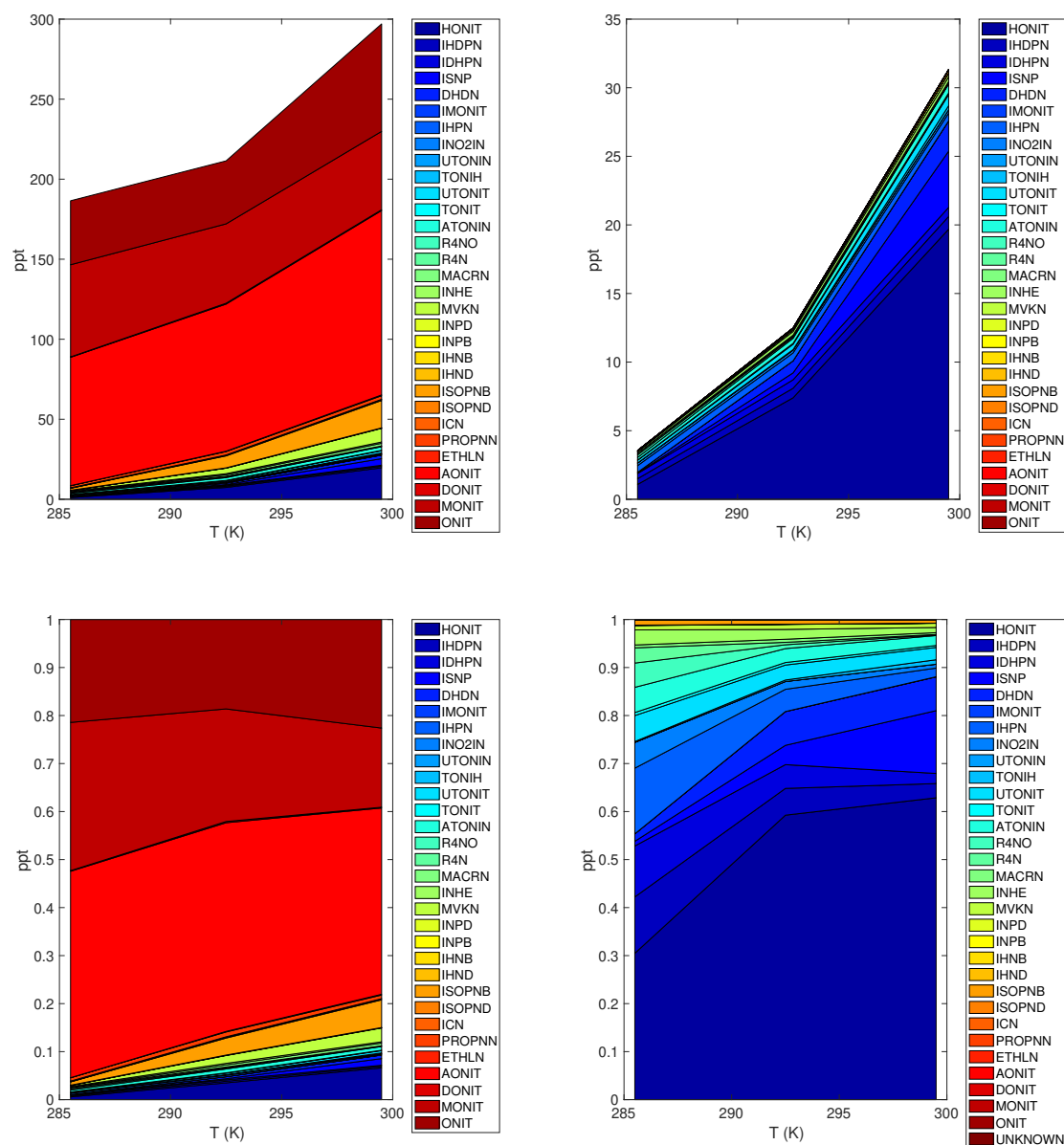
Figure C.16: CMAQ-modeled $RONO_2$ speciation for (left) $tRONO_2$ and (right) $pRONO_2$. Mixing ratios are shown in the top row, and the fractional, normalized speciation is shown in the bottom row. Species are ordered by vapor pressure: as the colors move towards red, species are more volatile and as the colors move towards blue, the species have lower volatility. Definitions of species names can be found in Browne et al. (2013) and Zare et al. (2019).
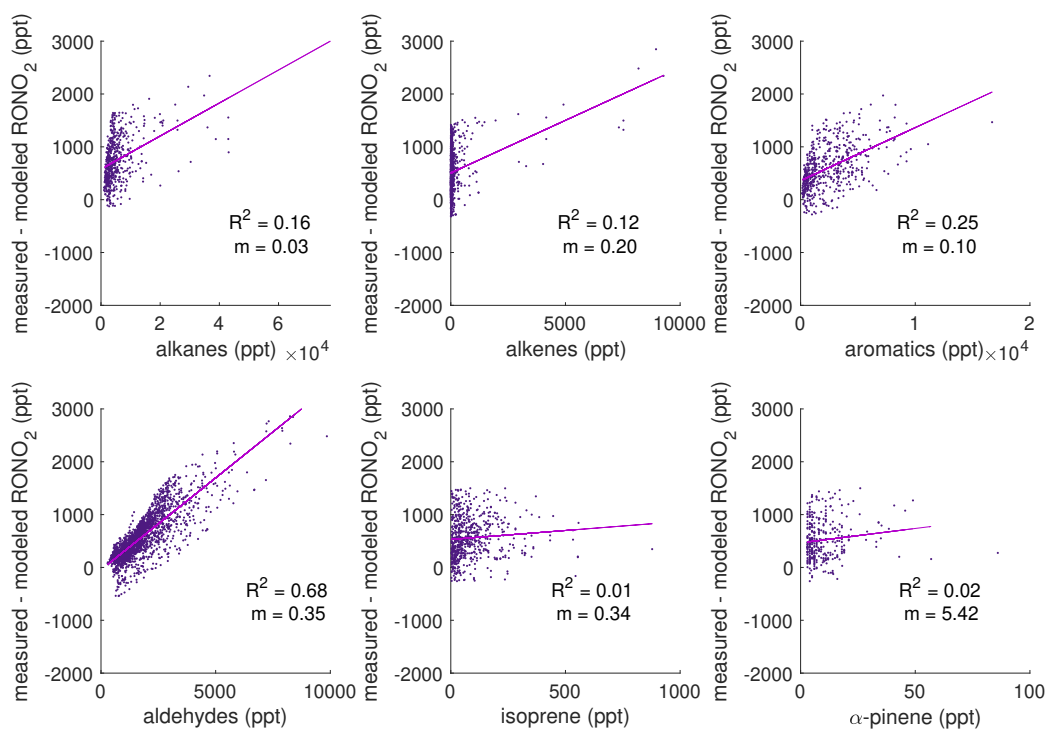
Figure C.17: Comparisons between the difference in between TD-LIF measured and CMAQ modeled $RONO_2$ ($RONO_{2,\text{diff}}$) and various VOCs and VOC classes. Outliers, defined as data $> 1.5\sigma$ on from either side of a linear fit through the data, have been removed. A second linear fit was then calculated once the outliers had been removed; this second fit is shown here. The R^2 and slope (m) of each linear fit is shown. Relatively weak correlations ($R^2 < 0.05$) between the $RONO_{2,\text{diff}}$ and both isoprene and α-pinene suggest that the missing source of $RONO_2$ is not biogenic in origin. The relatively stronger correlations between $RONO_{2,\text{diff}}$ and alkanes, aromatics, and aldehydes suggest an anthropogenic origin for the missing $RONO_2$.